MULTICOLOUR PHOTOMETRY OF GLOBULAR CLUSTER STARS

Christopher David Pike

A Thesis Submitted for the Degree of PhD
at the
University of St Andrews

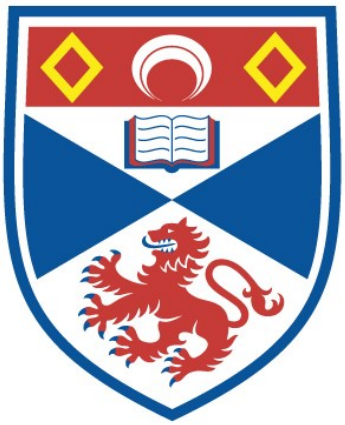

1977

MULTICOLOUR PHOTOMETRY OF GLOBULAR CLUSTER STARS

BY

CHRISTOPHER DAVID PIKE

A thesis submitted to the University of St. Andrews in fulfilment of the requirements for the degree of Doctor of Philosophy

JANUARY 1977

ProQuest LLC.
789 East Eisenhower Parkway
P.O. Box 1346
Ann Arbor, MI 48106 – 1346

CERTIFICATE

I certify that C. D. Pike has spent nine terms in research work at the Lick Observatory, University of California and at the University Observatory, St. Andrews, that he has fulfilled the conditions of Ordinance General No. 12 and Senate Regulations under Resolution of the University Court 1967, No.1, and that he is qualified to submit the accompanying dissertation in application for the degree of Ph.D.

ABSTRACT

The underlying theme of this thesis is the application of electronography to the study of stars in globular clusters through the use of both broad and intermediate-band photometric systems.

Introductions to both the study of globular clusters and to the use of electronography are given in Chapter 1. In Chapters 2 and 3 observations based upon electronographic exposures are presented for two little-studied clusters, NGC 5053 and NGC 6366. Both are loose, sparsely populated clusters but despite their similarity in appearance, the photometry shows that NGC 5053 is an unreddened, metal-poor globular, while NGC 6366 is found to be a highly reddened metal-rich cluster. One variable star in NGC 6366 is shown to be an a-type RR Lyrae - an unusual occurrence in a cluster of high metallicity.

Chapter 4 describes developments in the reduction of stellar electronographs made by the author. An automatic method of fitting Gaussian profiles to the density volumes is shown to produce photometry as accurate and linear as previous manual techniques, but with a much increased efficiency. This work is extended to investigate the use of more flexible profiles which are then shown to be useful for allowing photometry of crowded images. Finally, an application of the Gaussian profile fitting routines to photographic stellar photometry is discussed. Chapter 5 reports the use of this reduction scheme on photographic plates of the globular cluster M 15. Using the David Dunlap Observatory (DDO) intermediate-band photometric system, cluster members are easily distinguished from foreground dwarfs.

Chapter 6 describes the results of a programme of DDO electronography of the globular clusters M 5 and M 13. An accuracy of 0.03 is obtained for the DDO colours which, although comparable with some earlier photoelectric work, shows that, with the observational and reduction techniques employed, electronographic stellar photometry has not yet attained its potential as two-dimensional photoelectric photometry.

FOREWORD

The underlying theme of the work described in this thesis is the application of electronography to the photometry of stars in galactic globular clusters. The work is presented virtually in chronological order and therefore charts the progress of the changing techniques used and the programmes investigated.

At the time of the observations reported in Chapters 2 and 3, the only useful electronographic stellar photometry available was that of the Magellanic cloud clusters obtained at Cerro-Tololo in 1969 by Dr M. F. Walker. Some four years later, at the time of writing the final chapters, almost the only useful electronographic stellar photometry available was that of the Magellanic cloud clusters obtained at Cerro-Tololo in 1969 by Dr M. F. Walker. Far from being a typing error, this is a serious commentary on the state of electronographic photometry, particularly in regard to stellar work.

The observations described here represent attempts to amend this situation and the varying degrees of success achieved perhaps give an adequate explanation of its cause.

More specifically, after brief introductions to the astronomical and technical sides of the work, we describe in Chapters 2 and 3 photometric studies of two globular clusters based upon original electronographic material obtained in cooperation with Dr M. F. Walker. The reductions of the electronographs and the subsequent photographic and photoelectric observations were the work of the author.

The observations of NGC 5053 have since been published (Mon. Not. R. ast. Soc., 175, 525) as a joint paper with Dr M. F. Walker and Professor J. D. McGee. A paper based on Chapter 3 has also been published by the author (Mon. Not. R. ast. Soc., 177, 257).

The development of automatic routines for the reduction of electronographs is not unique, as stated in the text, but the work presented here was completely independent. The subsequent extension of the process to the reduction of multiple groups using a more realistic profile is, however, new and, we feel, holds much of the hope for the future of electronographic stellar photometry.

In Chapter 5, in a brief and enforced excursion from electronography, we describe a new application of the profile fitting programs to photographic photometry and describe the results of their use on plates of the globular cluster M 15.

The penultimate chapter represents an attempt to realise the full potential of electronography by obtaining accurate two-dimensional photometry in a photometric system that is capable of yielding important astronomical data. We believe that this is the first time such observations have been attempted.

I declare that the outline given above, together with the references cited in the text, give an accurate account of the extent to which this thesis is independent and original. I further declare that neither the complete thesis, nor any part of it, is substantially the same as that I have submitted or am submitting for any degree or other qualification to this or any other University. Under Ordinance General No. 12, I was admitted to the Faculty of Science of the University of St. Andrews as a research student on 1st October 1972 to carry out electronographic photometry of stars in globular clusters. I was accepted as a candidate for the degree of Ph.D. on 1st October 1973 under Resolution of the University Court 1967, No. 1.

C. D. Pike

January 1977

ACKNOWLEDGEMENTS

The results of this work have depended upon the cooperation and help afforded me by many people too numerous to mention individually - but to whom collectively I am deeply indebted.

In particular, it is a pleasure to thank my supervisors, Dr M. F. Walker at Lick Observatory, for not only the soundest possible training in the technique of electronography, but also more generally for instilling in me a part of his own meticulous approach to the art of astronomical observing; and Dr P. W. Hill at St. Andrews, for his overall supervision during the latter stages of the work and for his efforts in regard to the organisation of the original studentship and the observing described in Chapter 3.

At St. Andrews, the many conversations with Dr I. G. van Breda concerning the approach to profile fitting were invaluable and, after our move to the Royal Greenwich Observatory, Dr A. J. Penny's cooperation in freely giving of his own experience and knowledge in this field is much appreciated.

On the astronomical side, Dr R. J. Dickens' willing communication of his knowledge of this subject in its current, preprint and pre-preprint stages has proved of great help in our attempts to interpret the observations.

I am indebted also to the GALAXY group at the Royal Greenwich Observatory for their cooperation during my use of the machine; to Dr S. M. Faber for the loan of the DDO filters and to Mr D. M. Carr for his technical and culinary expertise at Izana.

I would like to thank the Directors of the Institutions where this work was pursued (Dr D. E. Osterbrock, Lick Observatory; Professor D. W. N. Stibbs, St. Andrews; Professor F. G. Smith, Royal Greenwich Observatory

and Dr D. Sadeh, Wise Observatory) for the unconditional use of their facilities.

The ever important financial support during the past four years has been generously provided by an SRC/NATO Studentship tenable at Lick Observatory and St. Andrews and, more recently, by a Junior Research Fellowship at the Royal Greenwich Observatory.

Finally, it is a pleasure to record the debt and gratitude I owe my wife, Jenny, who has withstood admirably (and usually in silence) the strains of astronomical widowhood over the past four years. My thanks are also due for her able assistance in all aspects of the preparation of this thesis, but most of all for her continual support, encouragement and often unfounded optimism in the face of many an electronographic disaster. Without all of these, her typing, proof reading and translations into English might never have been required.

TABLE OF CONTENTS

Foreword i

Acknowledgements iii

Table of Contents v

CHAPTER 1 Introduction 1

1.1 Globular Clusters
1.2 Electronography

CHAPTER 2 The Colour-Magnitude Diagram of NGC 5053 17

2.1 Introduction
2.2 Observations
2.3 Colour-magnitude diagram

CHAPTER 3 The Metal Rich Globular Cluster NGC 6366 32

3.1 Introduction
3.2 Observations
3.3 Colour-magnitude diagram
3.4 Reddening
3.5 Variable stars

CHAPTER 4 Reduction Techniques 55

4.1 Introduction
4.2 Profile fitting
4.3 Reduction of single images
4.4 Application to groups of images
4.5 Application to photographic images

CHAPTER 5 Intermediate band photographic observations of M 15 92

5.1 The photometric system
5.2 Calibration of the plates
5.3 Observations
5.4 Reduction for plates of M 15
5.5 Results

CHAPTER 6 Intermediate band electronography of M 5 and M 13 130

6.1 Introduction
6.2 Observations
6.3 Reductions
6.4 Sensitivity corrections
6.5 The globular cluster M 5
6.5.1 Introduction
6.5.2 Results
6.5.3 Discussion
6.6 The globular cluster M 13
6.6.1 Introduction
6.6.2 Results
6.7 Summary

CHAPTER 7 Conclusions 173

CHAPTER 1

INTRODUCTION

The study presented in this thesis is concerned with the photometry of individual globular cluster stars using, primarily, the technique of electronography. Since some readers are likely to be unfamiliar both in general and in detail with the programme and/or the use of electronography, we give here brief general introductions to the study of globular cluster stars and to electronography. The intention is that the details will be adequately discussed when they become relevant to the presentation in the later chapters.

1.1 Globular clusters

Our galaxy contains a multitude of stellar clusters which are as diverse in their characteristics as they are numerous. However, most clusters, with sufficient observation, can be classified unambiguously into either of two categories. This classification originated simply from the clusters' appearance. The term 'globular' was conceived for clusters such as M 3 and M 13 and the term 'open' reserved for those somewhat poorer in stellar content, typified by the Pleiades and M 67. Nevertheless, it was obvious from the outset that clusters covering the complete range of stellar densities existed and the discovery of 'globular cluster variables' in less well populated clusters, such as NGC 5053, only served to emphasise the shortcomings of a classification based upon appearance alone. Because of this, other criteria - the presence of many faint stars on long exposure photographs, the galactic latitude and the classification of the variables - were invoked to aid in the classification scheme. In the event, it was not until studies of the individual stars were attempted that the true nature and significance of the two kinds of clusters became apparent.

In the first years of this century, the colours and magnitudes of many nearby stars and of stars in the nearer open clusters had been

determined with sufficient accuracy to show that the majority still lay on the main sequence as we now know it. It was therefore a considerable surprise when the first investigations of globular cluster stars (Shapley, 1917) showed that the trend of colours with magnitude was the complete opposite of that previously found. Nonetheless, when accurate magnitude sequences were determined for example in Greenstein's (1939) study of M 4, these findings were confirmed. In that study the data defined the red giant branch and also a group of 'peculiar blue stars' near the plate limit. By the time Cuffey (1943) produced the colour-magnitude (C-M) diagrams of NGC 5053 and NGC 6838, it was apparent that indeed the separation of clusters into two distinct classes was justifiable but on the basis of a deep rooted physical difference in their observable stellar content. Hence it was that in Baade's (1944) discussion of stellar populations, globular cluster stars were identified as the prototype of Population II stars, while their open cluster counterparts were associated with Population I .

With the advent of larger telescopes and the accompanying possibility of extending magnitude sequences to fainter stars, the study of globular clusters, in particular their C-M diagrams, accelerated. An intensive study of the brighter northern clusters resulted in the identification of the Population II main sequence (Arp, Baum and Sandage, 1953), which showed for the first time how the giant sequences were related and joined to the main sequence. This work culminated a few years later in the C-M diagram of M 3 (Johnson and Sandage, 1956), which is still the most aesthetic of such diagrams.

Arp's (1955) comparative study of seven globular clusters was a landmark in the study of these objects. Three fundamental points emerged from his work, all of which have since been verified. Firstly, he found that the most striking difference between C-M diagrams is the morphology

of the horizontal branch; secondly, that the locus of the giant branch is correlated with the cluster's metal abundance; and thirdly that, although the sequences in most cases are intriniscally narrow, some of the stars found away from them in the C-M diagram are in fact cluster members.

The fundamental question of the heavy element abundance of globular cluster stars was also receiving a great deal of attention at this time. Mayall's (1946) data on integrated spectra had shown that the typical cluster spectrum was very weak in metals, but that stronger lined clusters did exist. Morgan (1956, 1959) was later to extend this work and demonstrate the existence of a continuous set of spectral types. Quantatative data on the metal deficiency only became available through the curve of growth analysis of red giants in M 13 and M 92 by Helfer et al (1959), although an indirect measurement of it had been provided by Sandage and Walker's (1955) discovery of the ultra-violet excess of globular cluster red giants, which they interpreted as a reduced line blanketing effect. Although a slight systematic trend with metallicity was apparent in the C-M diagrams observed by Arp (1955), the extension of these investigations to Morgan's (1959) clusters of later spectral type was given by Sandage and Wallerstein (1960). The C-M diagram for this metal rich cluster (metal rich in this context is used in the sense of being only a factor of about five deficient in metals compared with the sun) showed what today we take as characteristic features of high metallicity i.e. a horizontal branch only populated to the red of the variable star gap and a gently sloping giant branch.

During the next few years, C-M diagrams for a whole range of clusters were produced. All fitted, with various degrees of precision, into the scheme whereby metal abundance was seen as the principle parameter determining the C-M diagram morphology. From integrated photometry,

however, van den Bergh (1967) had suggested that at least two parameters were necessary to classify globular clusters. The most obvious manifestation of this was M 13 which, even though of intermediate metallicity, contained an extremely blue horizontal branch, thus presenting a violation of the otherwise unique relationship connecting horizontal branch morphology and metal abundance. Prior to van den Bergh's suggestion, there was no known galactic globular cluster which exhibited the reverse of the 'M 13 anomaly', although it had been observed in extragalactic systems by Baade and Swope (1961) (the Draco dwarf galaxy) and Tifft (1963) (NGC 121 in the SMC). This situation was changed dramatically by observations of two clusters reported within a week of one another. The C-M diagrams of NGC 7006 (Sandage and Wildey, 1967) and NGC 362 (Menzies, 1967) both showed a heavily populated red horizontal branch, which for these clusters was in contradiction to the other metallicity indicators. The theoretical work of Faulkner (1966) and Faulkner and Iben (1966) on the structure of the horizontal branch suggested strongly that variation in the helium abundance could be responsible. Indeed, Hartwick (1968) and Castellani et al (1970) have since presented classification schemes in which they adopt helium as the second parameter.

More recently, Hartwick and McClure (1972) have presented results from intermediate band photometry of the giants in NGC 7006 which purport to show that these stars have anomolously strong CN bands, indicating an overabundance of nitrogen. Subsequent theoretical calculations showing how an increased nitrogen abundance (through its influence on the CNO cycle) can mimic an overall increase in the heavy element abundance were presented by Hartwick and Vanden Berg (1973). Promising as this suggestion for the second parameter was, it was not to receive much support. Indeed, a similar study of NGC 362 (McClure and Norris, 1974) was unable to distinguish the giants in this anomalous cluster from these in M 5,

even though Eggen (1972) had found significant differences in the (R-I) colours of stars in the two clusters.

Unfortunately, the search for this second parameter has recently begun to lose some of its momentum. This is a direct result of further theoretical work, principally by Rood (1973), which has shown that, not only are age and helium abundance both likely to be ingredients of the parameter, but also that only very small changes ($\Delta Y = 0.03$; $\Delta T = 1$ billion years) in these are required to produce the range of characteristics observed. The probability is, therefore, that variations in helium and metal abundance, together with slight age differences have effects upon the stellar properties that are too small to be detectable easily at present, other than by the effect they have on the horizontal branch morphology.

Until recently, apart from broad band photometry, the only data generally available for cluster stars were low-intermediate dispersion spectra. These studies had nevertheless led to a number of interesting discoveries such as the CH stars in ωCen (Harding, 1962; Dickens,1972; Bond,1975), abundance anomalies in other clusters (Strom and Strom,1971; Zinn,1973a) and lately the recognition of the weak-G-band effect of the asymptotic giant branch (Zinn,1973b; Norris and Zinn,1976).

It was in the hope that an intermediate band study of a large number of globular cluster giants would yield further information on the occurrence of such effects, as well as giving physical data for the normal stars, that the observations described in the later chapters were obtained.

1.2 Electronography

Electronography has developed from an idea put forward by Kiepenheuer (1934) who proposed that a system whereby the electrons emitted from a photocathode could be accelerated, focussed and recorded directly would have many of the properties desirable for astronomical photometry. The two most important properties that should result are a high quantum efficiency and a linearity between output signal and input intensity. Viewed in these terms, electronography provides an opportunity for two-dimensional photoelectric photometry.

The time interval between the original suggestion and the production of the first important astronomical results - over two decades - remains as a testimony to the difficulties experienced in making a functional system. Lallemand (1936) is generally credited with the development of the first electronographic camera and, despite the delay between the conception and inception of a viable camera, once one was interfaced to a telescope important astronomical discoveries resulted almost immediately (Lallemand, Duchesne and Walker, 1960).

The practical difficulties encountered in developing a workable system were due mainly to two restraints imposed by the physical nature of the constituents. Firstly the photocathode can exist and the electrons only be imaged suitably in a vacuum. Secondly the photocathode and nuclear emulsion - the recording medium for the electrons - are incompatible in the sense that outgassing from the emulsion at room temperature in a vacuum will very quickly poison the photocathode. The system originally designed by Lallemand to overcome these difficulties still unfortunately suffered from the two fatal drawbacks of being unwieldy in operation and needing many hours of preparation, since a new photocathode had to be generated after each batch of plates had been exposed. The problem of the poisoning of the cathode was essentially solved by Kron et al (1969)

in their version of the electronographic camera. Here it was possible to seal off the photocathode from the film container by means of a coin valve. This valve was therefore closed when film changing was taking place and prior to the exposures the film space could be pumped down to the level of the cathode cavity. The whole system was cooled, as in the Lallemand camera, by liquid nitrogen. Under these conditions the amount of gas released by the emulsion during actual exposures is small enough for the photocathode to remain active for many months. The single greatest drawback of the Kron camera is that, in order for the film to be exchanged, the whole apparatus has to be removed from the telescope so that it may be attached to a parent vacuum system. Since this is a lengthy process, it effectively limits an observer to one film of six exposures per night. For many programmes this is clearly a serious handicap. Again in practical terms, the fact that exposures cannot be inspected to assess their quality - e.g. focus and exposure time - until the end of the night makes the system unattractive and potentially time wasting for the astronomer.

Probably as a direct consequence of the above considerations, the most widely used electronographic image tube to date has been the Spectracon developed by Prof. J. D. McGee and his collaborators at Imperial College (McGee et al, 1966). In this image tube, the problem of the incompatibility of the photocathode and emulsion is solved by the construction of a completely sealed vacuum tube containing the photocathode. The film then always remains external to this. The innovation which made this configuration feasible was the introduction into the back end of the tube of a four-micron-thick mica window. Such a window is vacuum tight but still electron permeable, since it has seventy-five percent transmission for the electron energies involved here. Hence the images can be recorded by simply bringing the film into intimate contact with the mica

window.

In an excellent review of image tubes used in astronomy, with particular emphasis on the Spectracon, McGee (1973) summarizes the five principal advantages of such a system.

1) There is no possible interaction between the photocathode and the nuclear emulsion.
2) The image tube is permanently sealed, so there is no need for auxiliary vacuum equipment.
3) The film can be developed and its quality assessed immediately.
4) Having a sealed-off high vacuum system enables more sensitive and delicate photocathodes (S1 and S20) to be used.
5) The image tube in its solenoid is compact and not excessively heavy, making it usable at all telescope foci.

As indicated above, the first of these points is the essential one which makes the system functional. The others are consequences of this which make the Spectracon a convenient and workable device. To redress the balance slightly, mention should be made of two drawbacks. In order to impart sufficient energy to the electrons for them to penetrate the mica window and still retain enough energy to activate the emulsion grains, the operating potential of the tube must be -40 kv. At such a high voltage, problems can arise with electrical breakdown and coronal discharges. Secondly, the mica window is severely limited in size by the atmospheric pressure which it has to withstand. The mica window is moreover quite fragile, but if reasonable care is taken in handling the tube, particularly when advancing the film towards the window, breakages are rare.

We should add, however, it is common experience that the Spectracon's performance does not always reach the levels expected of it from the above considerations. When the quality of the tubes produced by McGee's group was at its peak and when these were being used competently

(e.g. Walker 1970), then there is no doubt that the device was reliable, convenient to use and capable of yielding a wealth of important astronomical data. It appears though that Spectracons can become unreliable in use if the quality of and care taken in the manufacturing process are impaired. These affect the quality of the photocathodes and the general condition of the encapsulation of the tube, increasing its susceptibility to the development of background problems.

The two most important features of electronography are its high quantum efficiency and linearity. The first of these varies from cathode to cathode and can change during the tube's lifetime. The only complicating factor that does arise is from variations in sensitivity across a single photocathode. This can be allowed for, however, as will be described later. The debate as to the linearity of the whole process is a lively and continuing one. Given that the number of electrons leaving the photocathode is a linear function of the number of impinging photons, then it is possible that both the mica window and photographic process in the nuclear emulsion could be responsible for introducing some non-linearity into the results. There exist in the literature numerous claims and counter-claims for linearity. Kahan and Cohen (1969) performed exhaustive tests on Spectracon output. Their results indicated that for L4 emulsion there was no detectable departure from linearity up to a density of at least five, while with G5 emulsion linearity was accurately maintained up to a density of D = 2.5. Recently Penny (1976) has arrived at much the same conclusions, but finds a slight deficiency in observed density at densities greater than approximately D = 3 for L4 and attributes this to multiple interactions between the electrons and grains in the emulsion. Several groups, however, (see proceedings of the Texas symposium on Electronography and its Astronomical Applications) have reported their inability to produce linear results, even at low

densities. Since there seems little doubt that linearity is achieved in many instances, the easiest way out of the problem is to dismiss the negative results as being due to the use of incorrect developing and/or measuring techniques - an allegation vehemently denied of course. In the circumstances, it would seem prudent for each investigator to satisfy himself that his own complete development and measurement procedure produces the desired effects. This was done for the set-up employed to make and reduce the observations to be described later.

The test exposures were made in the laboratory using Spectracon B 289 operated at -40 kv. A light source with a stabilized power supply was used to project a spot of light approximately 3 mm in diameter on to the photocathode. A series of eight exposures could then be taken on a single strip of film. The standard development procedure used throughout was:

1) Develop for 5 min in D19 at 65° F with constant agitation.
2) Rinse for 30 sec in dilute acetic acid.
3) Fix for twice the clearing time (3 - 4 min usually, though it is very temperature dependent) in a solution of hypo and hardener.
4) Wash in filtered, running water for 45 - 60 min.
5) Rinse in alcohol and dry in dust free area.

A rotating disc was used to time the various exposures. Dr Walker had had this machined to strict tolerances so that there were three evenly-spaced clear sectors of 60° cut from it. The disc was rotated by a synchronous motor. The exposures could then be made by exposing the film to the passage of any number of the clear sectors. The need to operate the whole system in complete darkness necessitated having some means of recording the number of sectors exposed. Since this had to be non-mechanical so as not to interfere with the motion of the disc, we constructed a simple system which comprised a faint collimated beam

about 1 mm in diameter and a photo-diode, which when switched on by the light source activated a relay, which in turn operated a digital counter. Since the counter could be mounted well away from the test bench and read by luminous digits, it provided a convenient way of recording the exposure. The light source and detector were placed either side of a fork mounting as illustrated in Figure 1, with the disc passing between them.

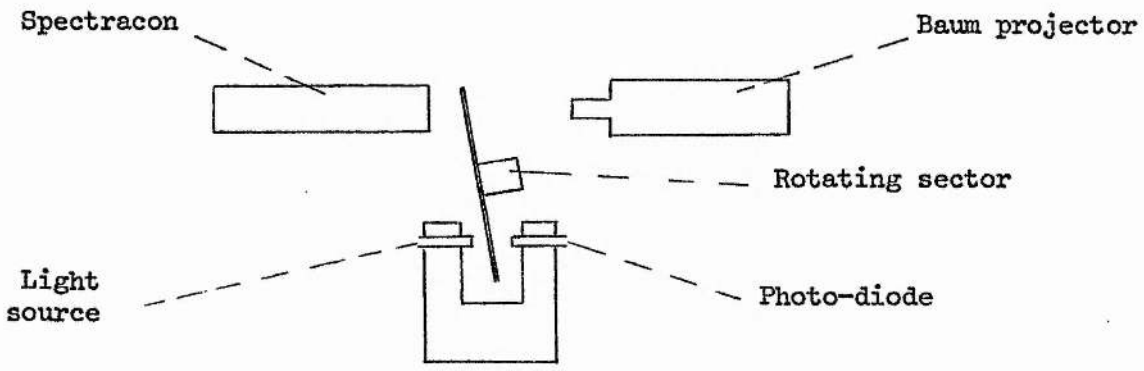

Figure 1

Using this apparatus, many test films were exposed. The results for one set of exposures which cover the correct range in density are illustrated in Figure 2. The images were scanned on the Joyce-Loebl at the Royal Greenwich Observatory, using a long slit to reduce the grain noise. Care was taken to trace the same region on each image to eliminate any effects of cathode sensitivity variations. This was rather easily done by employing the cathode defects as fiducial marks. Different wedges were used to record the short and long exposures, while measurement of a common exposure was used to determine the conversion factor. As can be seen, the measured density increased linearly with exposure time. The slight discrepancy noted at the highest density could be the effects of multiple hits beginning to manifest themselves.

A number of Spectracons used at Lick Observatory developed background

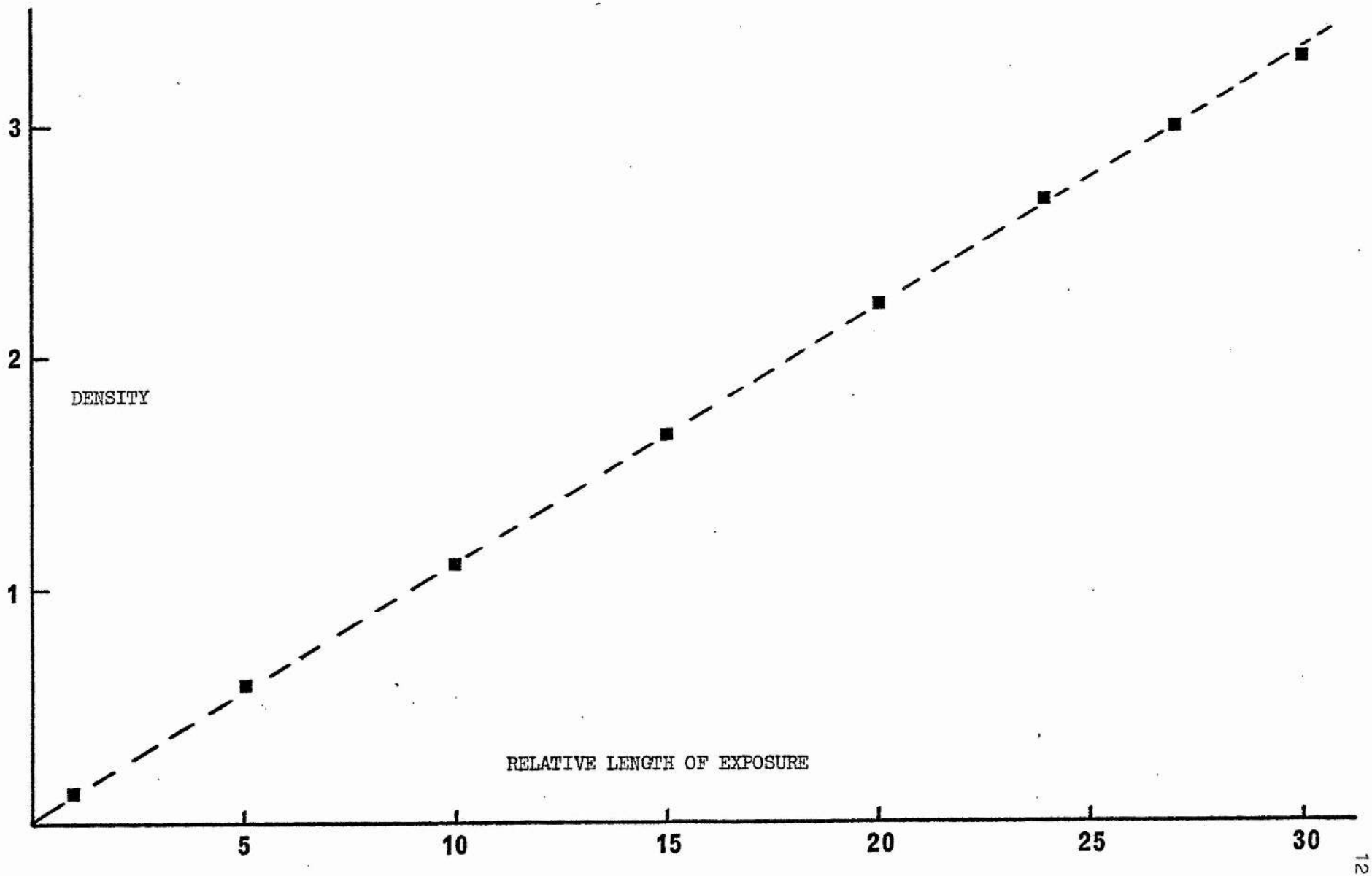

Figure 2. The linearity test for Spectracon output.

emission problems during use and it was found that this could be reduced considerably by lowering the operating voltage to -38 kv or even -36 kv. This is an undesirable thing to have to do of course, since there is a corresponding loss in speed of the tube. More importantly, it was found that when linearity tests were run at the lower voltages, then the degree to which the recorded density fell below the linear prediction at the higher densities increased considerably as the voltage fell. As a result, it would be erroneous to make the assumption of linearity over any large range in density under these circumstances.

Taken in isolation, this simple test of linearity might seem an insufficient foundation on which to base investigations that depend critically upon precisely this result. However, the physics of the linearity of nuclear emulsions and investigations into the properties of the microphotometers used to reduce the exposures have recently been given by Worsick (1975) and Penny (1976). They set out in detail the capabilities and shortcomings of the kind of procedures employed here and give confidence that meaningful data can be derived in this manner.

More recently, the supply of Spectracon tubes has all but dried up and their use for direct work has been less in the last two years than previously. For direct electronography this might well turn out to be a permanent situation since the tubes developed by McMullan et al (1972), which are direct descendants of the Spectracon, are seeing more and more use. The critical limitation of the Spectracon for many astronomical investigations is the small cathode area. The obstacle to enlarging this is the mica window which, having to withstand atmospheric pressure, must itself be limited in size. McMullan has solved this by having the mica window enclosed in an evacuated chamber so that the pressure it has to withstand can be controlled and limited to a few torr. The size of the mica window can thus be enlarged to match an increased cathode size.

Having the mica window in an evacuated chamber has not been allowed to hinder the operation of the tube, since the bringing of the film into contact with the window is completely automatic and controlled by sophisticated pneumatic engineering. For the electronographic work described in the later chapters, a McMullan 4 cm camera attached to the Wise Observatory's 1-metre reflector was used. In practice, the camera was found to be at least as easy to use as the Spectracon and of course has a vastly increased field of view - just the two properties most desirable in this kind of system.

References

Arp, H., 1955. A.J., 60, 317.

Arp, H., Baum, W. & Sandage, A., 1953. A.J., 58, 4.

Baade, W., 1944. Ap. J., 100, 137.

Baade, W. & Swope, H. H., 1961. A.J., 66, 300.

Bergh, S. van den, 1967. A.J., 72, 70.

Bond, H. E., 1975. Ap. J. (Letters), 202, L47.

Castellani, V., Gionnone, P. & Renzini, A., 1970. Astroph. & Sp. Sci., 9, 418.

Cuffey, J., 1943. Ap. J., 98, 49.

Dickens, R. J., 1972. Mon. Not. R. ast. Soc., 159, 7P.

Eggen, O. J., 1972. Ap. J., 172, 639.

Faulkner, J., 1966. Ap. J., 144, 978.

Faulkner, J. & Iben, I., 1966. Ap. J., 144, 995.

Greenstein, J. L., 1939. Ap. J., 90, 387.

Harding, G. A., 1962. Observatory, 82, 205.

Hartwick, F. D. A., 1968. Ap. J., 154, 475.

Hartwick, F. D. A. & McClure, R. D., 1972. Ap. J. (Letters), 176, L57.

Hartwick, F. D. A. & Vanden Berg, D., 1973. P.A.S.P., 85, 355.

Helfer, H. L., Wallerstein, G. & Greenstein, J. L., 1959. Ap. J., 129, 700.

Johnson, H. L. & Sandage, A., 1956. Ap. J., 124, 379.

Kahan, E. & Cohen, M., 1969. Adv. in E. & E.P., 28B, 725.

Kippenheuer, K. O., 1934. Die Sterne, 9, 190.

Kron, G. E., Ables, H. D. & Hewitt, A. V., 1969. Adv. in E. & E.P., 28A, 1.

Lallemand, A., 1936. C.R. Acad. Sci., Paris, 203, 243 & 990.

Lallemand, A., Duchesne, M. & Walker, M. F., 1960. P.A.S.P., 72, 76.

Mayall, N. U., 1946. Ap. J., 104, 297.

McClure, R. D. & Norris, J., 1974. Ap. J., 193, 139.

McGee, J. D., 1973. Vistas in Astronomy, 15, 61.

McGee, J. D., Khogali, A., Ganson, A. & Baum, W. A., 1966. Adv. in E. & E.P., 22A, 11.

Menzies, J., 1967. Nature, 214, 689.

McMullan, D., Powell, J. R. & Curtis, N. A., 1972. Adv. in E. & E.P., 33A, 37.

Morgan, W. W., 1956. P.A.S.P., 68, 509.

Morgan, W. W., 1959. A.J., 64, 432.

Norris, J. & Zinn, R. J., 1976. Preprint.

Penny, A. J., 1976. Thesis, University of Sussex.

Rood, R. T., 1973. Ap. J., 184, 815.

Sandage, A. & Walker, M. F., 1955. A.J., 60, 230.

Sandage, A. & Wallerstein, G., 1960. Ap. J., 131, 598.

Sandage, A. & Wildey, R. L., 1967. Ap. J., 150, 469.

Shapley, H., 1917. Ap. J., 45, 123.

Strom, S. E. & Strom, K. M., 1971. Astr. & Astroph., 14, 111.

Tifft, W. G., 1963. Mon. Not. R. ast. Soc., 125, 199.

Walker, M. F., 1970. Ap. J., 161, 835.

Worsick, S., 1975. Thesis, University of London.

Zinn, R. J., 1973a. Astr. & Astroph., 25, 409.

Zinn, R. J., 1973b. Ap. J., 182, 183.

CHAPTER 2

THE COLOUR-MAGNITUDE DIAGRAM OF NGC 5053

2.1 Introduction

The electronographic observations to be described below were made with the aid of a Spectracon mounting designed by Dr Walker for use at the prime focus of the 120" reflector and the Cassegrain focus of the 24" reflector of the Lick Observatory. Since working at the prime focus of the 120" precluded the use of liquid coolants, a new solenoid incorporating Peltier electrical coolers was used. The mounting, which has been described by Walker (1973), has facilities allowing field acquisition, off-set guiding and knife-edge focussing with the Spectracon in place.

Dr Walker's experience in Chile at Cerro Tololo where he had obtained photometry of Magellanic Cloud globular clusters to $V \simeq 22.5$ on the 60" reflector, led us to expect that it would be possible to obtain photometry to somewhat fainter limiting magnitudes than this when using the 120", even when due allowance was made for the brighter sky ($\sim$1.5 magnitudes in V) at Mount Hamilton.

One of the astronomical programmes planned for the prime focus was to extend existing colour-magnitude (C-M) diagrams of globular clusters to provide main sequence photometry, since this was available for only a handful of the brighter clusters. This was an ideal programme since the small field (2'.2 x 5'.5 for the normal 10 mm tubes) was in most cases not too much of a handicap and also it was usually possible to employ existing photoelectric standard sequences.

One cluster for which it seemed the existing photoelectric sequence could be extrapolated to reach the main sequence was NGC 5053. This sparsely-populated, high galactic latitude ($\alpha = 13^h\ 15^m.1$, $\delta = +17^\circ\ 48'$, 1975) globular cluster had previously been studied by Cuffey (1943) and Purgathofer (1966). Indeed, Cuffey's C-M diagram, based on red and blue magnitudes derived from photographic transfers from the North Polar

Sequence, was amongst the first C-M diagrams of globulars which showed their distinction from Population I clusters. Purgathofer observed the cluster on the UBV system of Johnson and Morgan (1953) using photoelectric and photographic observations obtained with the 100" Hale reflector. Purgathofer's observations, which extend to V = 16.6 barely reach the horizontal branch. However, unpublished observations by Sandage (Arp, 1965) indicated that the mean V magnitude of the horizontal branch was V = 16.55. Relative to its total stellar content, the cluster is rich in variable stars (Kukarkin, 1973). The ten confirmed RR Lyrae variables (Mannino, 1963) have a mean period of 0.673 days which is consistent with an extremely low metal content, similar to that in M 92 and M 53 (Arp, 1965).

2.2 Observations

The electronographic observations used in this investigation were obtained by Dr Walker at the prime focus of the 120" reflector. The Spectracon used in this instance was a special tube described by McGee, Coleman and Phillips (1973). It had an S-11 photocathode but was of the 'double-window' variety with photocathode and exit window dimensions of 20 x 30 mm. Single 60 minute exposures in yellow and blue light were obtained through filters consisting of 2 mm of Schott GG14 and 1 mm of Schott BG12 plus 2 mm of Schott GG13. Details of these exposures are given in Table I. The electronographic images of stars with $V \geq 15.0$ were measured by the author using the method described by Walker (1970). The images were scanned several times with the Joyce-Loebl microphotometer at a magnification of x200 with a projected aperture size of 12.5 microns square. A standard profile for each exposure was determined by averaging the parameters of six good profiles and thereafter this standard profile was fitted by eye to the scans of the programme

Table I

Measured Electronographs

Exposure No.	Date 1973 (U.T.)	Exposure (min)	Hour Angle mid-exposure	Colour
SL-37	April 7	60	1-11 W	Y
SL-38	April 8	60	2-20 W	B

Table II

Measured Photographs

Exposure No.	Date (U.T.)	Exposure (min)	Hour Angle mid-exposure	Telescope*	Emulsion (Kodak)	Filter
CD- 495'	1957 April 21	5	3-37 W	36	103aO	GG-13
CD-1826	1974 April 30	10	0-04 W	36	103aD	GG-14
CD-1827	April 30	10	0-47 W	36	103aD	GG-14
AB-7773	May 16	20	0-43 W	20	103aO	GG-13

*Telescope: 36 = 36-inch Crossley reflector; 20 = 20-inch Carnegie Astrograph.

'Plate taken from plate files of Lick Observatory.

stars. Instrumental magnitudes were derived by planimetering the area under the constructed profile and taking 2.5 times the logarithm of this. Although present to some extent in all photocathodes used for electronography, variation in sensitivity across the cathode of the double-window Spectracon used for these exposures was particularly severe. This can be seen in Figure 1, which is a reproduction of the yellow light exposure. Such large variations necessitated a star by star correction to the instrumental magnitudes. This was achieved by obtaining exposures of an area of the twilight sky (with the telescope on the meridian at $+60^{\circ}$) where no object had been visible when it was dark. These exposures provide a uniform illumination of the cathode and thereafter any measured variation in density on the developed film is ascribed to cathode sensitivity variations. In theory, the magnitudes in each colour should be corrected independently, although when twilight exposures were obtained in conjunction with U, B and V filters, no colour dependence of the sensitivity was ever found. This result applies specifically only to the S-11 photocathodes used here, since Penny (1976) has shown that, with the S-20 cathodes used in the McMullan cameras, there are large colour as well as spatial variations in the sensitivity, particularly in the red. A Joyce-Loebl isodensitracer map of the twilight exposure was then obtained at a magnification of x20 and a corresponding density scan across the image was traced in order to ascribe an absolute density and percentage change to the contours. The map used in the final analysis here had contours representing a 3% variation in sensitivity. By matching an enlarged print of the exposure with the Joyce-Loebl map it was possible to obtain point by point corrections accurate to the order of 1-2% by interpolating between the contours.

Despite the larger dimensions of the photocathode of the Spectracon

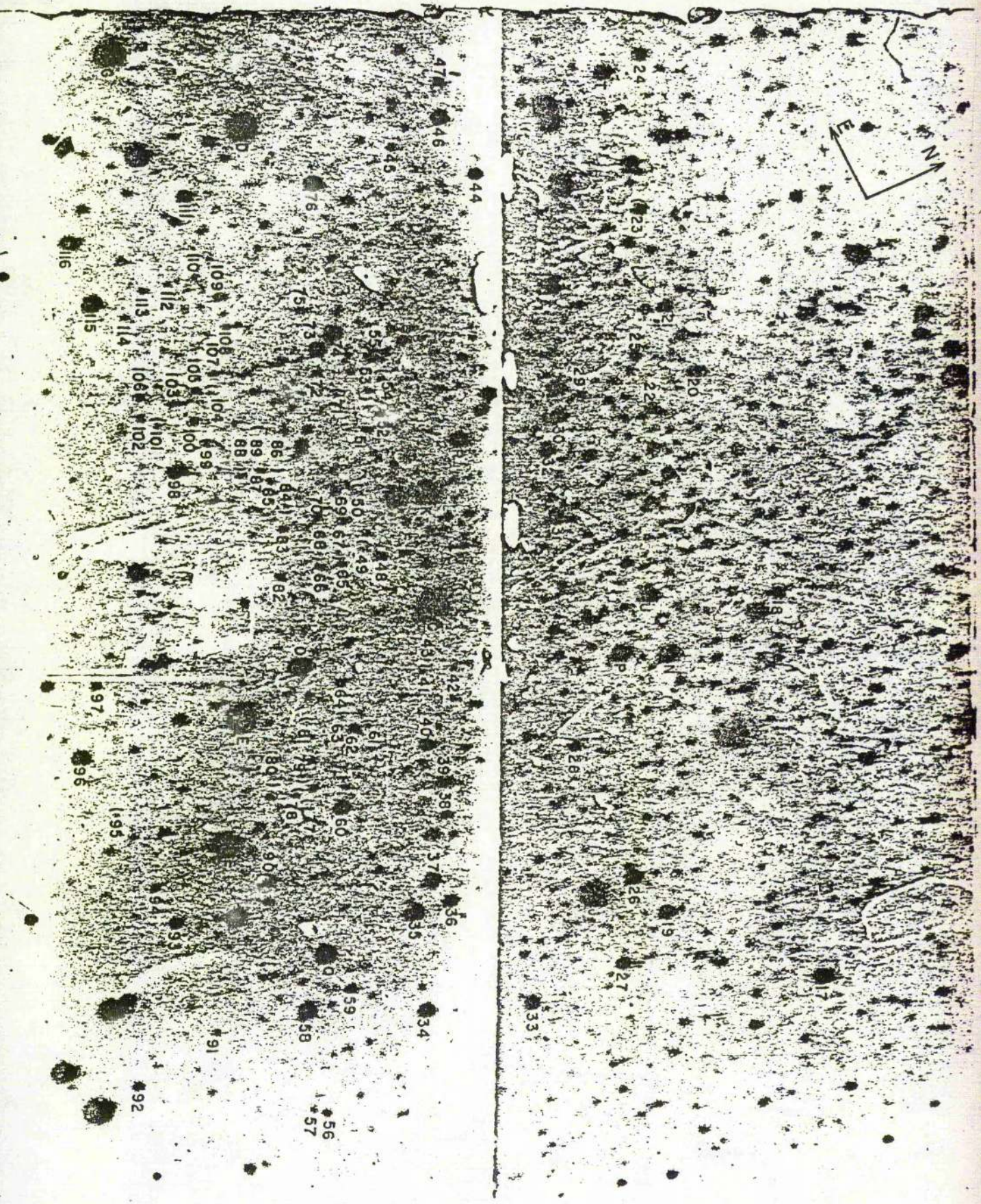

Figure 1

The yellow light electronograph of NGC 5053
The discontinuity down the centre results from the joining of two 10 mm cathodes to form the 20 mm size

used here, the sparse nature of the cluster resulted in very few red giants being contained in the field studied. This, together with the fact that the image density of stars brighter than V = 15.0 was too high for accurate measurement by the technique described, made it impossible to derive the form of the upper end of the red giant branch from the electronographic observations alone. Additional photographic observations, covering the entire area of the cluster, were therefore obtained by the author with the 36" Crossley reflector and the 20" Carnegie Astrograph. Details of these observations are given in Table II. On these exposures, most of the brighter stars within a radius of 4' of the cluster centre were measured using the Sartorius iris diaphragm photometer of the Lick Observatory. The stars measured photographically are identified in Plate I. The lettered stars are the original photoelectric standards identified by Purgathofer (1966).

The initial reduction of both photographic and electronographic measurements was made using the photoelectric data published by Purgathofer (1966) to provide the conversion to the BV system of Johnson and Morgan (1953). Since the colours of most of the standards fell within a rather small range, it was not possible to detect colour-equations in either the photographic or electronographic measures of the cluster stars. Comparison of the resultant C-M diagram with previous data for NGC 5053 (Arp, 1965) and with the diagrams of other globular clusters such as M 3 and M 92 suggested the presence of a zero-point error in the V magnitudes and possibly an undetected colour equation, since the mean magnitude of the horizontal branch did not agree with that quoted by Arp (1965) and the colours of the blue and red edges of the variable star gap were apparently anomalous. Fortunately, at this point Dr A. Sandage kindly made available to us his unpublished photoelectric and photographic observations of stars in NGC 5053 with

Plate I

Identification for the brighter stars in NGC 5053

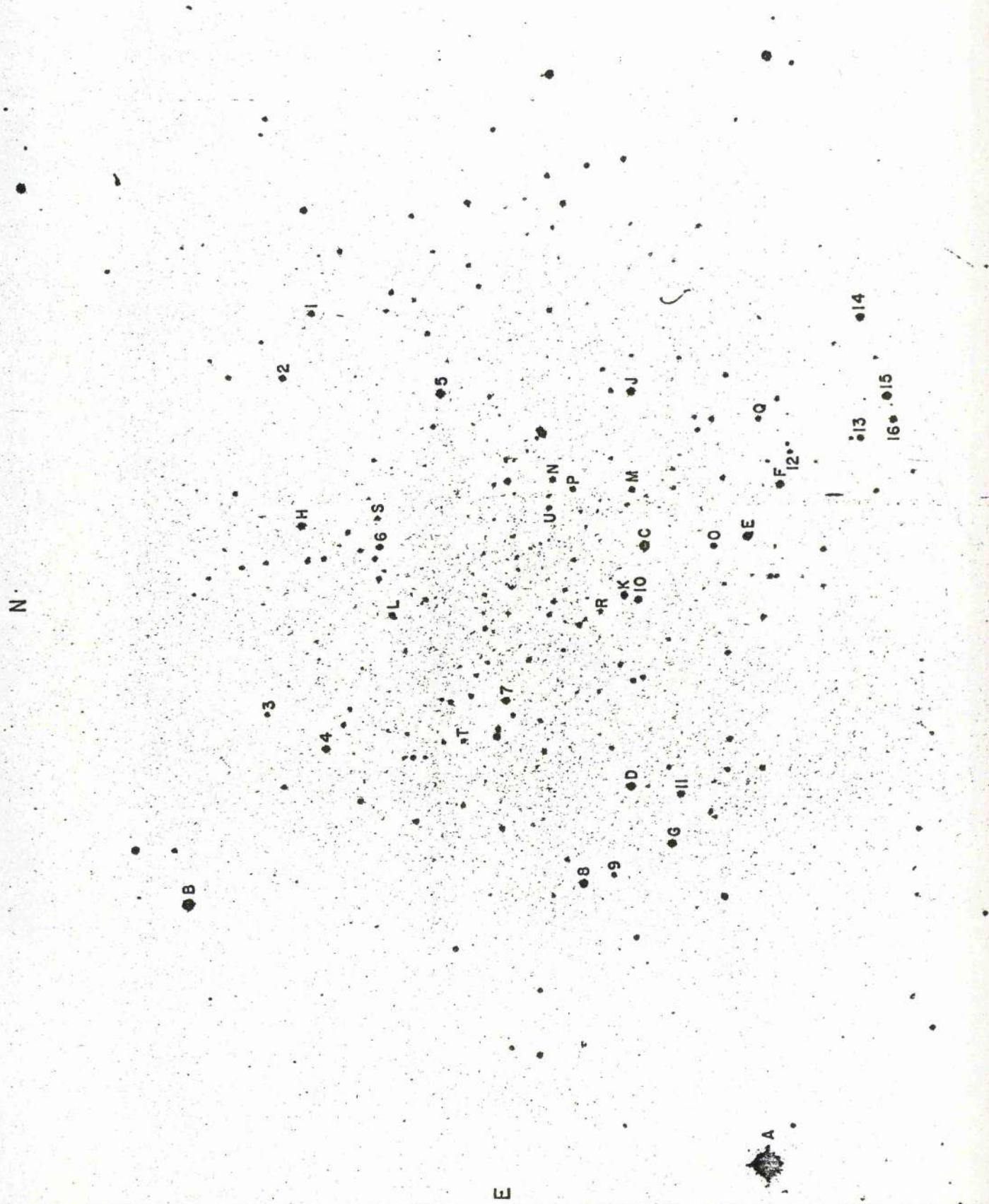

$V \leq 17.3$. These data made possible a detailed recalibration of the observations.

To ensure the use of as many stars as possible, the recalibration was done using, with equal weighting, the photographic magnitudes obtained by Sandage for all of the stars observed in both studies. The photographic and electronographic observations were treated separately. For the photographic magnitudes, corrections as a function of magnitude were deduced from plots, for both B and V, of the residuals between the magnitudes determined by Sandage and those obtained in the present study using Purgathofer's standards. After correcting both B and V in this manner, a remaining colour equation of the form

$$(B-V) = 0.82(B-V)pg + 0.14$$

was found and the colours corrected for this. The electronographic magnitudes were first transformed approximately to the BV system by means of zero-point corrections determined using Sandage's photographic magnitudes. A small colour equation

$$(B-V) = 1.06\ (B-V)elect + 0.04$$

was then found from a comparison of the two sets of magnitudes and colours, and the electronographic observations were corrected accordingly.

2.3 Colour magnitude diagram

The finally adopted values of the magnitudes and colours are given in Tables III and IV, and the C-M diagram plotted from them is shown in Figure 2. Table III lists the photographic observations, while Table IV contains the electronographic measurements. The average probable error of the photographic observations in Table III is ±0.03 mag. The probable error of the electronographic observations is not directly measureable since only single observations are available. However, from the dispersion of the residuals in (B-V) of the subgiants about a mean line in

Table III

Photographic Observations

STAR		V	B-V	STAR	V	B-V
C		14.04	+1.11	1*	15.92	+0.77
D*		14.59	0.98	2*	15.61	0.54
E*	**	14.65	0.98	3*	16.48	0.48
F*	**	14.68	1.27	4*	15.14	0.93
G*		14.87	0.99	5*	14.55	0.84
H*		15.01	0.85	6*	15.71	0.67
J*		15.05	0.95	7*	15.27	0.77
K		15.26	0.86	8*	14.71	0.65
M*		15.91	0.73	9	16.75	0.10
N*		15.90	0.75	10	15.40	0.78
O*		16.04	0.74	11*	15.68	0.68
P*		16.13	0.76	12	16.58	0.47
Q*		16.35	0.73	13*	15.63	0.77
R*	**	16.57	0.53	14*	15.17	0.89
S*		16.48	0.25	15*	14.58	0.80
U		16.56	0.55	16*	15.17	0.89

*Stars in common with Sandage (1975), used to transform the present observations to the B, V system.

**Remarks:

E. Appears double on the Crossley plates.

F. (B-V) differs substantially from Sandage (1975) and Purgathofer (1966).

R. Present photographic and electronographic measures agree, but not with Sandage (1975) or Purgathofer (1966).

Table IV

Electronographic Observations

STAR	V	B-V	STAR	V	B-V	STAR	V	B-V
N*	16.08	+0.61	46*	16.97	-0.03	81	20.96	0.44
O*	16.09	0.83	47	18.62	+0.52	82	18.78	0.54
P*	16.23	0.71	48	19.69	0.37	83	19.36	0.49
Q*	16.46	0.63	49	20.61	0.17	84	20.20	+0.41
R*	16.74	0.57	50	20.37	0.28	85	19.61	+0.39
U	16.69	0.60	51	19.91	0.41	86	21.09	0.25
17*	16.47	0.43	52	19.86	+0.42	87	19.32	0.69
18	16.08	+0.80	53	19.90	+0.59	88	20.08	0.26
19*	17.01	-0.07	54	20.26	0.30	89	21.11	0.59
20	17.69	+0.58	55*	17.12	0.70	90	17.91	0.70
21*	17.06	0.68	56	18.89	0.56	91	19.81	0.30
22	17.53	0.65	57	19.37	0.44	92	18.19	0.59
23	17.55	0.71	58*	16.81	0.07	93	18.05	0.67
24	17.29	0.61	59	18.67	0.61	94	19.56	0.38
25	17.96	0.65	60	17.03	0.76	95	20.11	0.52
26*	16.73	0.01	61	20.35	0.37	96*	16.73	0.76
27	17.54	0.58	62	18.73	0.58	97	18.46	0.56
28	17.85	0.58	63	20.52	0.41	98*	17.14	0.58
29	18.54	0.53	64	18.79	0.53	99	19.85	0.46
30	16.99	+0.76	65	19.34	0.48	100	19.65	0.52
31	17.19	-0.03	66	18.89	0.67	101	19.89	0.40
32	17.80	+0.74	67	20.43	0.53	102	19.65	0.17
33	17.04	0.65	68	20.37	0.10	103	19.73	0.36
34*	16.68	0.15	69	19.60	0.24	104	20.53	0.24
35*	16.58	0.73	70	19.67	0.43	105	19.45	0.31
36	17.33	0.69	71	19.97	0.41	106	19.64	0.40
37*	16.90	0.04	72	19.59	0.48	107	19.38	0.58
38	18.61	0.58	73*	17.10	0.70	108	19.31	0.66
39	17.84	0.62	74*	16.68	0.38	109	18.32	0.74
40	17.61	0.62	75	19.15	0.55	110	19.10	0.58
41	19.85	0.34	76*	17.01	0.65	111	17.62	0.69
42	20.11	0.07	77	21.10	0.42	112	19.87	0.39
43	20.74	+0.27	78	20.68	0.47	113	19.63	0.57
44*	17.23	-0.32	79	20.73	0.27	114	19.84	0.28
45	19.15	+0.59	80	20.42	0.60	115*	16.41	0.72
						116*	16.73	+0.13

*Stars in common with Sandage (1975), used to transform the electronographic measures to the B, V system.

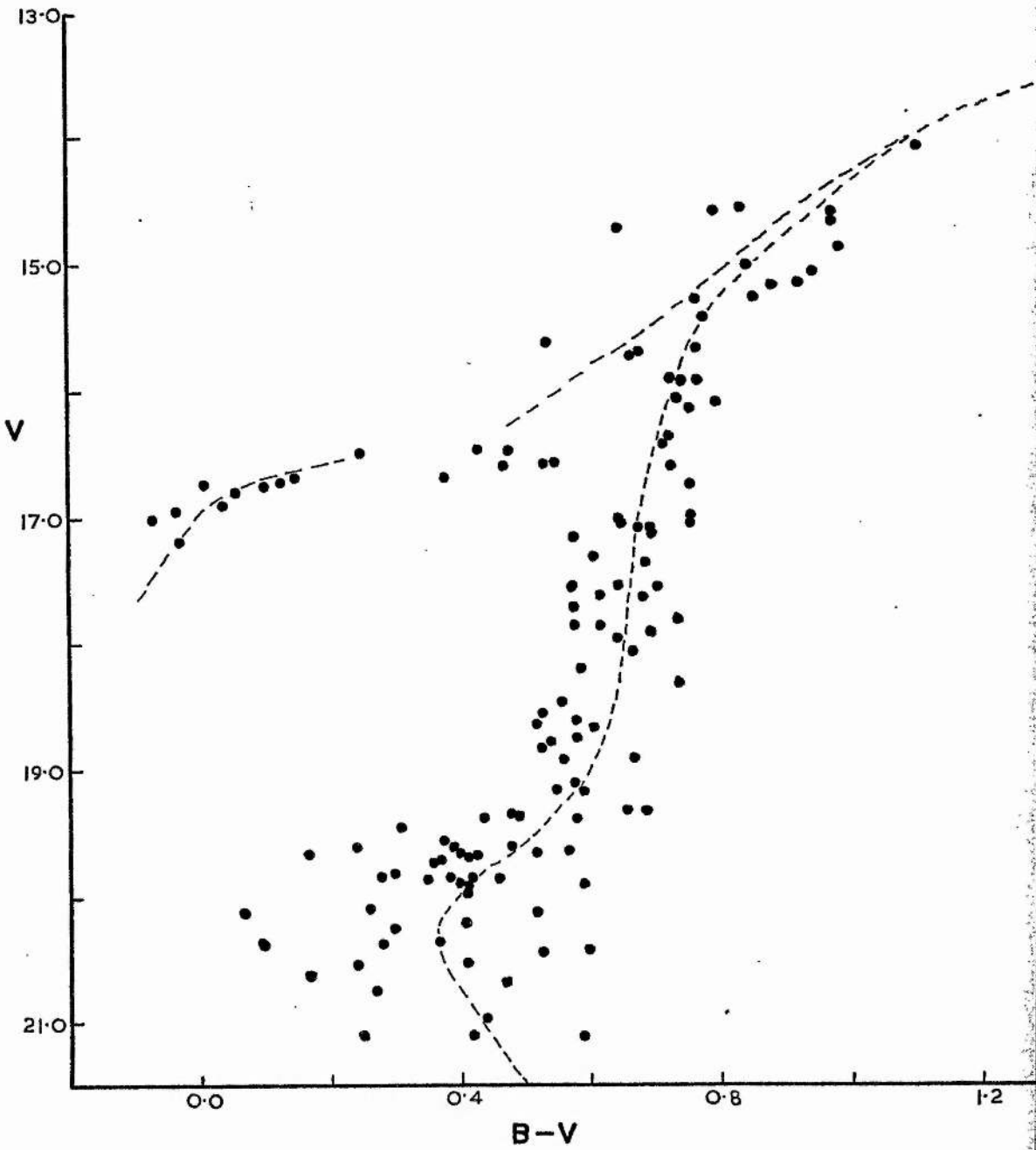

Figure 2

The Colour-Magnitude Diagram of NGC 5053

The dashed lines are the sequences of M 92
given by Sandage and Walker (1966)
and Sandage (1970)

the C-M diagram, and making no allowance for any intrinsic width of the cluster sequence, it would appear that the probable error of a single measurement in (B-V) is ±0.04 mag. in the range $17.00 < V > 19.99$, increasing to ±0.14 mag. for $20.00 < V > 20.99$. Thus, it appears that good photometric accuracy can be obtained even with a tube with a markedly non-uniform photocathode, provided that careful point by point correction for the variations in cathode sensitivity is carried out.

The C-M diagram of NGC 5053, reproduced in Figure 2, most closely resembles that of M 92. In the Figure, the red giant, asymptotic giant, and blue horizontal branches of M 92 (Sandage and Walker 1966, Sandage 1969), adjusted by V = 1.46 mag., are shown as dashed lines. The red giant, subgiant and blue horizontal branches fit the observations of NGC 5053 quite well. In particular, the unreddened colour of the subgiant branch at the level of the horizontal branch has the value $(B-V)_{o,g} = 0.70$, in agreement with the value quoted by Sandage and Smith (1966) for M 92 and the other clusters having the lowest metal content. These characteristics, together with the mean period of the RR Lyrae variables mentioned earlier, would indicate that NGC 5053 has an extremely low metal content like M 92. However, in NGC 5053 a red horizontal branch is more evident than an asymptotic giant branch, and the structure of the horizontal branch is reminiscent of clusters with an intermediate metal content, in conflict with the criteria just discussed. Below V = 19.0 in Figure 2, the dashed line represents the turn-off region of M 92 (Sandage, 1969) and appears to fit the observations of NGC 5053 well, though further measures extending to at least V = 22.0 will be necessary if the main sequence is to be used to calibrate the diagram.

If the comparison between NGC 5053 and M 92 is a valid one, then from the fit of the various parts of the C-M diagram, it appears that the reddening of the stars in NGC 5053 is similar to that in M 92 where

E(B-V) = 0.02 mag. (Sandage, 1969), and is thus essentially unreddened, not surprisingly in view of the high galactic latitude (+79°) of this cluster. Adopting the distance modulus of M 92, (m-M) = 14.62 as derived by Sandage (1969), the apparent distance modulus of NGC 5053 is (m-M) = 16.08 ± 0.08.

The motivation for observing clusters with existing photoelectric sequences was, as we have said, to be able to use the linearity of electronography to extrapolate these sequences with the hope of reaching the main sequence. Figure 2 demonstrates that we were only partly successful in this, since the limiting magnitude reached is at least two magnitudes brighter than we had anticipated. This was a general feature of the results obtained electronographically at Lick Observatory. A further demonstration of this is apparent in the data on NGC 6366 given in the following chapter. There, two-hour electronographs taken with the 24" telescope have limiting magnitudes of V = 17.0. This does not compare favourably with results obtained elsewhere. Penny (1976), for instance, gives a limit of B = 20 for a three minute exposure with the McMullan camera on the Wise Observatory 40" telescope. Only part of this discrepancy can be due to the use of different emulsions (L4 at Lick; G5 at Wise).

We were unable to pinpoint any single cause of these poor results, though there were several possible contributors. The seeing conditions, certainly, were never ideal and this can have significant effects upon limiting magnitudes. The cathode sensitivities of the many tubes used were never exceptional and the bright sky at Mt Hamilton limited exposures on the 120" to a maximum of about ninety minutes.

Our suspicions that a combination of such factors was mainly responsible were reinforced by the results from some exposures taken in July 1973. Two ninety minute electronographs of the faint photoelectric

sequence in M 13 (Baum et al, 1959; Sandage, 1970) were obtained under optimum conditions with a very sensitive S-20 photocathode Spectracon (it 'died' the following week) mounted on the 120". On these exposures the measurable limit was V = 22.0, which was approaching the expected performance.

References

Arp, H., 1965. In Galactic Structure, Stars & Stellar Systems, 5, 401.

Baum, W. A., Hiltner, W. A., Johnson, H. L. & Sandage, A., 1959. Ap. J., 130, 749.

Cuffey, J., 1943. Ap. J., 98, 49.

Johnson, H. L., & Morgan, W. W., 1953. Ap. J., 117, 313.

Kukarkin, B. V., 1973. Proceedings of IAU Symposium No 21. Pg 8.

Mannino, G., 1963. Bologna Publ., 8, No 12.

McGee, J. D., Coleman, C. I. & Philips, E. G., 1973. Nature, 241, 264.

Penny, A. J., 1976. Thesis, University of Sussex.

Purgathofer, A., 1966. Mitt. Univ. Sternwarte Wien, 13, No 3.

Sandage, A., 1969. Ap. J., 157, 515.

Sandage, A., 1970. Ap. J., 162, 841.

Sandage, A., 1975. Private communication.

Sandage, A., & Smith, L. L., 1966. Ap. J., 144, 886.

Sandage, A. & Walker, M. F., 1966. Ap. J., 143, 313.

Walker, M. F., 1970. Ap. J., 161, 835.

Walker, M. F., 1973. Texas Symposium on Electronography and its Astronomical Applications.

CHAPTER 3

THE METAL RICH GLOBULAR CLUSTER NGC 6366

3.1 Introduction

Although generally catalogued as a globular cluster, the true nature of NGC 6366 ($l = 18^{\circ}$, $b = +16^{\circ}$) could not formerly be discerned with any certainty (Baade, 1928). None of the previously observed properties of this little-studied cluster in Ophiuchus enabled a definitive classification to be made. The cluster has an extremely low central concentration, so that no integrated spectrum has been observed. Moreover, it could not be classified on the basis of its variables, since the only two detected (Sawyer, 1973) had not had their periods determined. Nevertheless, recently published integrated UBV photometry by Zaitseva et al (1974) indicated a relatively high metal content consistent with the cluster's low galactic latitude. The cluster could then either have been a misclassified open cluster, or more interestingly, a globular having only moderate metal deficiency of which insufficient have so far been studied. From an early measurement of its colour excess (Stebbins and Whitford, 1936) NGC 6366 was known to be highly reddened and Sawyer (1940) surmised that the general similarity in appearance between NGC 5053 and NGC 6366 is due to a large extent to this obscuration. A photometric investigation of NGC 5053 was presented in the previous chapter. Here we describe the study of NGC 6366 using photoelectric, photographic and electronographic photometry.

3.2 Observations

The initial observations were obtained in co-operation with Dr M. F. Walker, using a Spectracon image-converter at the Cassegrain focus of the Lick Observatory 24" photometric reflector. The Spectracon used was the same 'double-window' tube used in the photometry of NGC 5053. Sensitivity corrections for the non-uniformity of the photocathode were derived and applied as previously. The electronographic images were

scanned on the Joyce-Loebl again as described above. Although Walker (1970) has indicated the procedure for obtaining magnitudes from the density scans, we will briefly describe the mechanics of it here, since the final method adopted differs slightly from Walker's. From the set of profiles from one plate, six or seven are selected to define the standard profile of the exposure. For the exposures discussed here, this essentially involved finding those images on a nearly level background and free of both cathode defects and crowding problems. The procedure can then best be described with reference to Figure 1. The sky background AB is drawn and the midpoint of the profile, C, judged and drawn on AB. Lines DE and FG are then drawn so as best to fit the linear part of the profile sides. The intersections of these lines with the background line AB, say D' and F', are then recorded and their distance from C noted. It is these dimensions that determine the size of the profile to be fitted to the scans. At this juncture, Walker's procedure is to determine the characteristics of the wings of the profiles by first finding the point at which they 'break' from the linear sides of the profile and then measuring the distance from point C at which they have a height of one tenth the maximum density.

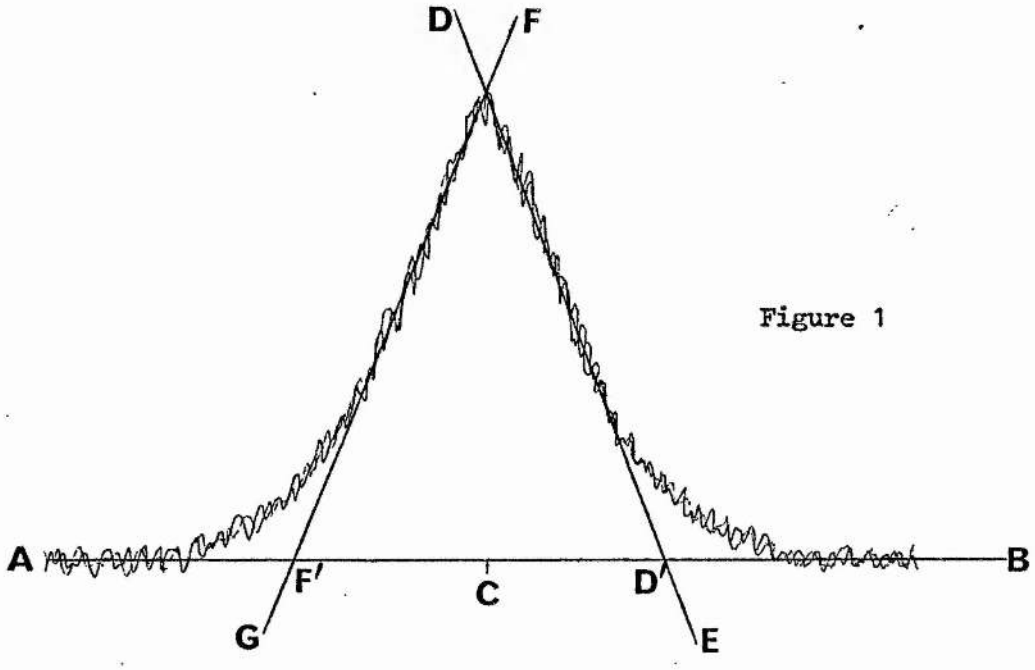

Figure 1

All these relevant properties are subsequently averaged to form the standard profile, which is afterwards fitted to the scans of the programme stars. The area under the profile is then planimetered and -2.5x the logarithm of the area gives the instrumental magnitude. We felt that no information was gained by fitting the wings and then planimetering the area of the profile; indeed, error may be introduced by the difficulty of drawing in the wings consistently. Furthermore, planimetering the profile is a time consuming and tedious task, which is best avoided. We therefore proposed that comparable results could be obtained by terminating the profile construction after lines FG and DE had been drawn and then using the height of the intersection above AB to find the instrumental magnitude. As a test, several profiles with typical parameters, including wings, were constructed with height being the only variable. These were planimetered and the height plotted versus the area. The results are illustrated in Figure 2 and from this we see that there is no advantage in including the profile wings. On numerous occasions when both methods were applied, almost identical results were obtained and it was found in addition that the height method was less susceptible to accidental errors. In view, therefore, of the great saving in time occasioned by measurement of only the height, we feel justified in the application of this method.

Four plates of NGC 6366, two in each of blue and yellow light, were reduced in this manner. The instrumental magnitudes deduced were averaged and these data used to plot the preliminary C-M diagram. Despite the larger dimensions of the cathode used for this investigation, the sparse nature of the cluster meant that still insufficient numbers of stars had been observed to interpret the C-M diagram unambiguously. To remedy this, further photographic observations were obtained. These consisted of three B (103aO + GG13) and two V (103aD + GG14) plates taken at the prime focus of the 36" Crossley reflector of Lick Observatory. In an attempt

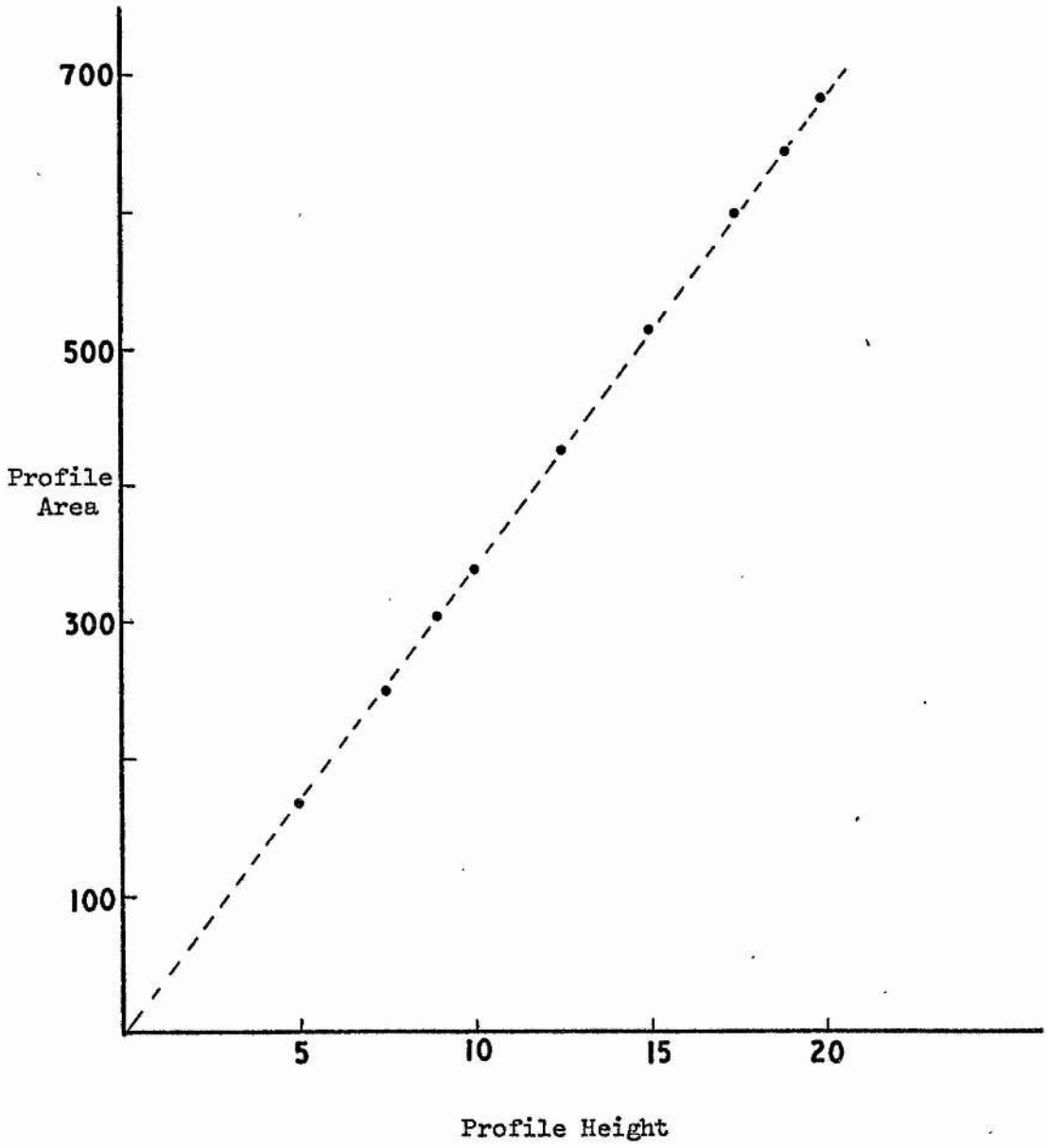

Figure 2

Comparison of height and area for standard profiles

TABLE I

Plates measured for the colour-magnitude diagram

Exposure Number	Date mid-exposure (UT 1974)	Time	Exposure (min)	Telescope	Emulsion	Filter
CD1830	April 30	11.40	10	Crossley	103aO	GG-13
CD1831	April 30	11.55	10	Crossley	103aO	GG-13
CD1835	May 1	10.54	10	Crossley	103aO	GG-13
CD1836	May 1	11.28	10	Crossley	103aD	GG-14
CD1838	May 1	12.02	7	Crossley	103aD	GG-14
AD1593	July 20	8.05	30	12"	103aD	GG-14
AD1599	July 22	4.45	30	12"	103aD	GG-14
AD1601	July 22	6.00	30	12"	103aD	GG-14

to obtain a classification for the variable stars in the cluster, an additional thirteen plates using a 103aD + GG14 plate-filter combination were obtained with the 12" refractor at Lick Observatory. Three of this latter group of plates were selected for measurement to provide additional data for the C-M diagram. Table I contains details of the plates used to derive the magnitudes and colours of the cluster stars. All eight plates were measured on the Sartorius iris diaphragm photometer of the Royal Greenwich Observatory. Since no photoelectric sequence was available, we have employed the mean of the electronographic magnitudes to determine the calibration curve for the iris photometer measures. Typical calibration curves, those plotted for the plates AD 1599 and CD 1831, are shown in Figures 3 and 4 respectively. The fitted lines are the solutions given by the second order polynomial least-squares fitting program, available on magnetic tape for use in conjunction with the Wang 600 desk calculator. For the 12" refractor plates, the faintest stars were not included in the least-squares solution since these are seen to deviate significantly from the smooth trend of the rest, and instead the curve through these points was drawn by hand. In judging these calibration curves, it must be remembered that we are not using highly accurate photoelectric standards for comparison and we must therefore expect increased scatter due to the additional errors in the electronographic magnitudes. However, it can be clearly seen that due mainly to the comparatively large number of 'standards' used, the objective of linearizing the photographic measures has been achieved. In the previous chapter, we detected a colour equation for the filter-photocathode combination used also to obtain the electronographs of NGC 6366. However, all of the stars studied in this investigation are redder than those in NGC 5053 and it is therefore not certain that the same colour equation should be applied. Consequently we have chosen to present the data

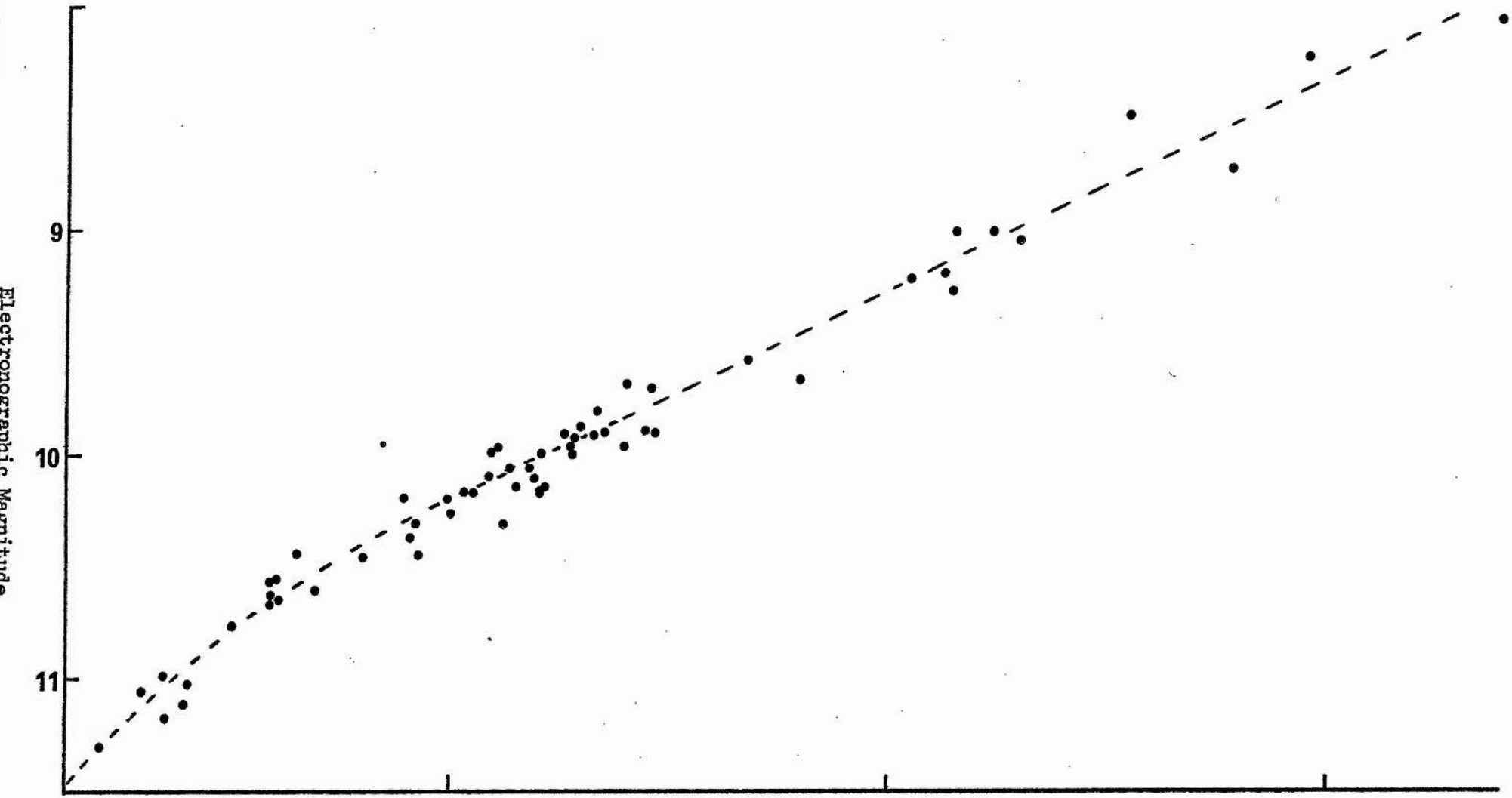

Figure 3
Calibration curve for plate AD 1599

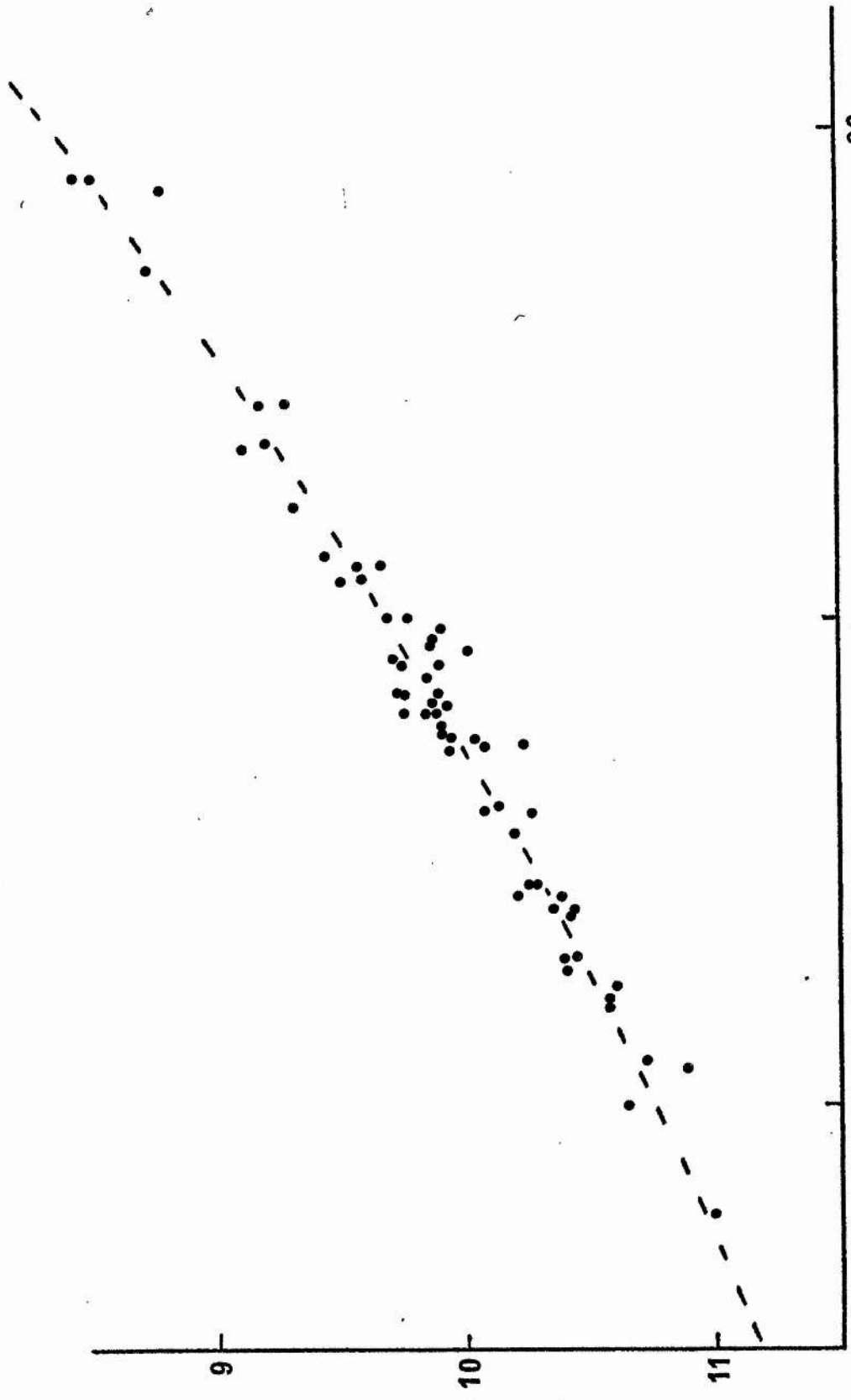

Figure 4

Calibration curve for plate CD 1831

uncorrected for that particular effect. With the photographic measures linearized, all that is required (apart from the determination of any inherent colour equations) are zero points to place the instrumental magnitudes on the standard BV system.

Five nights were generously allocated by the Infra-red Astronomy panel on the 60" Flux Collector at Izana, Tenerife, to enable the zero points to be determined. A modified student photometer from the University of St. Andrews was employed. Originally, it had been hoped to operate this in a pulse counting mode, using the Nova computer in conjunction with CAMAC modules for data acquisition and initial reductions. To this end, a program was written in BASIC for the NOVA which would have controlled the integrations, sky subtractions, averaging of counts and air mass calculations. In the event, however, despite the efforts of Mr D. M. Carr, the photomultiplier housing of the photometer was found to be insufficiently shielded and therefore unsuitable for modification to a pulse counting mode and in any case, the full NOVA-CAMAC facility was not fully commissioned before the observing run. This background is only given by way of explanation for the eventual set-up, where despite the programme stars being rather faint, a conventional photometer with an uncooled 1P21 and d.c. output was employed. The signals from the programme stars were a factor of 2-3 down from those expected from prior calculations of photon statistics, and, coupled with the dark current of the 1P21, this rendered observation in the U band impracticable. We were not aware of any previous optical photometry using the Flux Collector and it was therefore imperative that sufficient numbers of standard stars were observed to determine the extinction coefficients at these wavelengths and also to enable a reliable transformation of the instrumental magnitudes to the standard BV system. This was achieved by observations each night of stars in the network of faint UBV standards given by Landolt (1973). Three

stars in each of the relevant areas given by Landolt were chosen both for their range in colour and ease with which they could be located. Several sets of these stars were then observed through different air masses each night to provide the necessary constants. In addition, the four bright field stars near the cluster (labelled ABC and D in Plate I) had previously been observed photoelectrically on three separate occasions with the Lick Observatory 24" reflector and these were used as secondary standards. The mean magnitudes and colours of these stars as derived from the three observations are listed below:

STAR	V	B-V
A	10.26	0.96
B	10.93	0.95
C	12.47	1.06
D	11.92	0.86

From the internal agreement between the three nights' observations, we estimate the errors in these values to be ±0.01 mag. for stars A and B, increasing to ±.02 mag. for stars C and D. For the two or three weeks preceding our five nights observing at Izana, the site was badly affected by the presence of high-altitude Sahara dust. Fortunately this did clear to some extent as the run progressed. However, when the data were analysed to determine the extinction coefficient for each night, it was found that on two nights the principal extinction coefficient was unacceptably high and probably subject to large variations with azimuth. On the nights of the 3/4 and 5/6 August 1975, the extinction coefficients had mean values of 0.73 and 0.32 mag./air mass respectively. Due to the large uncertainties which this kind of abnormal extinction can cause in the final magnitudes, the data from these two nights were not considered further. For future reference, this is perhaps a rather serious situation, since apart from a moderate haze visible on the horizon during the day, the night looked

excellent for observing and yet the results indicate quite clearly that this kind of photometry was impossible. Due mainly to the mechanics of the telescope which made moving and setting it a time consuming business, and the need to observe a large number of standard stars, the number of programme stars observed each night was lower than had been anticipated. As a consequence, the majority of the stars were observed only once. Nevertheless, these data have proved sufficient to determine the zero points of the photographic data and further to detect a colour equation in the V photographic data of the form

$$Vpe = Vpg + 0.10\ (B-V)\ pg \qquad (1)$$

No similar effect was found in the B measurements and so equation (1) has been applied to all the photographic data.

All stars within a radius of 5'.5 of the nominal centre of the cluster were measured photographically. To try and ensure that as many cluster red giants as possible were detected, some of the brighter stars outside of this radius were also measured. A finding chart for all the stars measured is given in Plate I and the photographic colours and magnitudes derived are given in Table II where the stars observed photoelectrically are denoted by an asterisk. The notation for the star numbers is such that the first figure of the star numbers indicates the quadrant in which it is to be found. The internal standard errors of the final magnitudes are ±.02 in V and ±.03 in B.

3.3 Colour magnitude diagram

The C-M diagram plotted from the data given in Table II is shown in Figure 5. It shows a heavily populated red horizontal branch and a gently sloping red giant branch – both features characteristic of a globular cluster with only a moderate metal deficiency. The continued slope of the subgiant branch to the blue is not real and probably results

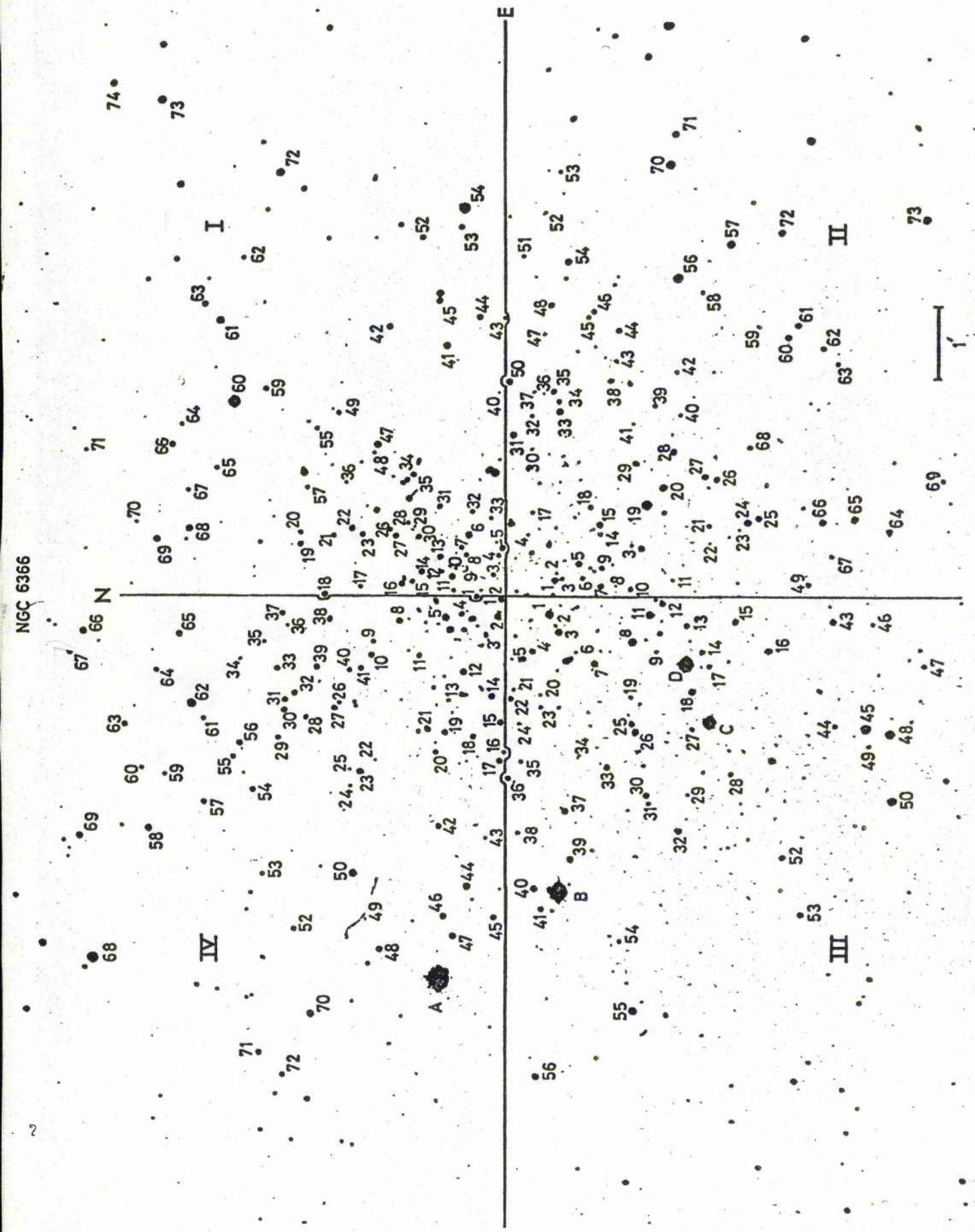

Plate I. The identification of stars in NGC 6366

TABLE II

Magnitudes and colours of stars in NGC 6366

QUADRANT I

STAR	V	B-V	STAR	V	B-V	STAR	V	B-V
101	15.70	1.42	124	15.59	1.67	152	15.63	1.80
102	17.18	1.21	125	17.30	1.17	153	16.14	1.52
103	16.13	1.66	126	16.67	1.01	154	13.37	1.01
104	16.24	1.59	127	15.77	1.58	155	16.63	1.40
105	15.41	1.58	128	16.29	1.58	157	16.35	1.66
106	14.78	1.68	129	17.46	1.09	158	16.54	1.59
107	16.13	1.55	130	15.71	1.54	159	15.86	1.55
108	16.33	1.43	131	15.95	1.63	160*	12.77	1.11
109	17.39	1.18	132	15.92	1.79	161	14.13	1.97
110	17.03	1.20	133	16.98	1.22	162	16.44	1.49
111	14.87	1.90	134	15.70	1.50	163	15.80	1.39
112	16.62	1.42	135	15.49	1.52	164	16.76	1.37
113	15.51	1.63	136	17.10	1.28	165	16.31	1.63
114	15.57	1.53	140	17.37	1.22	166	15.40	1.91
115	16.13	1.66	141	14.68	1.93	167	16.65	1.54
116	15.58	1.50	142	15.76	1.56	168	14.44	2.09
117	16.32	1.56	143	16.56	1.44	169	14.61	2.00
118	14.73	1.85	144	15.76	1.54	170	16.96	1.45
119	16.15	1.19	145	15.62	1.63	171	16.71	1.44
120	16.35	1.56	146	15.41	1.22	172*	13.87	1.92
121	16.19	1.62	147	14.86	1.69	173	13.84	2.12
122	15.77	1.44	148*	16.89	1.45	174	15.01	1.93
123	15.79	1.76	149	16.37	1.56			

QUADRANT II

STAR	V	B-V	STAR	V	B-V	STAR	V	B-V
201	15.24	1.59	220	14.72	1.72	238	16.41	1.37
202	17.10	1.23	221	16.31	1.58	239	16.69	1.23
203	16.65	1.43	222	17.29	1.28	240	17.07	1.21
204	17.00	1.33	223	17.24	1.29	241	17.37	1.16
205	15.62	1.51	224	14.93	1.74	242	17.06	1.17
206	16.45	1.41	225	15.81	1.50	243	16.72	1.51
207	15.61	1.41	226	15.80	1.50	244	16.18	1.52
208	17.14	1.29	227	15.45	1.68	245	16.64	1.40
209	16.20	1.45	228	15.21	1.78	246	16.16	1.62
210	16.42	1.44	229	15.56	1.64	247	17.18	1.25
211	17.06	1.27	230	17.22	1.14	248	15.59	1.56
212	15.60	1.53	231	15.63	1.20	249	16.21	1.55
213	17.08	1.28	232	16.69	1.40	250*	15.15	1.73
214	17.14	1.01	233	15.63	1.44	251	17.03	1.25
215	15.42	1.62	234	16.67	1.38	252	17.40	0.97
217	16.68	1.50	235	15.73	1.64	253	16.70	1.37
218	16.10	1.59	236	17.37	1.18	254	15.66	1.47
219	13.74	1.26	237	17.20	1.22	256*	14.29	1.02
257	14.73	1.65	263	16.72	1.50	268	16.21	1.73
258	16.61	1.61	264	15.86	1.54	269	16.70	1.45
259	17.51	1.08	265	15.55	1.42	270	13.50	2.09
260	15.75	1.51	266	15.41	1.65	271	15.70	1.45

TABLE II - continued

QUADRANT II - continued

STAR	V	B-V	STAR	V	B-V	STAR	V	B-V
261	15.69	1.59	267	17.03	1.06	272	15.78	1.30
262	17.04	0.85						

QUADRANT III

STAR	V	B-V	STAR	V	B-V	STAR	V	B-V
301	14.25	1.75	320	17.28	1.17	338	16.62	1.50
302	17.19	1.16	321	16.91	1.31	339	15.73	1.47
303	15.92	1.09	322	15.97	1.56	340	15.74	1.39
304	15.70	1.48	323	17.12	1.21	341	16.02	1.63
305	15.48	1.75	324	16.99	1.34	342	15.61	1.39
306	17.13	1.19	325	15.55	1.68	343	15.73	1.52
307	14.74	2.39	326	15.43	1.41	344	16.34	1.63
308*	13.94	1.90	327	16.67	1.38	345	14.27	1.06
309	16.96	1.34	328	17.00	0.94	346	17.10	1.17
311*	14.35	1.76	329	17.32	1.18	347	16.99	1.11
312	15.53	1.72	330	15.46	1.63	348*	13.75	1.77
313	16.05	1.59	331	16.56	1.47	349	16.94	1.36
314	16.20	1.53	332	15.58	1.39	350*	13.60	2.20
315	15.74	1.46	333	15.62	1.65	352	16.07	1.33
316	15.44	1.62	334	17.38	1.07	353	16.21	1.30
317	16.62	1.21	335	16.87	1.38	354	16.44	1.63
318	15.38	1.51	336	16.06	1.56	355	13.69	2.16
319	17.00	1.13	337	15.67	1.42	356	14.90	1.71

QUADRANT IV

STAR	V	B-V	STAR	V	B-V	STAR	V	B-V
401	15.47	1.25	414	15.75	1.48	427	15.76	1.55
402	15.58	1.25	415	15.12	1.78	428	16.16	1.61
403	16.38	1.40	416	16.85	1.20	429	16.17	1.56
404	16.00	1.64	417	15.66	1.59	430	15.66	1.69
405	14.79	1.68	418	15.86	1.69	431	15.79	1.67
406	14.65	1.83	419	15.65	1.54	432	15.82	1.50
407	16.06	1.51	420	16.19	1.50	433	15.74	1.56
408	15.55	1.54	421	15.60	1.54	434	16.98	1.38
409	15.69	2.40	422	17.22	1.17	435	16.76	1.37
410	15.57	1.54	423	15.40	1.65	436	17.03	1.36
411	15.99	1.70	424	17.35	0.96	437	15.85	1.63
412	15.03	1.86	425	17.38	1.00	438	15.68	1.67
413	15.58	1.74	426	16.68	1.45	439	15.75	1.57
440	16.25	1.67	451	16.85	1.35	462*	14.51	1.03
441	15.80	1.66	452	15.90	1.69	463	16.12	1.20
442	15.89	1.70	453	16.30	1.54	464	16.23	1.58
443	17.14	1.18	454	15.79	1.60	465	15.34	1.79
444	14.65	1.90	455	15.78	1.75	466	14.93	1.56
445	15.81	1.60	456	15.73	1.63	467	15.54	1.67
446	15.69	1.50	457	15.93	1.56	468*	13.27	1.06
447	15.23	1.79	458	14.89	1.86	469	15.63	1.35

TABLE II - continued

QUADRANT IV - continued

STAR	V	B-V	STAR	V	B-V	STAR	V	B-V
448	15.74	1.57	459	16.89	1.25	470	14.26	2.08
449	17.25	1.14	460	16.72	1.28	471	15.72	1.55
450*	13.60	2.25	461	16.44	1.48	472	16.00	1.58

TABLE III

Observations of the variable star no. 303

Plate AD	Time Mid Exposure (JULY 1974 UT)	Phase	V
1593	20.337	0.957	15.54
1594	21.212	0.679	16.08
1595	21.238	0.730	16.07
1596	21.267	0.788	16.07
1597	21.304	0.860	16.28
1598	21.333	0.917	15.94
1599	22.198	0.620	16.03
1600	22.222	0.667	16.01
1601	22.250	0.722	16.07
1602	22.278	0.777	16.06
1603	22.305	0.831	16.07
1604	22.333	0.866	16.12
1605	22.358	0.935	15.85

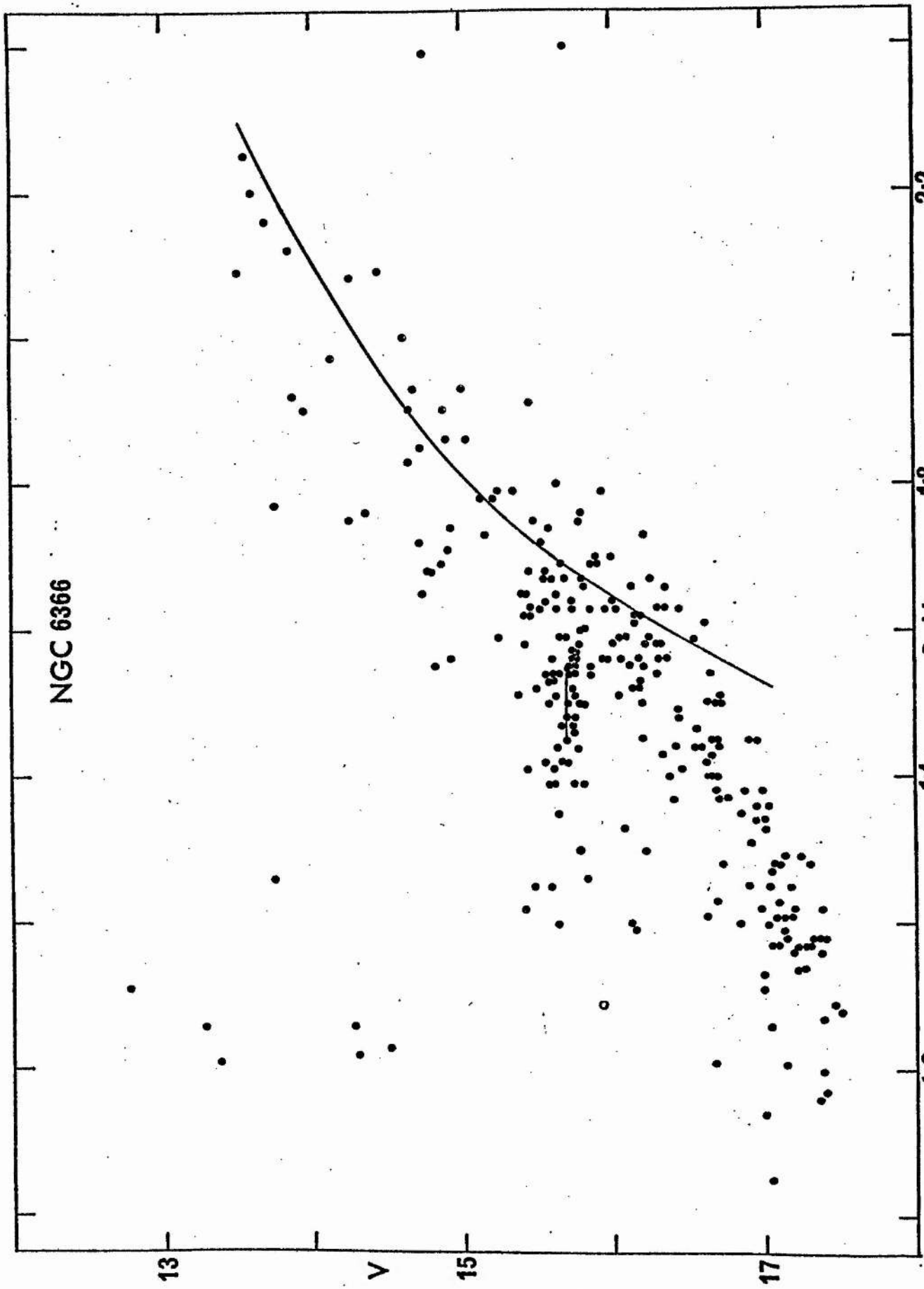

Figure 5. The colour-magnitude diagram of NGC 6366

from a combination of the cut-off of the blue plate and possibly the presence of an undetected colour equation at the fainter magnitudes. It is apparent that there exists a considerable spread in colour on the giant branch. This could be the result of the presence of a substantial number of asymptotic giant branch stars - a situation similar to that in NGC 6171 (Dickens and Rolland, 1972) - although at this galactic latitude, variable reddening across the cluster may well contribute to this effect. For comparison, the standard lines of 47 Tuc (Menzies, 1973) are shown in Figure 5. The overall agreement is good, except that the separation of the red horizontal and subgiant branches clearly seen in 47 Tuc is not so apparent here. Despite the scatter on the giant branch, we can estimate a value of S = 3.7 ±.3 for the Hartwick (1968) parameter, indicative of [m/H] = 0.5 ±.2 (Kraft, 1972). From Figure 5 we adopt an observed mean magnitude for the horizontal branch of $\bar{V}_{HB}$ = 15.7 ±.1, which yields a corrected distance modulus of $(m - M)_o$ = 12.6 ±0.3, using M_v = 0.9 ±0.2 for the mean luminosity of the horizontal branch (Hartwick and Hesser, 1974) and a reddening of E(B-V) = 0.72 derived in the following paragraph. NGC 6366 is thus not as close as had once been conjectured (Sawyer, 1940), but nevertheless the main sequence turn-off will occur at an apparent magnitude of 19<V>20 and should be easily observable on a medium sized telescope if electronography is used.

The C-M diagram shows the presence in the field studied of seven bright blue stars. Similar stars are noted in the C-M diagrams of many other clusters (Zinn et al, 1972) and have been the subject of a thorough observational and theoretical investigation by Strom et al (1970). They distinguish two groups of bright blue stars: 1) the AHB (above horizontal branch) group, which are the proposed progeny of the blue horizontal branch stars and 2) the Von Zeipel (VZ) 1128 group, named after the prototype in M 3, which are considered to be the progeny of the double shell source

stars on the asymptotic giant branch. Of the bright blue stars in NGC 6366, only the four most luminous fall distinctly into the VZ 1128 region, although if the fainter three are true cluster members, they must also be assumed to be of this type, since the lack of any observed blue horizontal branch should preclude the occurence of the AHB group. We note that although these stars are indeed 'bright blue stars' relative to the cluster sequences, due to the heavy reddening of the cluster these stars also have colours compatible with them being foreground field stars, a fair number of which could be expected at this galactic latitude. The presence of stars at the magnitude level of the horizontal branch, but to the blue of the cluster sequence, is also indicative of contamination of the C-M diagram by field stars and it seems, therefore, that in this instance the most feasible interpretation of the bright blue stars is in terms of them being little-reddened, foreground dwarfs.

3.4 Reddening

Since neither ultra-violet measurements of the individual stars, nor an integrated spectrum are available, we have obtained a value of the reddening of NGC 6366 primarily from a differential fit of the C-M diagram sequences relative to those of 47 Tuc. Hartwick and Hesser (1974) give $E(B-V) = 0.04$ for 47 Tuc. A more recent study by Crawford and Snowden (1975), who used a reddening-distance relation for the field stars in the line of sight of the cluster, yielded a slightly smaller reddening of $E(B-V) = 0.03$. Since this latter value is possibly only a lower limit, we have adopted $E(B-V) = 0.04$ for 47 Tuc. The differential fit of the two C-M diagrams then yields $E(B-V) = 0.72$ for NGC 6366. Moreover, if we ignore the difference in topology of the horizontal branches in NGC 6366 and NGC 6171, a differential fit using the red horizontal and giant branches yields $E(B-V) = 0.74$, if the value for the reddening of NGC 6171

given by Dickens (1970) is used. A less certain reddening value can be deduced from the cosecant reddening law (Arp, 1965) whence E(B-V) = 0.22. However, from inspection of the Palomar Sky Survey charts, NGC 6366 is seen to be in a region of highly variable extinction, making this estimate extremely uncertain.

Racine's (1973) investigation of the intrinsic colours of globular clusters enables one further estimate of the reddening. Values of the observed integrated colours of NGC 6366 are available from Zaitseva et al (1974), who find (B-V) = 1.47 and (U-B) = 1.01. Harris and van den Bergh (1974) give (B-V) = 1.6, but ascribe a low weight to the observation. A comparison of the results for the clusters observed in common between the above reveals no systematic differences, but there are observational errors producing differences commonly of the order of 0.05 magnitudes. We will use a weighted mean of (B-V) = 1.50 which gives E(B-V) = 0.70. In view of these results, we adopt a reddening of E(B-V) = 0.72 ±0.02.

3.5 Variable Stars

Sawyer Hogg (1973) lists two variables in the vicinity of NGC 6366 and describes each as having a large amplitude but an undetermined period. Only the one nearer the cluster centre (Table II: No. 303) was within the field studied here. As described above, thirteen plates of the cluster were obtained (twelve of them on two nights) in an attempt to follow any short period variations of this star. These plates have been measured on an iris photometer. Apart from the known variable stars, the group of stars lying to the blue of the red horizontal branch were also monitored to test for any variability. No variation on the time scale covered by these observations was found for any of the stars in this group.

The light curves for star 303 were plotted for the two main nights of observation. These essentially showed little or no variation except

that for both nights the last data point indicated that the star had brightened quite rapidly. By adjusting these plots relative to one another and including the single observation of the previous night, it was apparent that all of the observations could be reconciled with a period of 0.508 days. The data for the variable are given in Table III where the phase of an observation has been calculated from the tentative ephemeris:

$$\text{zero phase} = \text{JD } 2442249^{d}.875 + 0.508E$$

As can be seen in Figure 6, where the final light curve of the variable is shown, the observations cover less than half of the suggested period. However, they do fortuitously indicate the beginning of a very sharp rise to maximum and on this basis it was suggested that the variable should be classified as an a-type RR Lyrae. From the C-M diagram where it is represented by an open circle, the instantaneous V magnitude and B-V colour place the star near the variable star region on the horizontal branch. After this independent study of the variable was concluded, a private communication from Dr H. B. Sawyer Hogg intimated that she had much earlier completed an investigation of this variable and she kindly informed me that she had obtained the following ephemeris:

$$\text{zero phase} = \text{JD } 2428696^{d}.745 + 0.513162E$$

whilst at the same time confirming the above classification. It is gratifying that the meagre data given in Table III give the correct classification and period for the star, but they are unfortunately insufficient to enable us to say more than that they are consistent with Sawyer Hogg's initial ephemeris. The detection of this kind of variable in a metal rich globular cluster (we are here assuming membership of NGC 6366 purely on its location near the centre of the cluster and its position in the C-M diagram) is always of interest since it is a relatively uncommon occurence. Moreover, since as noted above, the main

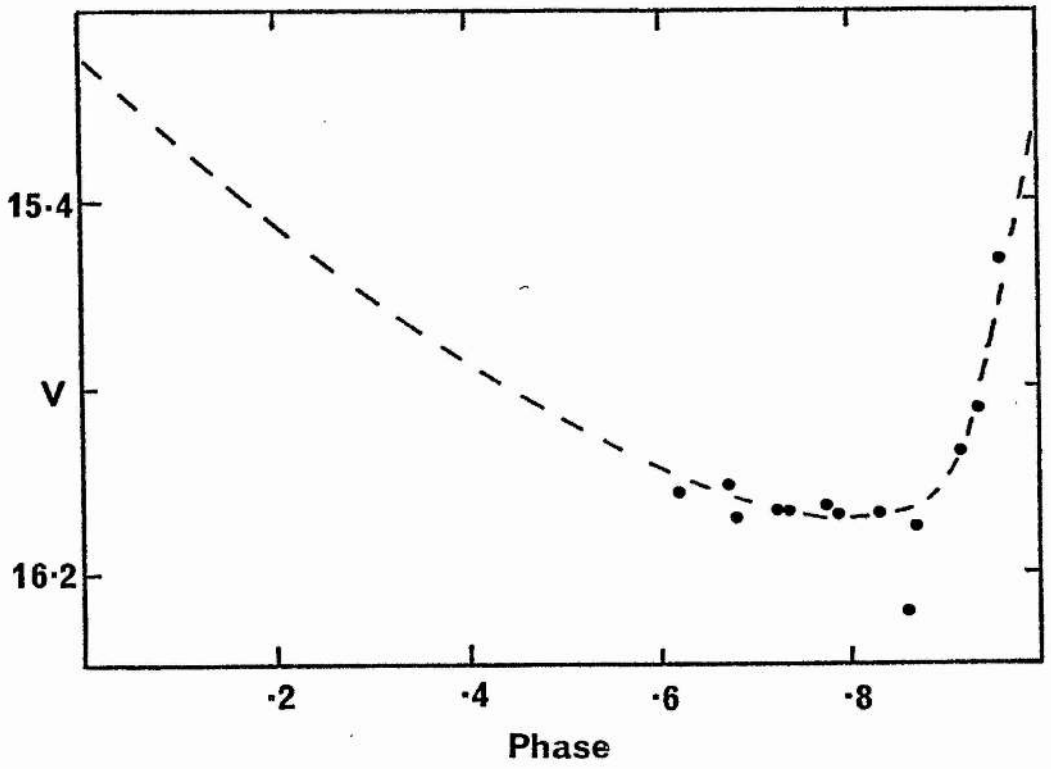

Figure 6

The light curve for variable 1 (No. 303)

sequence of NGC 6366 should be observable, the cluster provides another rare opportunity for the calibration of the absolute magnitude of a metal rich RR Lyrae star.

Dr Sawyer Hogg also intimated that she had had difficulty finding a consistent period for variable 2, on the assumption that it too had a short period. At her request, therefore, we measured variable 2 on some of our plates and found it to be very red - (B-V) = 2.3. The instantaneous magnitude placed it somewhat below the giant branch, but the photometry we obtained suggests strongly that this star lies at the tip of the giant branch and is likely therefore to have a long or an irregular period.

References

Arp, H., 1965. Galactic Structure. Stars & Stellar Systems, 5, 401.

Baade, W., 1928. A.N., 232, 200.

Dickens, R. J., 1970. Ap. J. Suppl., 22, 249.

Dickens, R. J. & Rolland, A., 1972. Mon. Not. R. ast. Soc., 160, 37.

Harris, W. E., & Bergh, S. van den, 1974. A.J., 79, 31.

Hartwick, F. D. A., 1968. Ap. J., 154, 475.

Hartwick, F. D. A. & Hesser, J. E., 1974. Ap. J. (Letters), 194, L129.

Kraft, R. P., 1972. Dudley Obs. Reports, 4, 69.

Landolt, A., 1973. A.J., 78, 959.

Menzies, J., 1973. Mon. Not. R. ast. Soc., 163, 323.

Racine, R., 1973. A.J., 78, 180.

Sawyer, H. B., 1940. Pub. D. D. Obs., 1, 5.

Sawyer Hogg, H. B., 1973. Pub. D. D. Obs., 3, 6.

Strom, S. E., Strom, K. M., Rood, R. T. & Iben, I., 1970. Astr. & Astroph., 8, 243.

Stebbins, J. & Whitford, A. E., 1936. Mt. Wilson Contrib. 547.

Walker, M. F., 1970. Ap. J., 161, 835.

Zaitseva, G. V., Lyutyi, V. M. & Kukarkin, B. V., 1974. Soviet Astr., 18, 257.

Zinn, R. J., Newell, E. B. & Gibson, J. B., 1973. Astr. & Astroph., 18, 390.

CHAPTER 4

REDUCTION TECHNIQUES

4.1 Introduction

We have described in previous chapters dealing with the photometry of NGC 5053 and NGC 6366 how the electronographs were reduced using one dimensional density scans followed by a procedure of manual profile fitting. The main disadvantages of this method are its slowness and its inability to use much of the information available on the electronograph. Experience by the author has shown that, even in crowded globular cluster fields where identification is an easy matter, the density scans can only be produced at a maximum rate of about ten per hour. This rate is further reduced for the fainter stars near the plate limit where firstly finding and identifying the star are problems and the subsequent centring of the image troublesome and uncertain. Nevertheless, a large amount of useful electronographic photometry resulting from the use of this technique has been published by Walker (1970, 1971, 1972, 1974).

It is apparent though that this kind of reduction method will be unable to keep pace with the ever-increasing amounts of data that will become available, particularly with the use of the new large window McMullan electronographic cameras. At the onset of this work (1974), we were not aware of any efficient system for reducing electronographs that was actually in operation. We were in fact unaware of the paper by Cullum and Stephens (1972), in which they describe a reduction system much the same as those in use today. In defence of this omission, we can only point out that such work only usually becomes well known by the results it produces. We therefore set about devising and putting into operation a suitable reduction process.

The scheme we envisaged was to digitize the stellar images and process this data by means of a least-squares fit to a standard profile. Lick Observatory at that time did not have any suitable means of digitizing the data and progress in this direction therefore had to await our return to

St. Andrews. Available there was a Joyce-Loebl microphotometer with auto-densidater attachment which was interfaced to a Honeywell H316 computer and a magnetic tape unit. Fortunately, the control programs for the Joyce-Loebl had already been developed by Mr R. J. Campbell and it seemed advisable to build our scheme around these. The capabilities of these existing programs, as relevant to our application, were as follows. The plate could be scanned on the Joyce-Loebl and the data, in the form of an array of up to 512 x 512 points, stored on magnetic tape. Using a separate program, the data could then be displayed on a Tektronix screen in the form of a contour map, essentially the same as the maps produced by the Joyce-Loebl in its isodensitracer mode. With the data displayed in this form, local areas within the display could be isolated using the cross-wires and the data within this 'window' redisplayed if necessary. The scanning program had been designed specifically for the reduction of galaxy images and in that form would have been very inefficient for performing separate scans over each individual star image. In the first instance it was therefore necessary to scan the electronograph in sections. Particularly for globular cluster fields, this was acceptable as the proportion of time spent scanning areas of sky was reasonably small. Since, as mentioned, all of the programs described so far were available for general use, our contribution has been the appending to these of the programs needed to reduce the data. The main steps in the finally adopted reduction scheme are enumerated below.

1) Areas of plate containing as many stellar images as possible are scanned with a sampling rate sufficient to give approximately twenty sample points across an image and the data stored on magnetic tape.
2) The data is displayed as a contour map on the Tektronix screen. Data to be analysed can then be isolated using the cross-wires and the 'window' facility.

3) Control is handed to the analysis subroutines to fit a profile to the data.

4) When a suitable fit has been achieved, control is given back to the operator who defines the next area for analysis.

4.2 Profile Fitting

If we make the simplifying assumption that the light distribution produced by the optics and seeing at the focal plane has a two-dimensional Gaussian distribution of intensity, then this will not be precisely the distribution of density within a stellar image on a photograph, since the distribution of intensity will be modified by the non-linearity and scattering within the emulsion. It has been shown that the intensity produced by the scattering decreases exponentially from the position of incidence of the light. Thus, following Gyldenkerne (1950) we may write

$$I(r) = C\int_{-\infty}^{+\infty}\int \exp\left\{-(x^2+y^2)/z^2 - K\left[(x-r)^2+y^2\right]^{\frac{1}{2}}\right\} dx\, dy$$

where the intensity I is now determined by the combination of the original Gaussian light distribution and the exponential decay occasioned by the scattering. The decay constant K is termed the constant of scattering and has values dependent upon the grain size in the emulsion. Typical values quoted by Gyldenkerne are K = 100/mm for fine grain emulsion and K = 50/mm for coarse grain emulsion. Clearly, measured in these terms, the action of the electrons in the fine grain emulsion used for electronography will be equivalent to a high value of the scattering constant, indicating that the initial light distribution will be only slightly distorted. It appears then that the density within a stellar image is likely to be adequately approximated by a simple Gaussian.

We find that, particularly with electronographic exposures obtained

with Spectracons, the images are occasionally elongated due to image drift within the camera, rather than to human errors. However, in order to avoid the necessity of introducing cross product terms into the Gaussian representation of the image, we note that the images can always be aligned so that the major axis of the electronographic image corresponds to the scanning direction. The reductions will then simply involve having different values for the x and y dispersions.

For any Gaussian distribution, the parameters which we need to determine are:

1) H; the central height of the profile above the sky background. This will be measured in density steps as designated by the encoder attached to the Joyce-Loebl density wedge carriage.
2) σ_x and σ_y; the dispersions in the scanning direction and at right angles to this. These will be treated separately in order, as noted above, to be able to take account of elongated images. They will be measured in units of the sampling interval used in the scans.
3) $\bar{x}$ and $\bar{y}$; the position of the centre, measured in a coordinate system where the first sample data point is (1,1).

We thus represent the profile as:

$$I(x,y) = H \exp\left\{-a_1^2(x-\bar{x})^2 - a_2^2(y-\bar{y})^2\right\}$$

where we have written

$$a_1 = 1/(\sqrt{2}\sigma_x) \qquad \text{and} \qquad a_2 = 1/(\sqrt{2}\sigma_y)$$

I(x,y) represents the measured density at the point (x,y).

The above five parameters are treated as variables and their determination will be via an iterative linearized least-squares procedure. Before this can be effective however, we need reasonably accurate initial approximations to the parameters. These we obtain using the method of moments. This method obtains values of the distribution parameters by equating the moments of the theoretical distribution to the corresponding

moments of the observed distribution.

The centre of the profile is easily found from the expressions

$$\bar{x} = \sum_{ij} D_{ij}\, x_i \;/ \sum_{ij} D_{ij} \qquad \bar{y} = \sum_{ij} D_{ij}\, y_j / \sum_{ij} D_{ij}$$

where D_{ij} i=1,N j=1,N are the observed data points.

The relevant moments of the observed distribution are then

$$m_0 = \sum_{ij} D_{ij}$$
$$m_{20} = \sum_{ij} D_{ij}\,(x_i - \bar{x})^2$$
$$m_{02} = \sum_{ij} D_{ij}\,(y_j - \bar{y})^2$$

The moments of the theoretical Gaussian distribution with parameters H, a_1, a_2, $\bar{x}$, $\bar{y}$ are

$$m'_0 = \int_{-\infty}^{\infty}\!\!\int I(x,y)\, dx\, dy \qquad m'_{20} = \int_{-\infty}^{\infty}\!\!\int (x-x)^2\, I(x,y)\, dx\, dy$$

$$m'_{02} = \int_{-\infty}^{\infty}\!\!\int (y-y)^2\, I(x,y)\, dx\, dy$$

these can be integrated analytically to give

$$m'_0 = H\pi/a_1 a_2 \qquad m'_{20} = H\pi/2a_1^3 a_2 \qquad m'_{02} = H\pi/2a_1 a_2^3$$

Thence equating the observed and theoretical moments we obtain

$$a_1 = (m_0/2m_{20}) \qquad a_2 = (m_0/2m_{02}) \qquad H = m\, a_1 a_2/\pi$$

These results were tested by generating 'data' points from a distribution of the form

$$I(x,y) = 10 \exp\left\{-(0.3536)^2 (x-9)^2 - (0.283)^2 (y-9)^2\right\}$$

for a 20 x 20 data array.

Generating the moments of the data points and applying the above equations returned values of

$$\bar{x} = 9.00 \quad \bar{y} = 9.00 \quad H = 10.034 \quad a_1 = 0.35361 \quad a_2 = 0.28396$$

part of the discrepancy arising from the use of only single precision on the NOVA computer. In practice the values returned from actual, noisy data were never as good as the above example. The position given for $\bar{x}$ and $\bar{y}$ for instance can be affected if only a slight contribution from a nearby image to the density readings is detected. Particularly troublesome for the denser electronographic images is the case where the centre of the image has exceeded the maximum measurable density on the density wedge used. In the event that this was detected by the program, it was dealt with by multiplying the returned height by a scaling factor which had been found empirically to correct approximately for the effect. Before the moments of the observed distribution can be calculated, the sky background has to be subtracted from the raw data; indeed, the answers returned by the moments solution depend critically upon this. Throughout the measurement of the electronographs the '1.5D' Joyce-Loebl wedge was used. Assuming the nominal range to be 1.5D, each of the 1024 density steps as measured by the encoder corresponds to approximately 0.0015D. Various tests were made to investigate the effects of changes in the background subtraction upon the moment solutions and it was found empirically that the initial approximations were closer to the final least-squares values if, in the moment calculation of the centre (x,y), all data points (after sky subtraction) with values of less than 25 were ignored. Similarly for the calculation of the dispersions a_1 and a_2 the estimates were improved if points with values of less than 50 were omitted. Despite these limitations

imposed by the real data, the solutions provided by the method of moments have been consistently within the limits of convergence for the linearized least-squares routines.

As mentioned, we proceed to find the parameters which give the best fit to the observed data by an iterative method. We assume that the Gaussian profile can be represented by a Taylor series expansion about the function containing the initial approximations to the parameters. Thus if we denote the initial estimates by superscript zero, then we require

$$I(x,y;H,a_1,a_2,\bar{x},\bar{y}) = I(x,y;H^\circ,a_1^\circ,a_2^\circ,\bar{x}^\circ,\bar{y}^\circ) + \partial I(x,y)/\partial\beta_\kappa \cdot \beta_\kappa'$$

where β_κ, $k = 1,5$ are the unknown parameters of the profile and β_κ' are the corrections to β_κ° which we require.

Then if we have a total number of NxN data points each with a weight w_s, $s = 1, N$ we require by the principle of least-squares that

$$\frac{\partial}{\partial\beta_\kappa}\left\{\sum^{N}\omega_s\left(I^\circ - H\frac{\partial I^\circ}{\partial H} - a_1\frac{\partial I^\circ}{\partial a_1} - a_2\frac{\partial I^\circ}{\partial a_2} - \bar{x}\frac{\partial I^\circ}{\partial \bar{x}} - \bar{y}\frac{\partial I^\circ}{\partial \bar{y}}\right)^2\right\} = 0$$

We can then obtain the normal equations which upon rearranging yield

$$H\sum w_s A^2 + a_1\sum w_s AB + a_2\sum w\ AC + \bar{x}\sum w_s AD + \bar{y}\sum w_s AE = \sum w_s \phi\ A$$

$$\vdots$$

$$H\sum w_s EA + a_1\sum w_s EB \quad . \quad . \quad . \quad . \quad . \quad . \quad . \quad . \quad . \quad . \quad . \quad . \quad . \quad .$$

here we have substituted $A = \dfrac{\partial I}{\partial H}$, $B = \dfrac{\partial I}{\partial a_1}$ etc. and ϕ is the value of (data point) − (value of the profile calculated with β_κ°).

More concisely in matrix form

$$\beta R = T \quad \text{where } R(1,1) = w_s A^2 \quad \text{etc.}$$

and hence

$$\beta = TR^{-1}$$

which gives the corrections to the parameters. These are added to and the analysis repeated until the corrections are found smaller than a prescribed value when convergence is assumed.

This analysis can be readily changed if it is desired to include more parameters. For instance if the background level, F, is to be treated as a variable such that

$$I(x,y) = H \exp\left\{-a_1^2(x-\bar{x})^2 - a_2^2(y-\bar{y})^2\right\} + F$$

then $\partial I/\partial F = 1$ and appropriate changes can be made to the dimensions of the matrices R and T. In particular for electronography, it is useful if the analysis can handle the reduction of overlapping profiles from a group of stars. We will return to this subject later.

4.3 Reduction of single images

In practice, electronographs are reduced by fitting to all the stars profiles of a fixed dispersion but with variable height. Fits for which all five of the parameters described are allowed to vary are therefore only performed on a few standard stars. The dispersions found for these stars are then averaged and this fixed-dispersion profile subsequently applied to the programme stars.

The program, in the form described earlier, was employed to reduce the electronographic plates SLT-7 and 8 which were V and B exposures of NGC 6366. These plates had previously been reduced by hand and a direct comparison between the two methods was therefore possible. The same stars were taken as profile standards as when previously measured and the averaged profile parameters applied to the programme stars. The results are compared graphically in Figures 1 and 2. The most encouraging result is that the linearity is accurately maintained. The increase in scatter on the blue plate is attributable

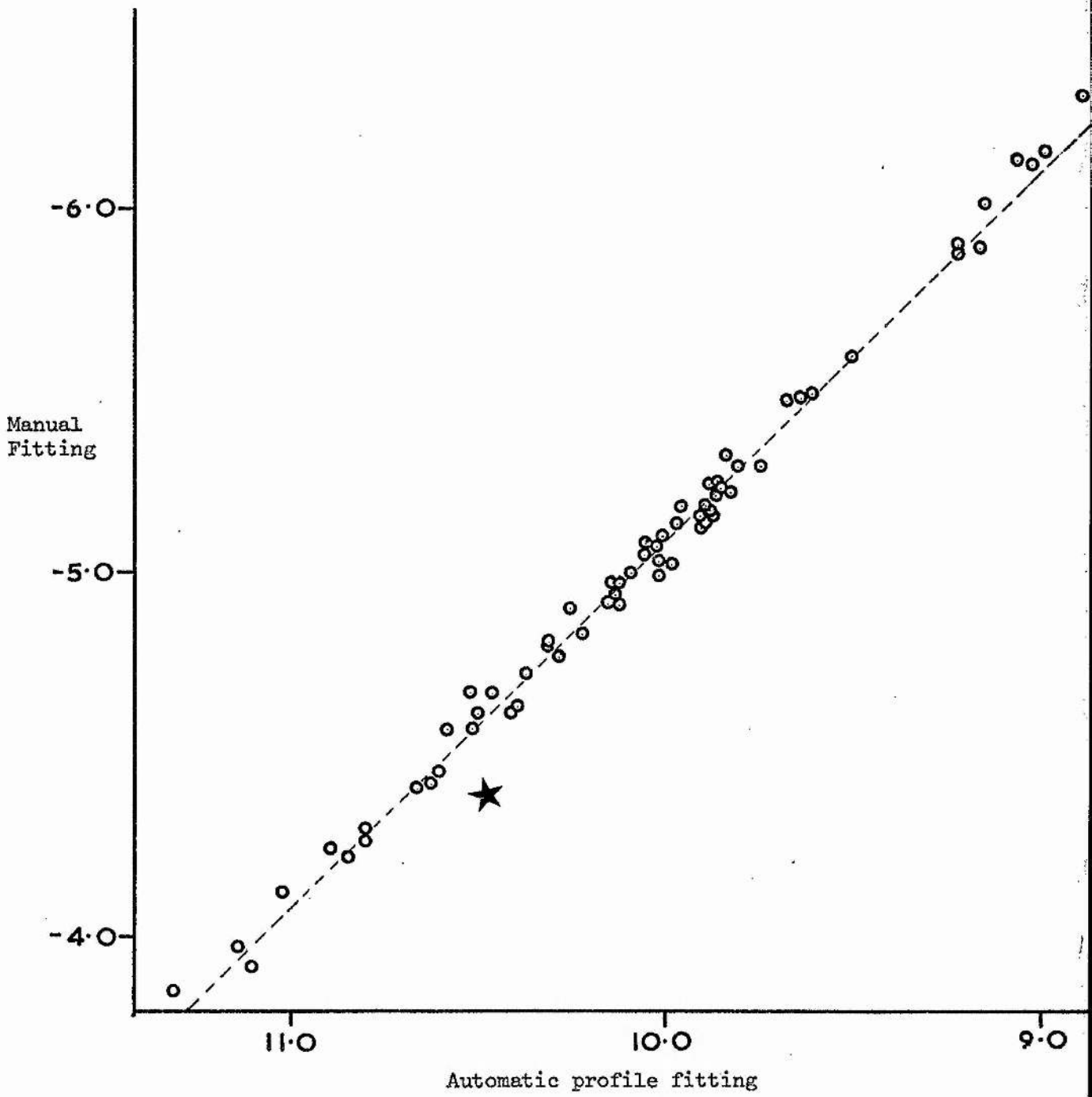

Figure 1

Comparison of manual and automatic magnitudes
from SLT-7, a V exposure of NGC 6366

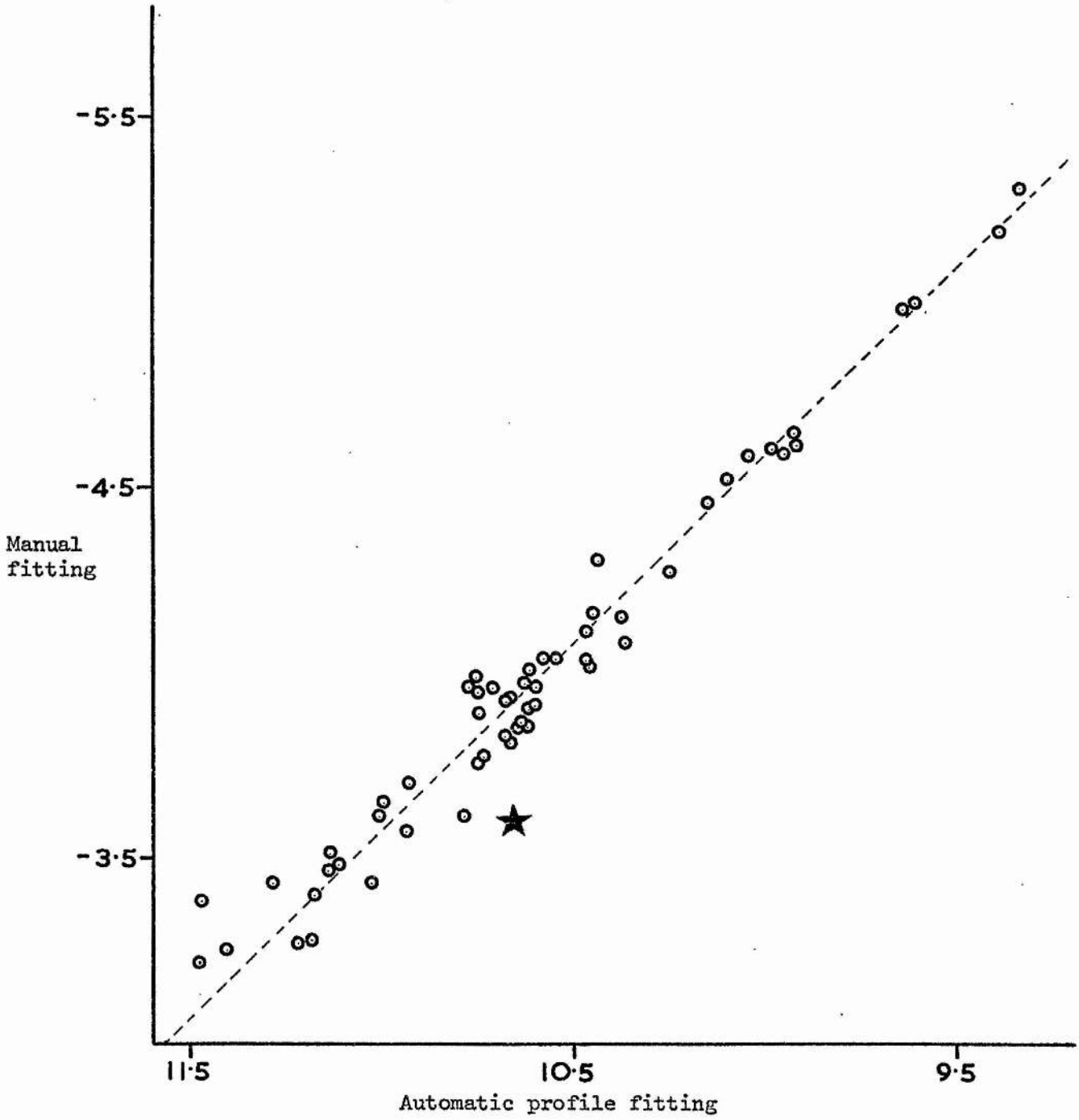

Figure 2

Comparison of manual and automatic magnitudes from SLT-8, a B exposure of NGC 6366

to the decreased image density on this plate.

For the reduction of these plates by this technique, the same Joyce-Loebl wedge is used for one complete set of measurements. For the brighter stars on SLT-7 (V), the central densities as measured were off the scale of the wedge. These points were subsequently ignored in the analysis by giving them zero weight. When the results were plotted a deviation from the straight line was apparent in the results for the brighter stars. These were the same stars that had been measured on a different wedge during the manual reductions. To place measures from different wedges on to the same scale, a zero point correction had been applied to the manual results. This was determined from measures of several stars on both wedges. The difference noted above thus could indicate the presence of an error in this correction factor. Penny (1976) however has illustrated that since the Gaussian is not a perfect fit to a stellar image - particularly in the centre and wings - if different weights are given to data points this will disturb the balance of the overall fit and the linearity of the final results cannot be assumed. The deviations in Figure 1 are likely to be a further demonstration of this effect. In Figure 3 we show the data and fitted profile in the x and y directions for star 416 on SLT-7. We see that on this scale, however, the Gaussian representation seems adequate in view of the noise in the data.

One problem encountered during the automatic reductions which was highlighted in the comparison between the two methods was the one of cathode defects. Defects, areas of zero cathode sensitivity which form pinholes and scratches on cathodes, are introduced during the production of the cathode and it is hoped that further refinements in production techniques (as has recently occurred for the McMullan cameras) will eventually eliminate these. However, the cathode used in this study

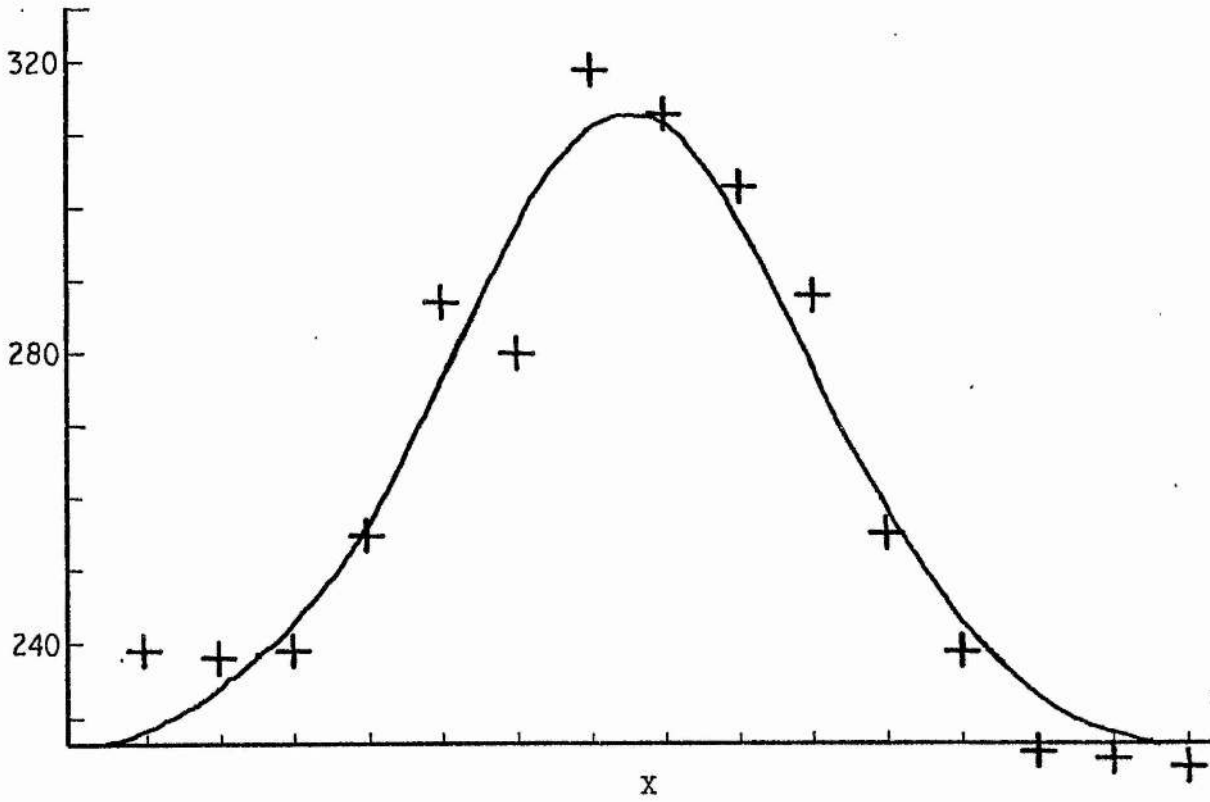

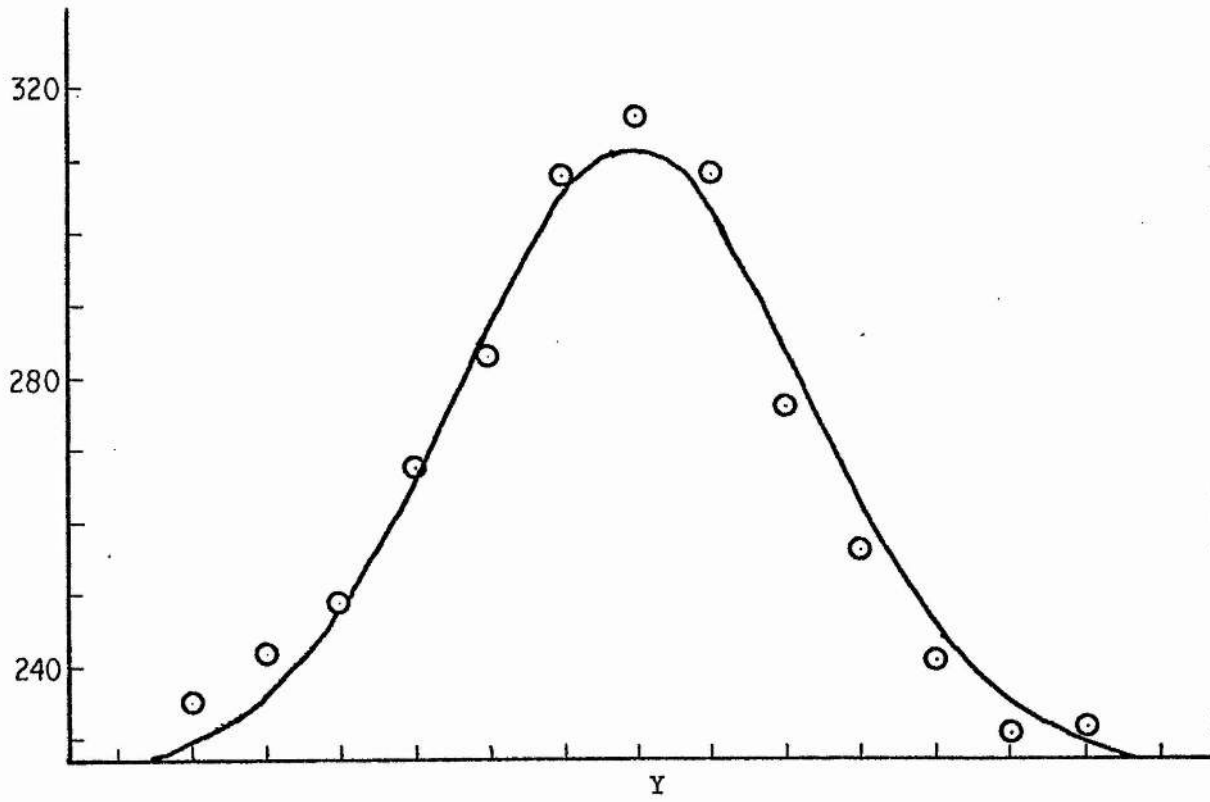

Figure 3

Observed and calculated profiles of star 416 on SLT-7

had liberal quantities of these defects. We note in passing that such defects do have their uses, primarily as fiducial points. They are thus extremely useful in searching for faint images and also in comparing the positions of images from exposure to exposure. The problems that arise in the reductions are exemplified in Figure 4 where a Joyce-Loebl scan of star 437 is shown. From this we can see that the image falls on the edge of a defect, such that the sky background to the right is lower and variable, compared to the 'true' level on the left. It is also clear from the tracing that the right hand side of the profile itself is adversely affected. Due to the linearity of the electronographic process, a reasonably accurate magnitude can be obtained by hand from such a profile. This is because the observer will recognise the presence of the defect, judge its extent and effect and compensate accordingly. It is virtually impossible however to program a computer to have the same recognition abilities since each defect will almost certainly manifest itself in a different way upon the data. For the particular example given in Figure 4, we see that this is the image denoted by a star in Figures 1 and 2. Clearly the automatic reduction is measuring the profile too bright. We can understand this as the result of it trying to reconcile the background values it finds on either side of the stellar image. The best it can do is to adopt a value somewhere between the two extremes. The densities within the stellar image are therefore artificially high and this had consequences for the final magnitude as we have seen. Returning to Figures 1 and 2, we have drawn the 45° line to indicate the linearity of the reduction process. The standard deviation of the points about these lines is 0.04 magnitudes for the yellow plate, increasing to 0.08 magnitudes for the weaker images on the blue plate. Since we have no photoelectric standard sequence available, there is no direct way to investigate the proportion of this

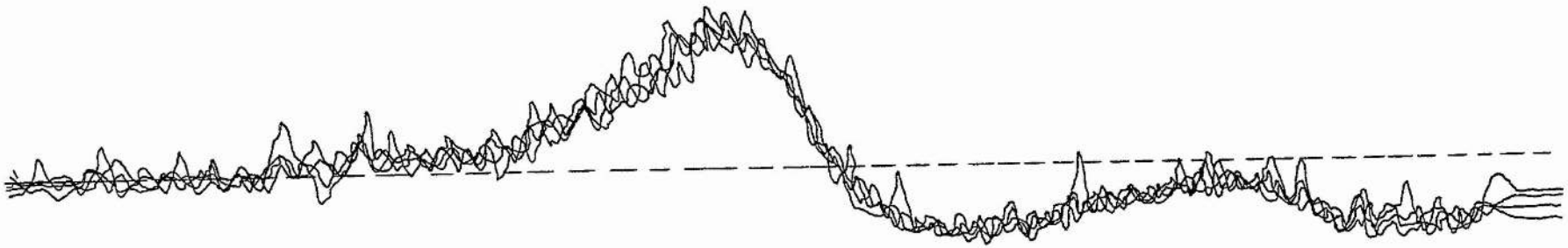

Figure 4

Joyce-Loebl scans of star 437 from SLT-7. The right-hand side of the tracing is affected by a cathode defect.

error which originates in each reduction method. However, from a comparison of the manual measures obtained from the two blue light electronographs, the standard deviation of the measures is estimated at about 0.05 - 0.06 magnitudes. This implies from Figure 2 a comparable error for the automatic procedure, when measuring images of this type whose central density was on the whole less than 0.15D. There will be in Figure 2 also an unknown contribution from the effects of cathode defects as described.

Wlerick et al (1974) have proposed using the sky background density on an exposure to provide a measure of the cathode sensitivity at any point. In addition, this method would not only take direct account of any emulsion variations, but would also by-pass any problems normally encountered in the matching up of exposures. Since in our analysis of the electronographs of NGC 6366, the background level was left as a variable in the fit, we may investigate the method of Wlerick et al by comparing the fitted background level with the independently determined sensitivity corrections. This is shown in Figure 5. Although there is general agreement, the scatter is disappointingly large. The errors associated with the sensitivity corrections are ±0.02 magnitudes at most and it seems therefore that much of the scatter in Figure 5 occurs in the fitted sky level. An estimate of the expected errors in this case can be obtained from a comparison of the sky levels fitted for the two exposures measured. Such a plot shows that the errors are a function of the density of the background level. In this particular example, we estimate the agreement to be ±3 Joyce-Loebl units in the denser regions, increasing to ±5 in the faint regions. For the density wedge used here, the latter figure corresponds, in density terms, to ±0.007D which again for manual density scans is equivalent to setting the background in Figure 4 to within one millimetre. Viewed in these terms, the scatter present in Figure 5 is understandable, but combined with the small slope

Figure 5

Fitted sky level compared to the independently determined sensitivity correction

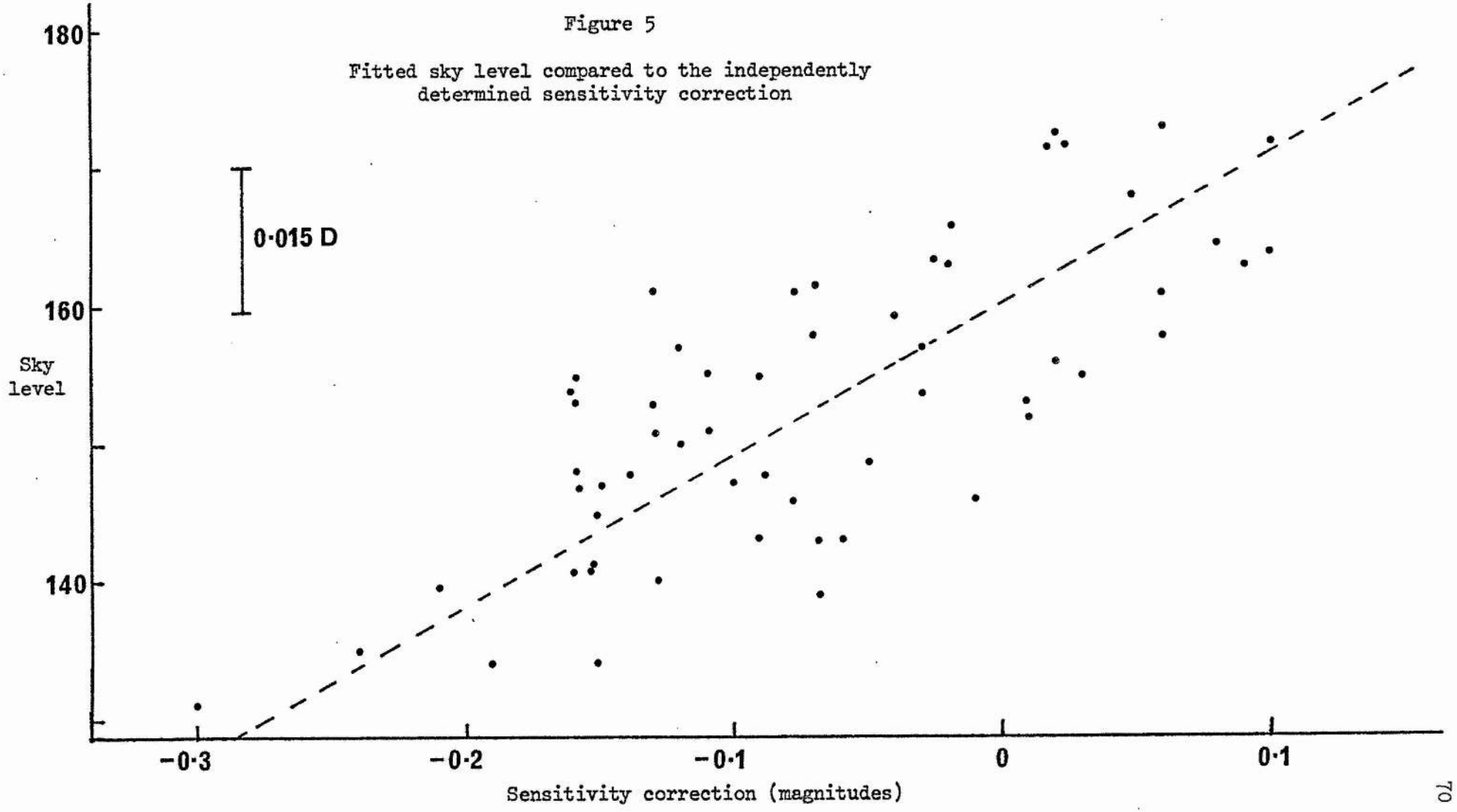

of the relation between sky level and sensitivity correction shows that this method could not be used here. Indeed, it appears that it could only be used where the background density is much higher, probably of the order of 1.0D, something which it is not always possible to achieve.

4.4 Application to groups of images

So far, we have only considered profile fitting in the context of analysing single, uncrowded images and in this sense have not utilised to the full the advantage that linearity offers over the normal photographic process. Because of linearity, we should in theory be able to disentangle multiple images to yield accurate information on the constituent images. Indeed, thus far the manual reduction technique has greater applicability, since the effects of other stars can be ignored quite easily when the fit is made. As a first step in developing an automatic system to handle crowded images, we extended the original Gaussian fitting program to enable it to fit up to six fixed-dispersion profiles simultaneously. In this situation, we have that the density at any point within the array is given by

$$I(x,y) = \sum_i H_i \exp\left\{ - a_1^2 (x-\bar{x}_i)^2 - a_2^2 (y-\bar{y}_i)^2 \right\} \qquad i=1,6$$

Again a number of experiments were performed with artificial data to gain some insight into the capabilities of such a scheme. The results indicated that convergence was as fast and assured as in the single image fit, providing that the initial approximations placed the images further apart than they actually were. In other words, it was found that the iterative scheme would pull the images together to effect a fit, but was likely to diverge if it attempted or needed to spread them out.

A simple illustration for the one-dimensional case of only two overlapping images is shown in Figure 6. This was one of the numerical tests performed where the profile P3 was generated from the sum of P1

and P2; profiles of the same dispersion and separated by one dispersion width. This circumstance is probably quite often met in practice as the source of the 'non-stellar' images often noted on electronographs. In this case, using the noiseless, generated data, convergence on to the two correct profiles was achieved in about four iterations, more or less regardless of the initial height and position estimates, with only the one proviso as noted above.

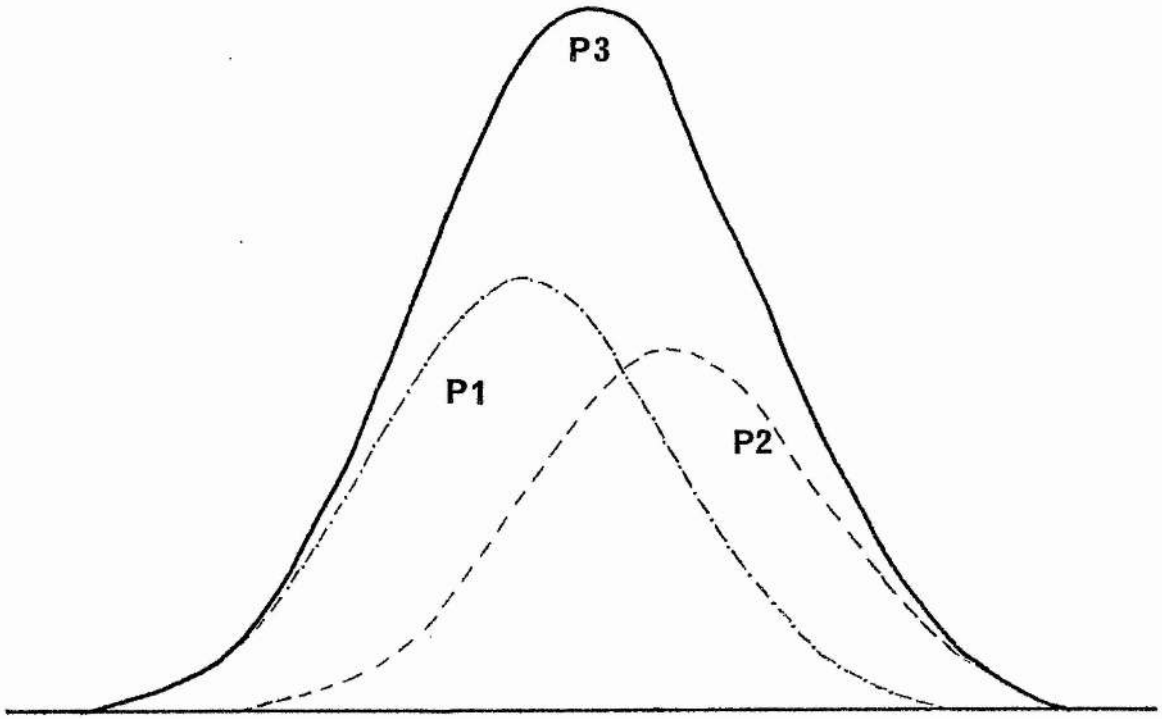

Figure 6

After successful tests on artificial data, a grouping of stars was chosen from plate SLT-26-3, a 90 minute, B exposure (G5 emulsion) of NGC 2158 taken with the 24" reflector. The initial approximations for such an analysis were obtained by the operator from the Tektronix screen - the centres were indicated by positioning of the cross-wires and the density at these points taken as the starting point for the height of the profile. The dispersions had previously been set by averaging the values obtained from some single uncrowded stars. The grouping of stars

analysed is shown in Figure 7, together with the identification and an indication of the direction of the scans shown in the following Figures. No magnitudes for these stars are available from the work of Arp and Cuffey (1962) on the cluster - reflecting the fact that the stars are too crowded to allow photographic photometry. One might argue that manual scanning techniques could provide adequate magnitudes for such a grouping, but this will only be true for some of the stars and particularly only if the scan direction can be chosen independently for each star. This of course would be unwise due to possible dependence of the dispersion upon direction. For this group the solution converged in 5 iterations with the resultant magnitudes given in Figure 7. In Figures 8 and 9, we show the results of plotting the data, together with the fitted curve for the cross-sections indicated in Figure 7. The highest peak in Figure 8 is due to star 3, with a large contribution from star 4. Shown also are the wings of star 2. The indications from this cross-section are that the wings of the stars are a lot stronger than those of a Gaussian. We show in Figure 10 Joyce-Loebl density tracings of the kind required for manual reduction of star 3, taken through approximately the same section as Figure 8. The effects of stars 2 and 4 obviously prohibit any sensible estimate of the magnitude of star 3.

Although the iterative scheme did converge satisfactorily for this grouping of stars, the shortcomings of the Gaussian representation become apparent in the preceding Figures and, as a consequence, it is not clear how valid the derived magnitudes are. It is important, however, that the approach to this kind of data analysis does not stop here and so we have pursued this question by employing a different form of profile. In his work on double stars using the photoelectric area scanner, Franz (1973) derived an expression for the intensity in an image of the form

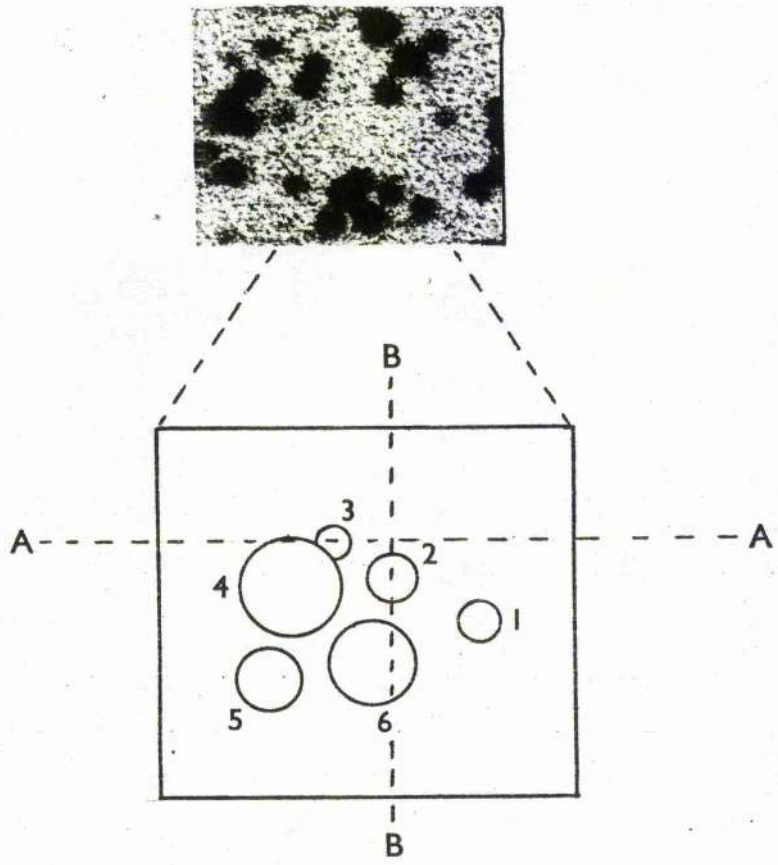

m(1) = 9.55
m(2) = 9.39
m(3) = 9.53
m(4) = 8.20
m(5) = 8.91
m(6) = 8.39

Figure 7

The six-star grouping analysed as described in the text. The derived magnitudes for the individual stars are given. Section AA is plotted in Figure 8 and section BB in Figure 9.

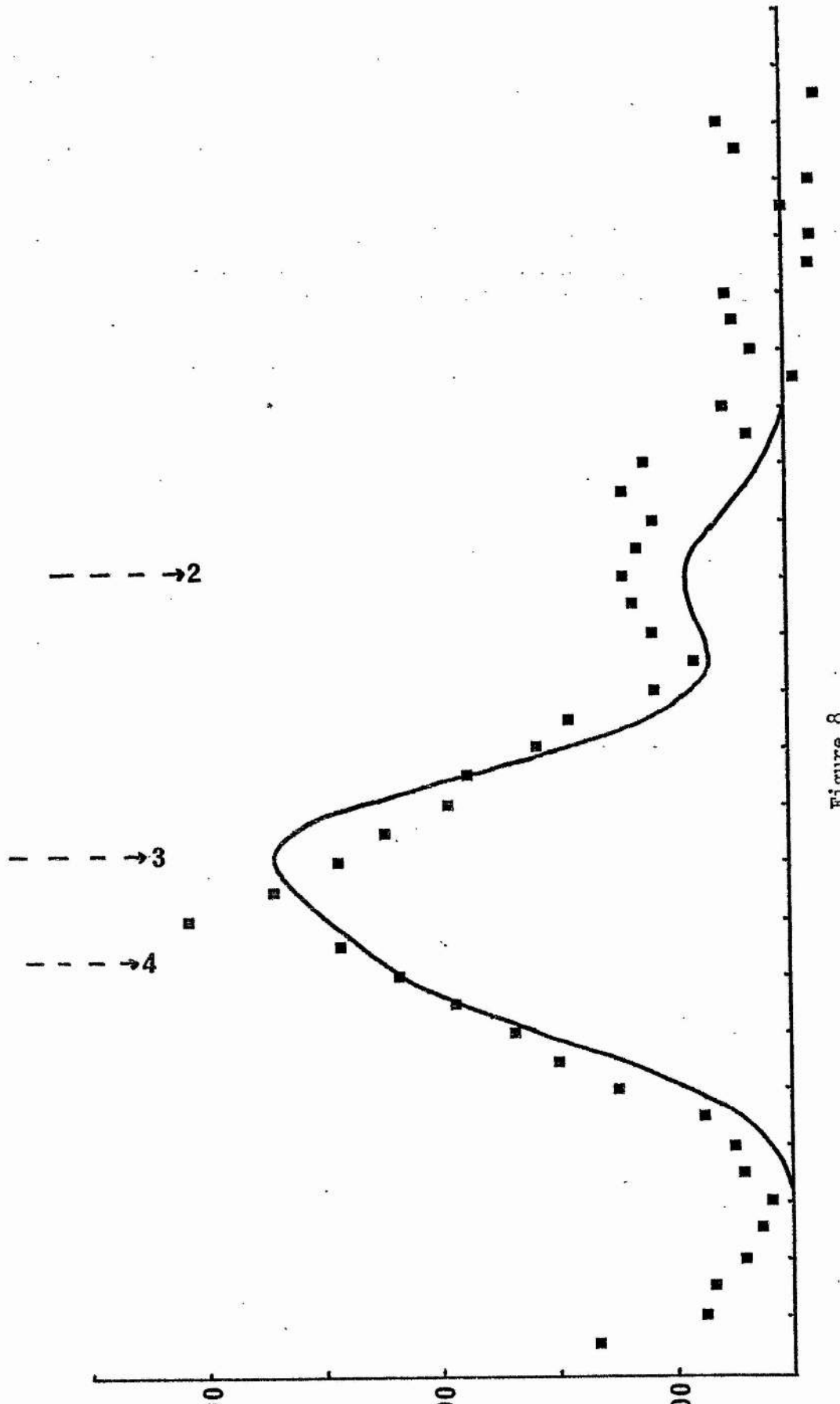

Figure 8

The section AA of Figure 7. Squares are the observed data points and the line is the final fitted profile

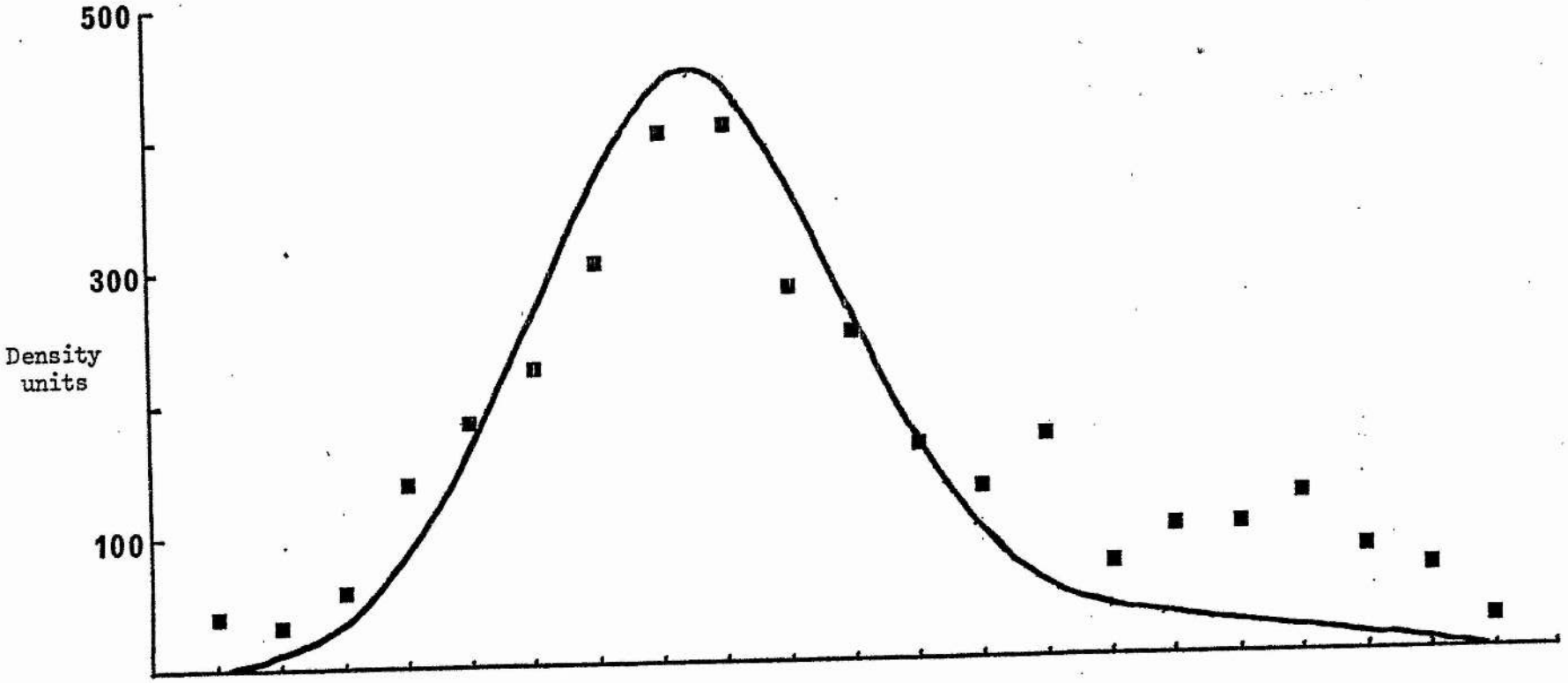

Figure 9

Section DD of Figure 7. The symbols are the same as in Figure 8.

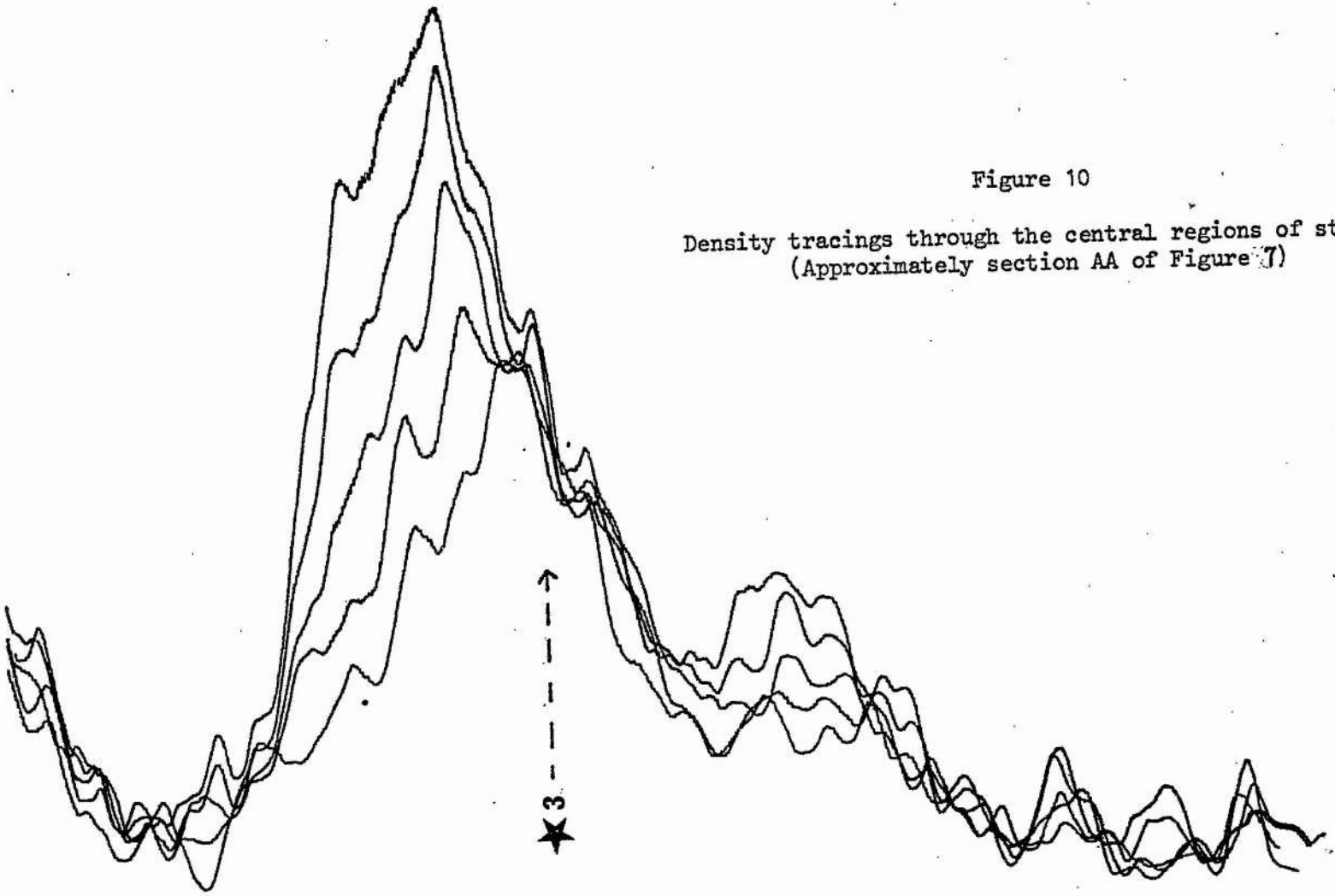

Figure 10

Density tracings through the central regions of star 3.
(Approximately section AA of Figure 7)

$$I(x) = \frac{I_o}{1 + \left(\frac{|x-\bar{x}|}{B_x}\right)^{P\left(1+\frac{|x-\bar{x}|}{C}\right)}}$$

where the centre of the profile is $\bar{x}$ and the parameters B, P, C are variable and determine the shape of the profile. B is clearly the distance from the profile centre at which the intensity is one half the peak intensity, while P and C combine to determine the rate of fall-off of the profile. Penny (1976) adopted the Franz expression for his electronographic photometry of double stars and it was from his success with this profile that this work springs.

We have taken a pseudo-two dimensional representation of the Franz profile of the form

$$I(x,y) = I_o/XY$$

where

$$X = \frac{1}{1 + \left(\frac{|x-\bar{x}|}{B_x}\right)^{P\left(1+\frac{|x-\bar{x}|}{C}\right)}} \quad \text{and} \quad Y = \frac{1}{1 + \left(\frac{|y-\bar{y}|}{B_y}\right)^{P\left(1+\frac{|y-\bar{y}|}{C}\right)}}$$

This is analogous in many ways to the Gaussian, since it is simply the product of two one dimensional arrays rather than a true two dimensional form. In some circumstances this could cause problems, in the sense that if the widths (B_x and B_y) are very different, the contours of this volume might assume rather awkward shapes with corners, tending to develop. We have checked this and find that when B_x and B_y are comparable, within 10 - 15%, then the contours are well behaved. This should cover most practical applications even for the worst guiders. An important advantage of this form though is that it makes it possible to separate the variables in the analysis, saving much computing time.

Since this profile is not easily integrated, we cannot use the method

of moments as previously to find the initial approximations. We have therefore adopted an empirical procedure of which the best that can be said is that it has been found to work. In Figure 11 we show a Franz profile having the parameters B = 6, P = 2, C = 50 together with the least-squares Gaussian fit to that data. Since the two profiles agree closely at around the half peak intensity point, the value of B can clearly be found from the dispersion of the associated Gaussian. We found that

$$B = 0.75/a$$

gives a good approximation (better than the theoretical B = 0.832/a which would be true if the heights matched accurately).

Obtaining automatic estimates of P and C proved more troublesome, since they have no simple and precise physical interpretation as has B. One approach which seemed promising at first was to take the ratios of the height of the actual profile at, say, distances of 0.8B and 2B from the centre. The parameter, P, then cancels out and with B already known, an estimate of C results. In practice, slight errors in the value of B affected the results and since the value of C deduced was in any case very sensitive to the ratio found, generally poor estimates of C resulted. In the end, no such technique was found satisfactory and we relied upon the results given by Penny (1976), who found that in most instances P has a value of about 2.0 and C, although showing a large range, in most circumstances had a value of between 50 and 100. One quirk of the fitting procedure which we did find was that the iterations converged on a value of C more or less regardless of the initial value, providing that the original estimate of C is lower than the true value. This means that in practice, getting the routine to converge is little trouble, since the initial approximation of C can be set to a small number.

In a similar manner to that already described, we have generalized

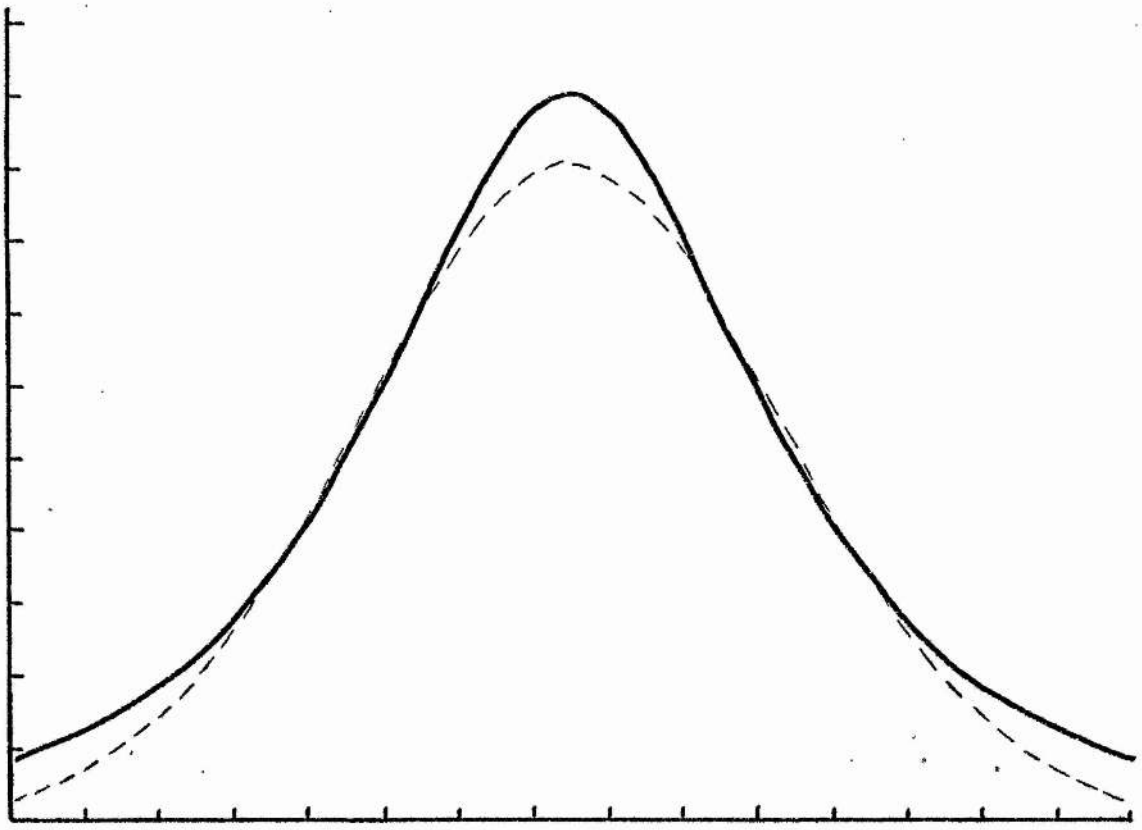

Figure 11

A comparison of a typical Franz profile (solid)
with the least-squares fit of a
Gaussian (dashed) to it

the program to handle multi-image groupings once the parameters of the profile (B, P and C) have been set from standard stars. To illustrate how well the Franz representation is able to follow the true image, we show in Figures 12 and 13 the data and fits from stars of the same plate as previously. For some reason, the image shape appears quite variable on this plate - something that was not readily apparent from the Gaussian fits. Nevertheless, using average parameters, we have analysed the same group of stars as before. Part of a section through the wings of stars 4, 5 and 6 is illustrated in Figure 14. It demonstrates the ability of this profile to reproduce the form of the stellar image and shows that improved magnitudes can be expected in this situation over those obtained with the Gaussian.

In conclusion, therefore, we have confidence that the reduction scheme developed is superior to those formerly available due to the following results:

a) The linearity and accuracy of the hand measures has been duplicated and possibly improved.

b) The facility to handle multiple groupings of stars has been developed. This means that a great deal of information hitherto unavailable can now be retrieved.

c) The efficiency of the data reductions has been greatly increased.

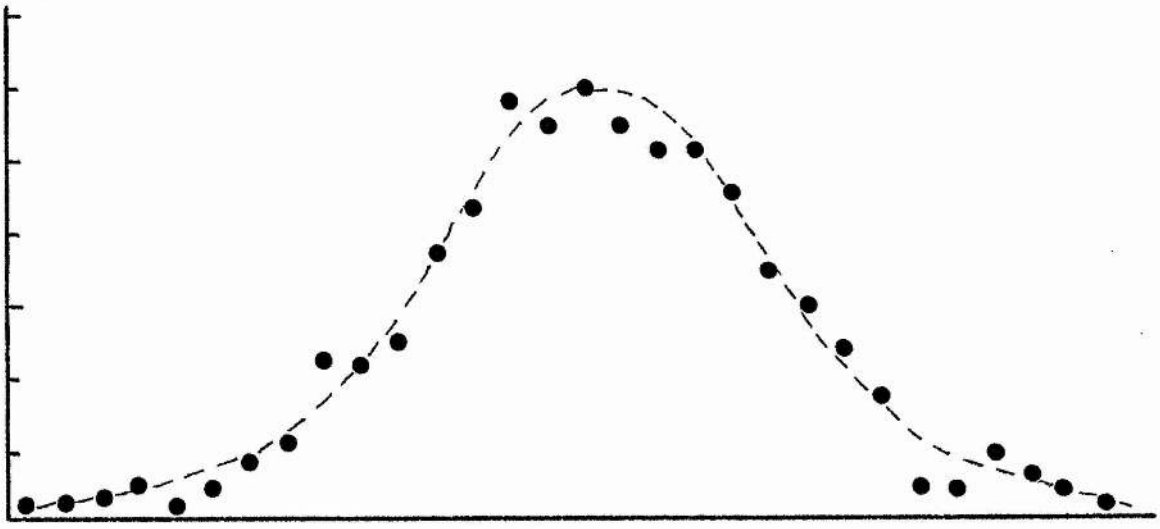

Figure 12

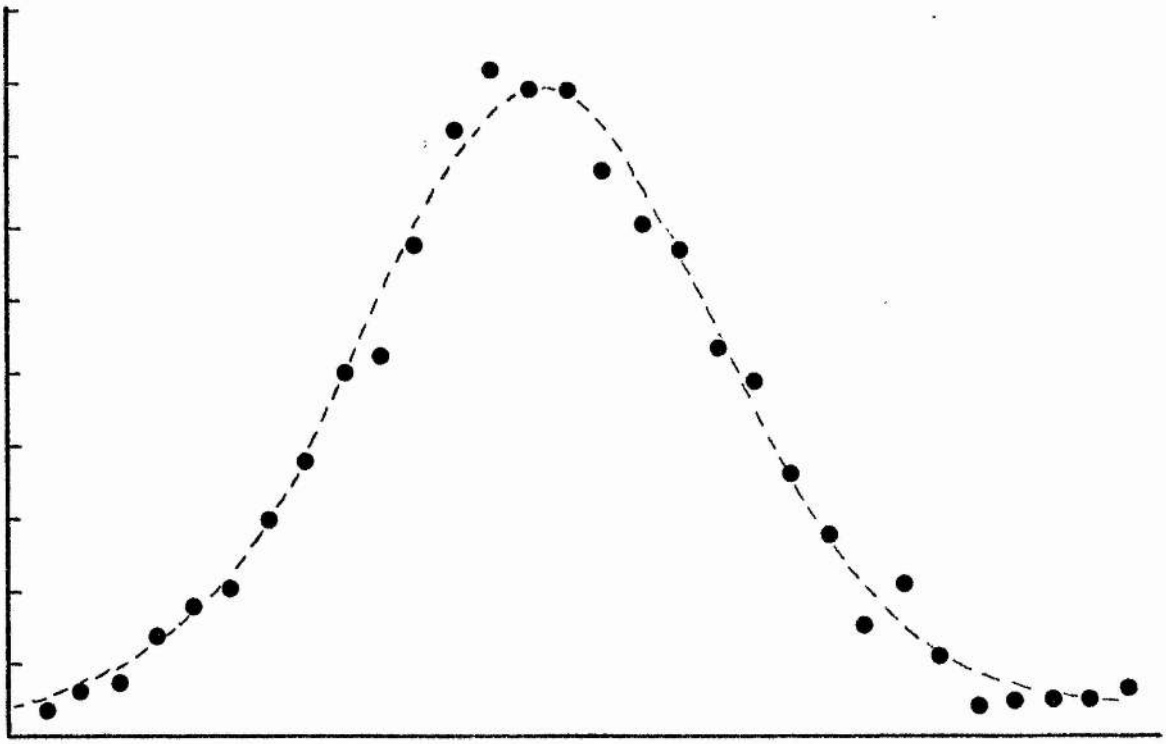

Figure 13

The data and fitted Franz profiles for two standard stars

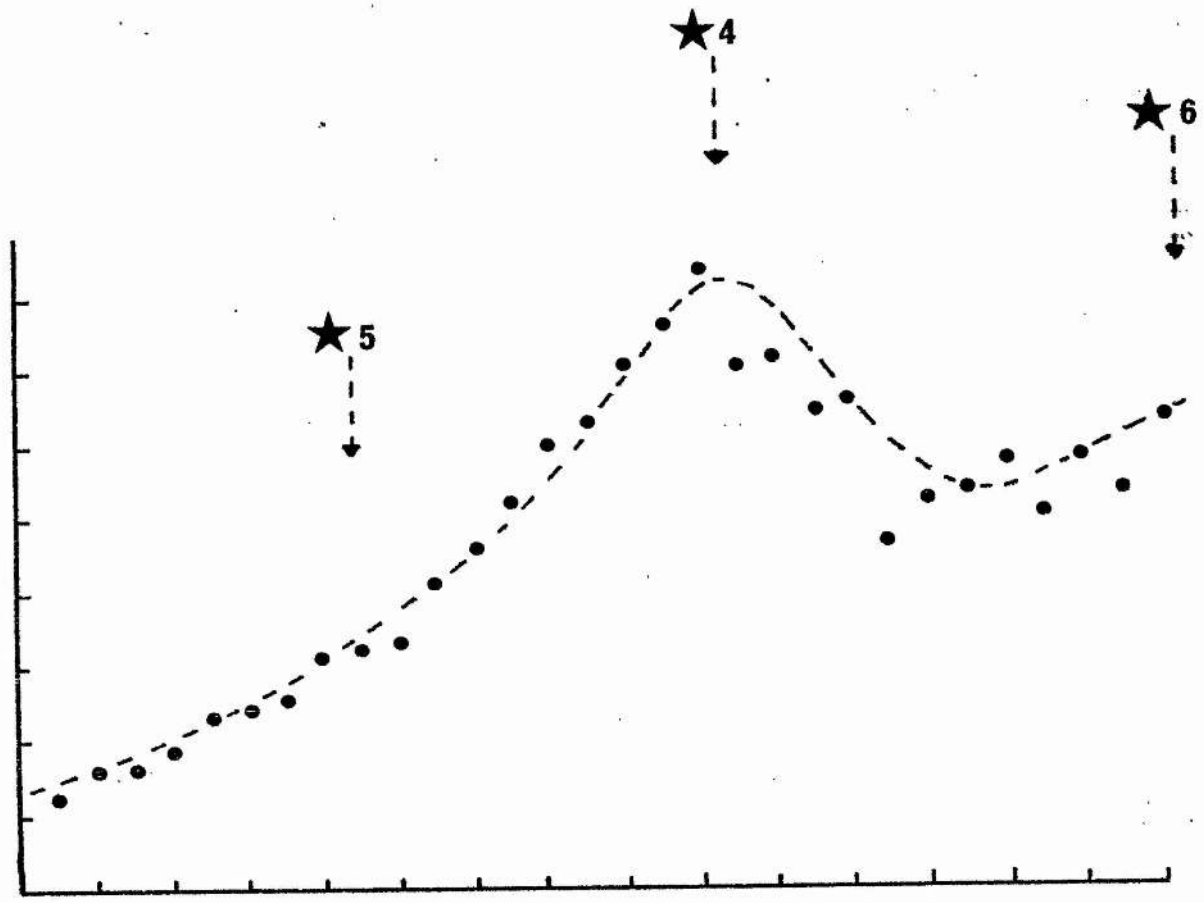

Figure 14

A multiple Franz profile fit to a section of the stellar grouping shown in Figure 7

4.5 Application to photographic images

In this section, we describe the extension of the reduction procedure for single electronographic images given above, to the measurement of photographic plates for the purpose of stellar photometry.

This work arose from the need to reduce the large amounts of data that had been obtained at the Lick Observatory. These consisted of photographic plates of bright northern globular clusters with up to 100 stars per cluster. An iris diaphragm photometer was available at St. Andrews, but preliminary measurements with it indicated that the results were extremely sensitive to external factors, particularly temperature, and while this can to some extent be corrected for, it was felt that we could not afford to lose any accuracy through such factors and an alternative method for reducing the plates was therefore sought.

If possible we wished to apply the Gaussian profile fitting technique, but clearly doubt arises as to whether by fitting a Gaussian profile to photographic images we can obtain anything near meaningful magnitudes. We expect that due to the non-linearity and increased grain size of the emulsion, the profile will bear less of a resemblance to a Gaussian even than did the electronographic images. However, as a test case, a photographic plate of M 67 was reduced. This cluster has photoelectric standards measured by Sandage and Johnson (1955). The images of interest were scanned on the Joyce-Loebl; the data stored on magnetic tape and various reduction procedures experimented with, using the IBM 360 computer at the Computing Laboratory, St. Andrews.

Plotting out the data in conjunction with the theoretical fits confirmed that the Gaussian profile was not a particularly good representation of the data, especially in the wings of the image. To try and allow for this, various weighting procedures were experimented with. For example, during tests the weight of a data point was taken as proportional

to Q; (Q/H); etc. where Q is the value of the predicted density at the position of the data point and H is the maximum height of profile. In the event, it was found that the resultant magnitudes were relatively insensitive to the weighting function used. However, to acknowledge the poor fit of the Gaussian, the final adopted weighting was such that equal weight was given to all data points, unless

1) after 2 - 3 iterations they still deviated by more than three standard deviations from the calculated value, or
2) they were at a distance from the centre of the image of greater than twice the dispersion of the profile, or
3) they were in the saturated centre of an image.

In these cases, zero weight was attributed to the data point. Initially, the reduction programs were written so as to include the background sky level surrounding the images as one of the variable parameters of the fit; thus providing the facility for compensation of any background variations. It was found in practice however that in order that sufficient data points measuring the background could be included to give a good determination of this level, a large area surrounding the image had to be scanned. In many cases such an area included at least the outer parts of a nearby image and accurate elimination of these effects is difficult. If different areas surrounding stars are scanned, there would probably then be the need for a correction of the final magnitude as a function of the area scanned. In view of these difficulties, the background was omitted as a variable and its value set from scans of nearby areas of image-free plate.

The easiest and fastest method of deriving a magnitude from a scanned profile is to take the logarithm of the volume of the image i.e. perform a simple summation of the data points within the profile area once the background level had been subtracted. For the noisy data

obtained from digitizing photographic plates, this does not yield accurate or consistent results. When a full fit of all five parameters is performed for the image, a more consistent and accurate magnitude results if the volume under the least-squares fit profile is calculated. By the nature of the photographic emulsion, the image size is related to the brightness of the star, this being the basis of photographic iris photometry. Consequently, we cannot retain the idea of a standard profile for each plate, as with the electronographs. By allowing the fitting procedure to adopt the image size as necessary, we find, as expected, a relationship between the image size and integrated density in the image (which in this instance gives a good enough approximation to the true value). The plot derived for the M 67 plate is given in Figure 15. As is seen, the relationship is fairly well defined except for the fainter images, whose radii are set by the seeing on the plate. The dotted line is a least-squares fit to the points. Since the equation of the line is of second order, the solution usually has a turning point in the region of the smaller images, but as this is an artefact of the solution, we have set the image size to the minimum value for fainter images. Using these calibrations for the dispersions in the x and y directions, we can calculate the 'correct' dispersions for the total density found in the image. Tests were made to see whether, by subsequently assigning these dispersions to the images and recalculating the least-squares fit, more accurate final magnitudes were produced. It was possible to check this in two ways. Firstly, by a comparison of the final magnitudes with the photographic results of Sandage and Johnson (1955) whose values we assume to be accurate since they are the mean of six plates. Secondly, a star in a clear field was measured several times using different sizes of scanning area and different positioning of the star within this area. On both counts the magnitudes given by performing a final fixed dis-

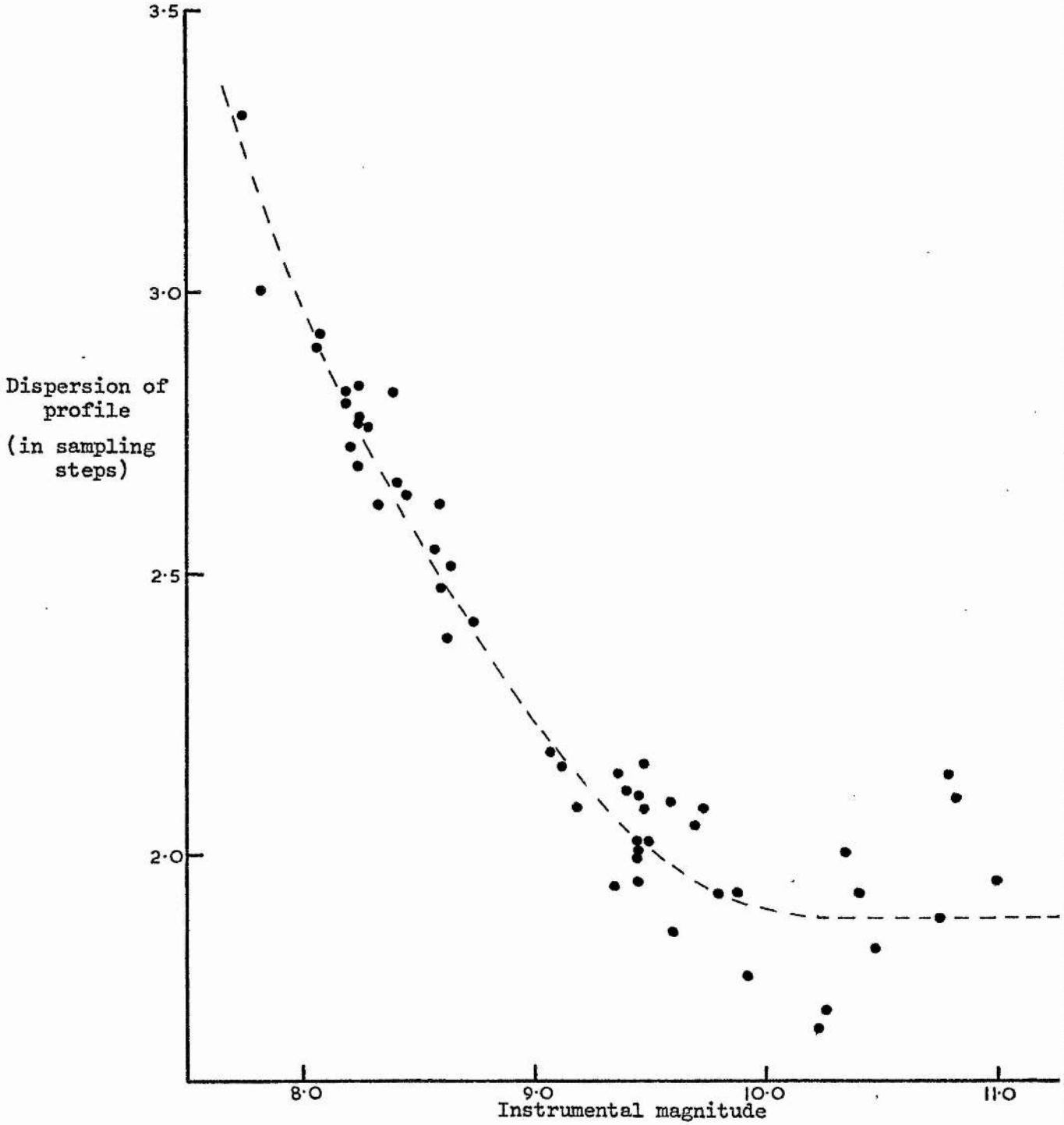

Figure 15

The image growth on the M 67 plate

persion fit were superior. With reference to the consistency checks, four measures of the same star were obtained with the image centred in varying sizes of scan area and then four scans were obtained with the image offset to the corners of the scanning area. For the total of eight measures, the standard deviation from the mean was ±.007 magnitudes. The two extreme values were obtained with exactly the same positioning of the image, indicating that most of the differences from scan to scan arise from variations in the digitizing of the data. The Joyce-Loebl samples the density at predetermined intervals - usually for the work described here this was two or three times the nominal step size of 5 microns. The accuracy of individual steps however is only accurate to ±5%, with the error being non-cumulative. When scanning over the steep density gradients found in stellar images, such errors in the spacing of individual samples can be expected to give significantly different density readings and hence affect the final magnitudes.

The final calibration curve for the M 67 plate is shown in Figure 16. The mean standard deviation of the points is ±0.04 magnitudes, indicating that a satisfactory accuracy can be obtained with this method. During the later stages of the development of the program, but at a point where the sky background level was still being treated as a variable, some of the photographic plates of NGC 6366, as given in the previous chapter, were measured and reduced using the above techniques. The resultant C-M diagram from three plates in each colour was very similar to the final diagram and demonstrated clearly for the first time the true nature of the cluster.

We conclude this section with a brief resume of the procedure used in the final computer program devised for the measurement of photographic plates. The program controlling the Joyce-Loebl was altered by Mr R. J. Campbell to enable a more operator-independent mode for scanning.

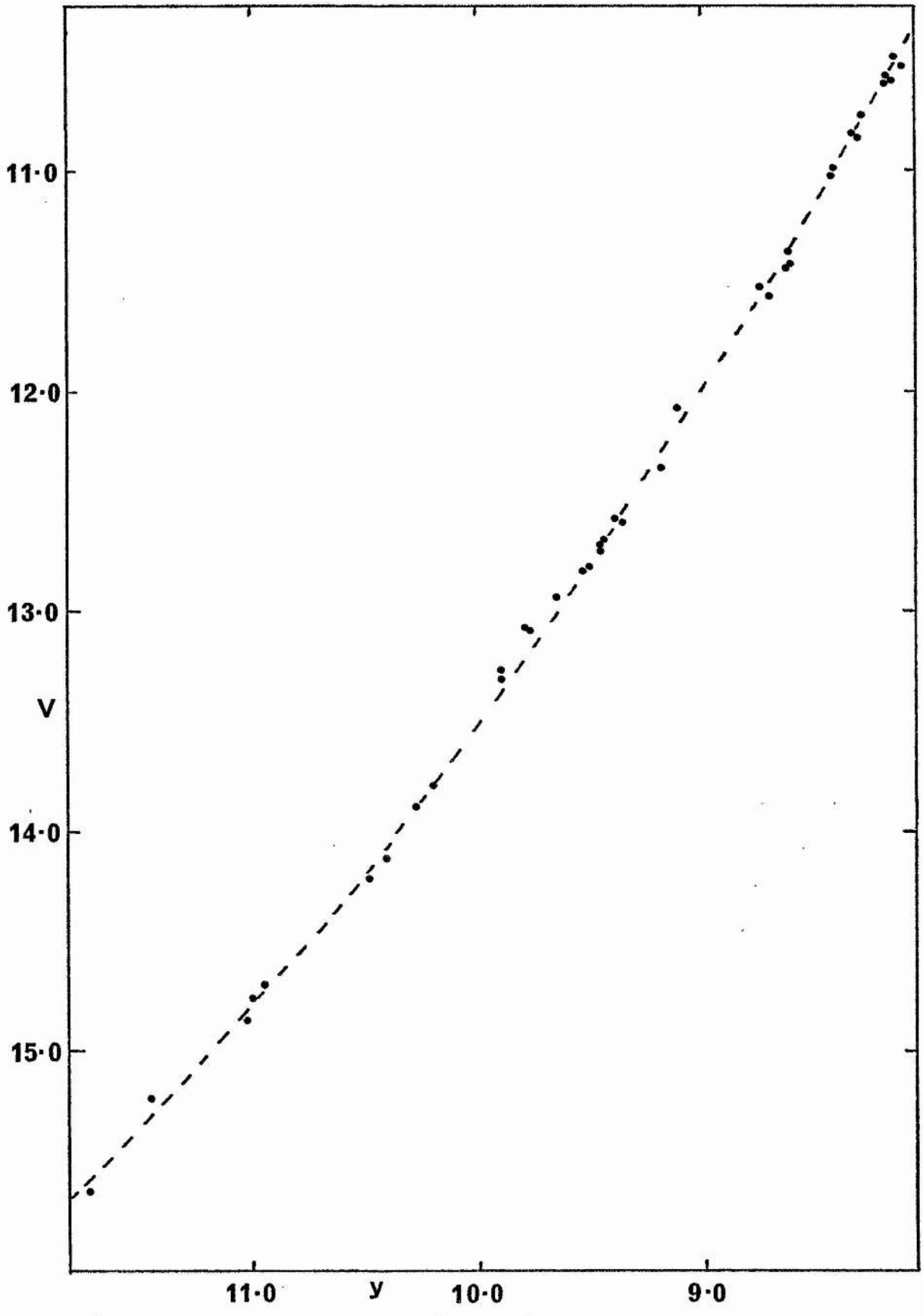

Figure 16

The photographic calibration curve for M 67

For the field to be measured, a path was devised to minimize as much as possible the travel of the carriage as it moved from star to star. The carriage was then driven by the operator to each star or area of sky that was to be scanned and the position was recorded in the computer memory. When all the positions had been so defined, the Joyce-Loebl returned to each position, scanning a preset size of area centred on them. Each separate scan was recorded as a separate file on magnetic tape for future analysis. Working through each tape file, the reduction program performed the usual Gaussian fit to the images. The dispersions and integrated density within the image were then calibrated as described; the dispersions for each image fixed and the profile refitted. The instrumental magnitudes for the standard stars were then calibrated by a least-squares fit to the standard magnitudes and the final magnitudes output.

References

Arp, H. & Cuffey, J., 1962. Ap. J., 136, 51.

Cullum, M. J. & Stephens, C. L., 1972. Adv. in E. & E.P., 33B, 757.

Franz, O. J., 1973. J. R. ast. Soc. Can., 67, 81.

Gyldenkerne, K., 1950. Annales d'Ap., 13, 97.

Penny, A. J., 1976. Thesis, University of Sussex.

Sandage, A. & Johnson, H. L., 1955. Ap. J., 121, 616.

Walker, M. F., 1970. Ap. J., 161, 835.

Walker, M. F., 1971. Ap. J., 167, 1.

Walker, M. F., 1972. Mon. Not. R. ast. Soc., 159, 379.

Walker, M. F., 1974. Mon. Not. R. ast. Soc., 169, 199.

Wlerick, G., Michet, D. & Labeyne, C., 1974. Texas Symposium on Electronography & its Astronomical Applications.

CHAPTER 5

INTERMEDIATE BAND PHOTOGRAPHIC OBSERVATIONS OF M 15

5.1 The photometric system

Although a great deal of information has been gleaned from observations of globular cluster stars using the broad band UBV photometric system, the progression to intermediate band systems was certain to open up new avenues of research and to yield valuable data on the physical characteristics of the stars. This is evidenced by the investigations of Newell et al (1969) and Newell (1970), which employed spectroscopy and narrow band photometry to obtain temperatures and gravities for blue horizontal branch stars in several globular clusters. This work was further complemented by Philip's (1972, 1973) observations of similar stars using Stromgren photometry.

The David Dunlap Observatory (DDO) system was designed by McClure and van den Bergh (1968) to allow measurement of the temperatures, gravities and abundances of late type stars. When Osborn's (1971) calibration of the system and its extension to Population II stars became available, it was clear that this system would play an important part in future investigations of globular cluster giants. Osborn's (1971) observations of some thirty-five stars in five bright northern clusters had given accurate abundances for the clusters, as well as providing data on the individual stars suitable for comparison with theoretical studies. He had also discovered two CN rich stars and one low gravity star in his sample.

It seemed, then, an appropriate time to extend these observations to as many stars as possible, with the intention of obtaining physical data for a large sample of stars, while at the same time being able to investigate the statistics of the occurrence of the CN and CH stars. We proposed to use electronographic photometry and to this end a set of 2" x 2" DDO filters was purchased for use with the Spectracon mounting. The specifications of the interference filters are given in Table I and the

transmission curves shown in Figures 1 and 2.

TABLE I

Specifications of the DDO interference filters

Filter	Central wavelength	Half width	Peak transmission
41	4166A	83A	37%
42	4257	73	35%
45	4517	76	59%
48	4886	186	55%

In the spectrum of a late type star, the 41 filter is centred on the 0-1 cyanogen (CN) band with the band head at 4216A. For Population II stars this band only becomes significant at low gravities - hence the ease with which CN rich stars can be detected.

The 42 filter is designed to measure the flux in a relatively line free region just shortward of the G-band of the CH molecule. The colour index obtained from the 41 and 42 filters, i.e. C(4142) in Osborn's notation, will therefore measure the strength of the CN band.

The 45 filter is a continuum measure well to the red of the G-band. C(4245) will then measure the break across the G-band. This is known to be a sensitive temperature indicator (Crawford, 1961) given that peculiar abundance variations are not affecting the strength of the G-band.

The 48 filter again gives a measure of the continuum flux in that region, though the pass-band does contain the lines of magnesium hydride. The presence of these lines contributes to the sensitivity of C(4548) to surface gravity (McClure, 1976).

The DDO system contains two other filters, the 35 and 38. The 35 - identical to the Stromgren u - is used for gravity determination in stars of spectral type earlier than G5. Since it is shortward of the Balmer jump, C(3538) measures the Balmer discontinuity.

The 38 filter of the system is now the one adopted by Osborn (1971).

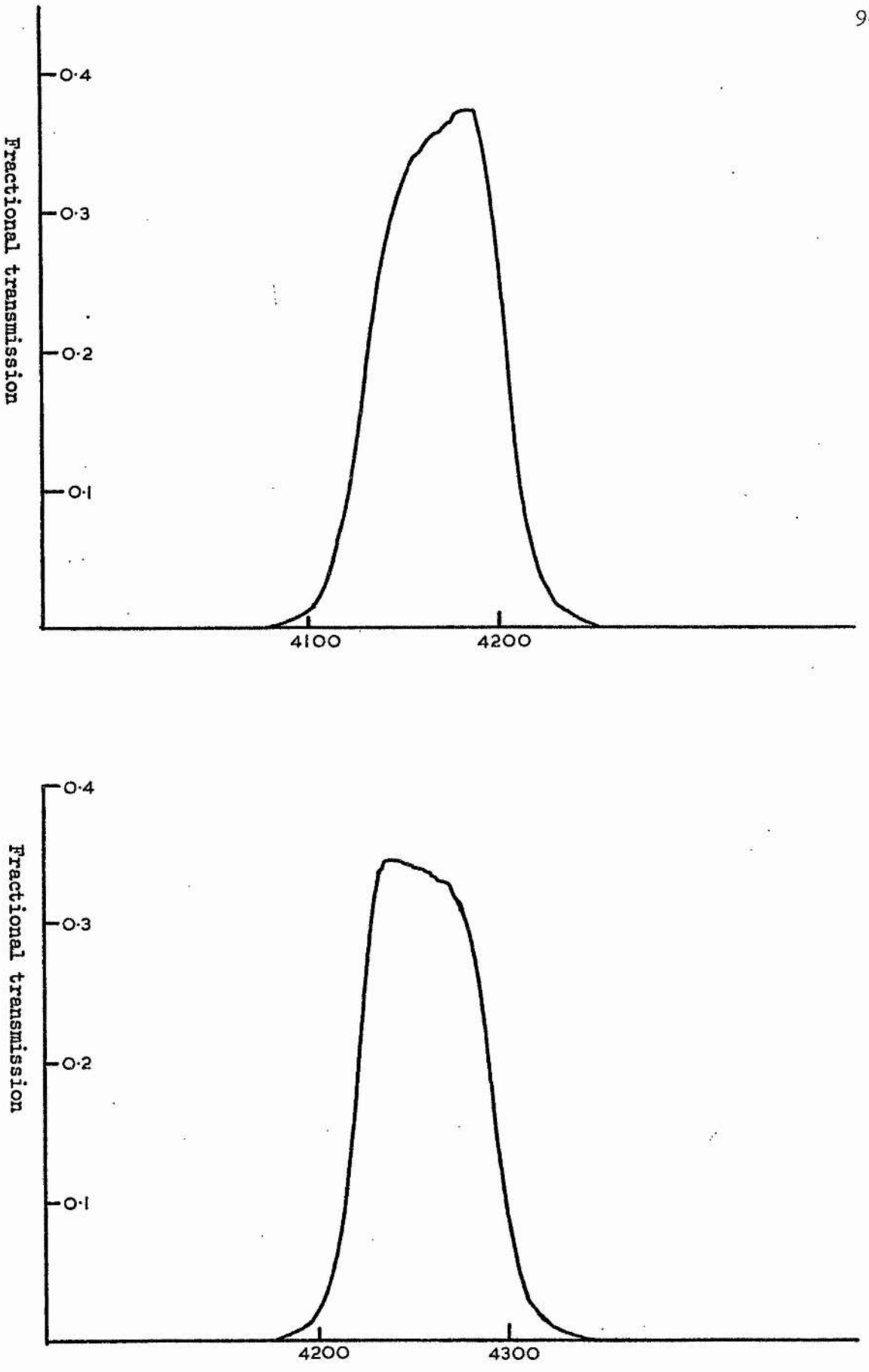

Figure 1

The transmission curves for the '41' and '42' filters

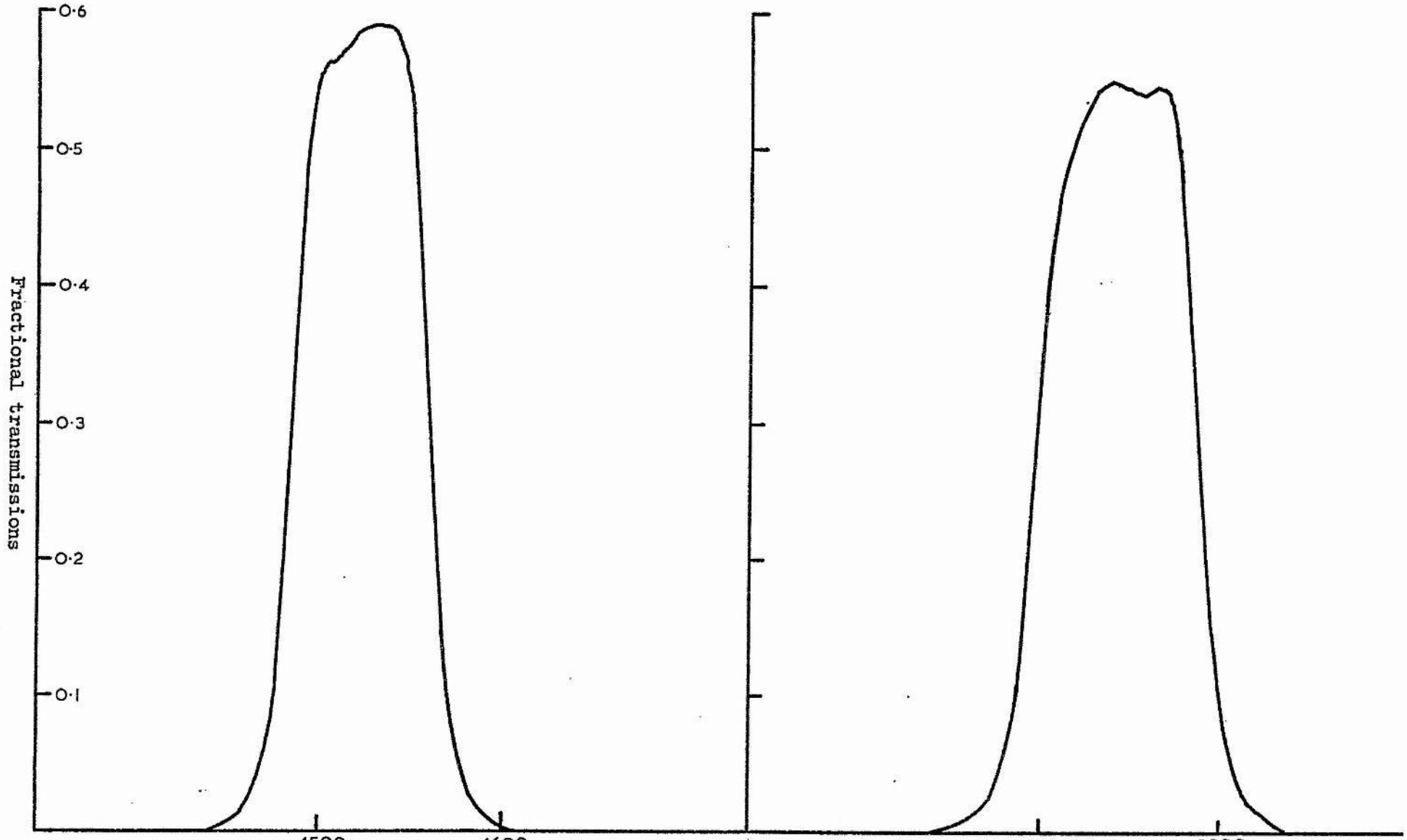

Figure 2. The transmission curves for the '45' and '48' filters

It is composed of 2 mm of Schott GG-18 plus 5 mm of Corning 7-51. This produces a peak transmission of about 30% at 3813A with a half width of 330A. This combination of glasses has a serious red leak beginning at around 6900A and so must be used in conjunction with a copper-sulphate cell if the detector has an S-20 response. The 38 filter is centred on a region of spectrum crowded with Fe I lines and so, when compared with either the 41 or 42 filters for Population II stars, it can be used as a metallicity indicator. There is now evidence for a complication here, since there is a strong CN band at 3800A and any enhancement of this band will mimic an increase in iron abundance, whereas abnormal atmospheric abundances of carbon and/or nitrogen could be responsible.

5.2 Calibration of the plates

During 1973-4, the unreliability of the Spectracons, alluded to earlier, finally overcame our efforts to observe with them. As a consequence, we were at that time unable to obtain the electronographic observations we had planned. Instead, we observed a number of clusters photographically, but still employing the DDO system. While clearly these observations would be unsuitable for use with Osborn's calibration, we felt it worthwhile to investigate the possibilities of such a set up.

Since the stars observed by Osborn were too few in number and, on the whole, outside of the photometric field of the plates, they could not be used for the photographic calibration. It was therefore necessary to find an alternative means of linearizing the photographic measures. Fortunately, Osborn (1971) gave magnitudes as well as colours for his observations of cluster giants - a practice which has now been generally adopted for the DDO system (McClure, 1976). Consequently, it is possible to ascribe to a star a magnitude for each filter. This we have done - the results are given in Table II. Now, since the four longer wavelength

TABLE II

Standard DDO and B magnitudes

Star	m(41)	m(42)	m(45)	m(48)	B	σ(B)
328	15.450	15.294	14.400	13.040	14.18	0.020
325	16.003	15.895	15.077	13.808	14.73	0.020
398	16.311	16.189	15.429	14.220	15.05	0.020
317	17.068	17.022	16.562	15.618	16.05	0.020
309	17.160	17.112	16.709	15.690	16.09	0.020
311	17.190	17.125	16.715	15.779	16.10	0.020
503	15.393	15.214	14.170	12.769	13.87	0.025
519	15.335	15.171	14.210	12.873	14.04	0.025
559	15.520	15.294	14.340	13.005	13.98	0.025
551	16.383	16.191	15.491	14.263	15.03	0.025
586	16.639	16.565	16.050	15.019	15.61	0.025
544	16.574	16.534	16.068	15.032	15.61	0.025
1085	15.495	15.372	14.500	13.163	14.14	0.025
1055	15.414	15.320	14.533	13.239	14.20	0.025
1076	15.544	15.465	14.745	13.510	14.46	0.025
1040	16.823	16.757	16.120	15.061	15.62	0.025
1083	16.182	16.129	15.603	14.585	15.30	0.025
13786	15.263	14.988	13.920	12.443	13.70	0.015
13371	15.382	15.291	14.455	13.208	14.04	0.030
13171	15.182	15.090	14.311	13.056	13.87	0.030
13651	15.485	15.363	14.597	13.360	14.24	0.020
13095	15.944	15.891	15.317	14.183	14.85	0.030
13818	15.790	15.723	15.174	14.049	14.74	0.030
92013	14.701	14.541	13.719	12.362	13.36	0.015
9218	14.740	14.571	13.768	12.430	13.43	0.010
9208	14.979	14.872	14.206	12.953	13.83	0.010
9210	15.510	15.436	14.766	13.586	14.37	0.005
9202	15.576	15.474	14.846	13.676	14.42	0.015
92114	15.811	15.733	15.118	13.967	14.70	0.020
9281	16.129	16.024	15.545	14.469	14.97	0.020
9212	16.112	16.053	15.596	14.534	15.06	0.010
92010	15.938	15.943	15.328	14.336	14.97	0.020

filters of the DDO system are all within the central regions of the B filter of the UBV system of Johnson and Morgan (1953), we might expect a reasonably good correlation between the DDO magnitudes and the B magnitudes. There will, of course, be scatter due to observational errors and to an intrinsic scatter due to the DDO magnitudes measuring much smaller regions of the spectrum - in some cases, including definite spectral features. The form of the correlations is shown in Figures 3 - 6, where we have plotted each set of DDO magnitudes against the B magnitude as given by Osborn. There is also a fairly tight correlation between the broad band U magnitude and the DDO 38 magnitude as shown in Figure 7. This could be used for a similar calibration of m(38), although the relationship does break down for the stars at the very tip of the red giant branch. To obtain the functional relationship, we have employed the method and fitting program described by Barker and Diana (1974). This is a modification of the normal least-squares technique, in which due account is taken of the fact that both variables have errors. As is well known, in making a normal least-squares fit the underlying assumption is that the independent variable has no error. If, however, both variables have uncertainties - as is usual in most practical situations - then a simple regression of x on y will give a different functional fit than a regression of y on x and indeed it is not necessarily correct that the mean of the two gives the true best fit (York, 1966). The method used here was adapted by Barker and Diana from work by Clutton-Brock (1967). The program weights each data point using an effective variance of the form:

$$\text{effective variance} = \left\{ \sigma_x + \{f'(x)\}\, \sigma_y \right\}$$

where σ_x and σ_y are the standard deviations in the measures of x and y and $f'(x)$ is the derivative of the fitted function. Since the effective variance requires an estimate of the function's derivative, an iterative

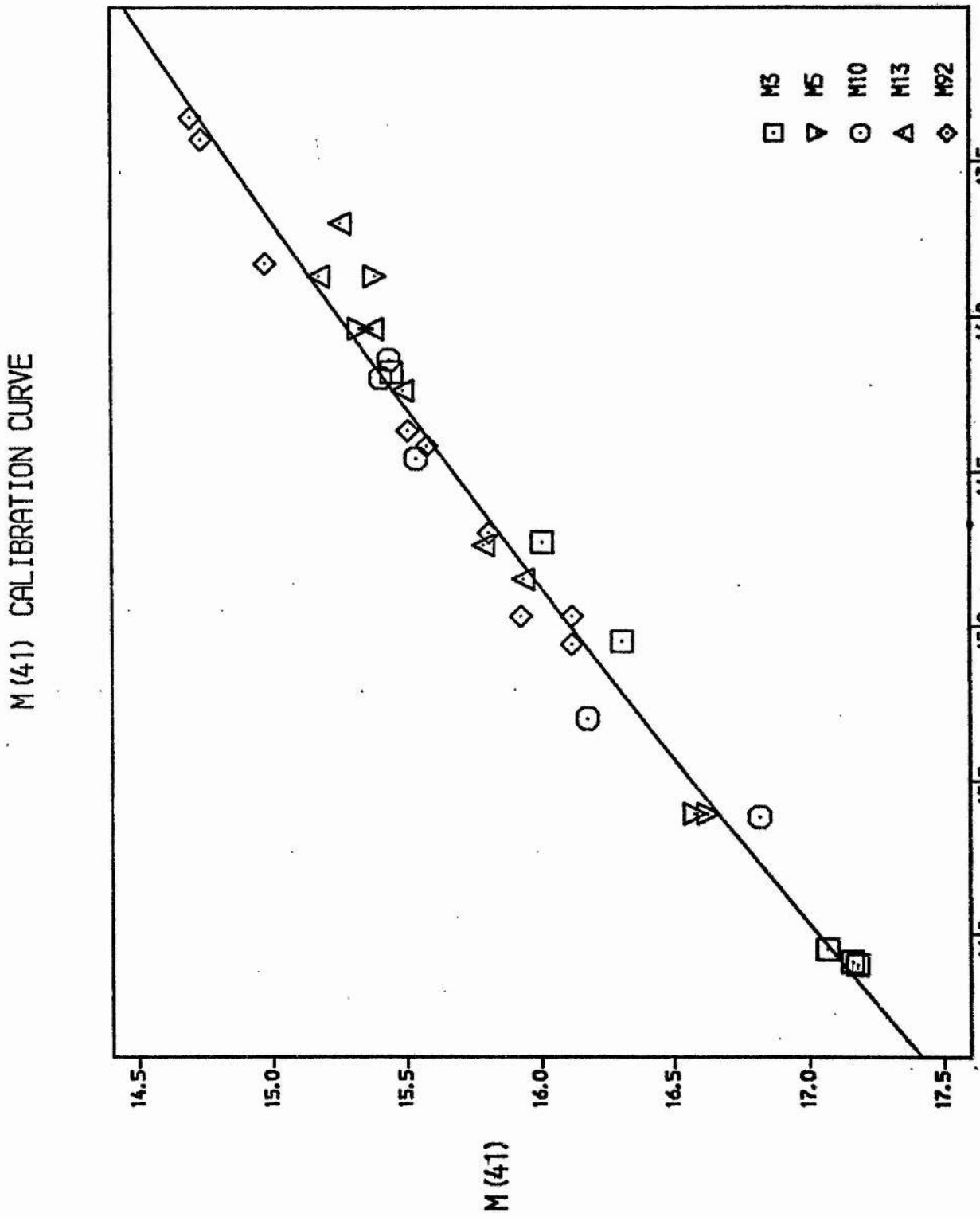

Figure 3

The calibration curve for M(41)

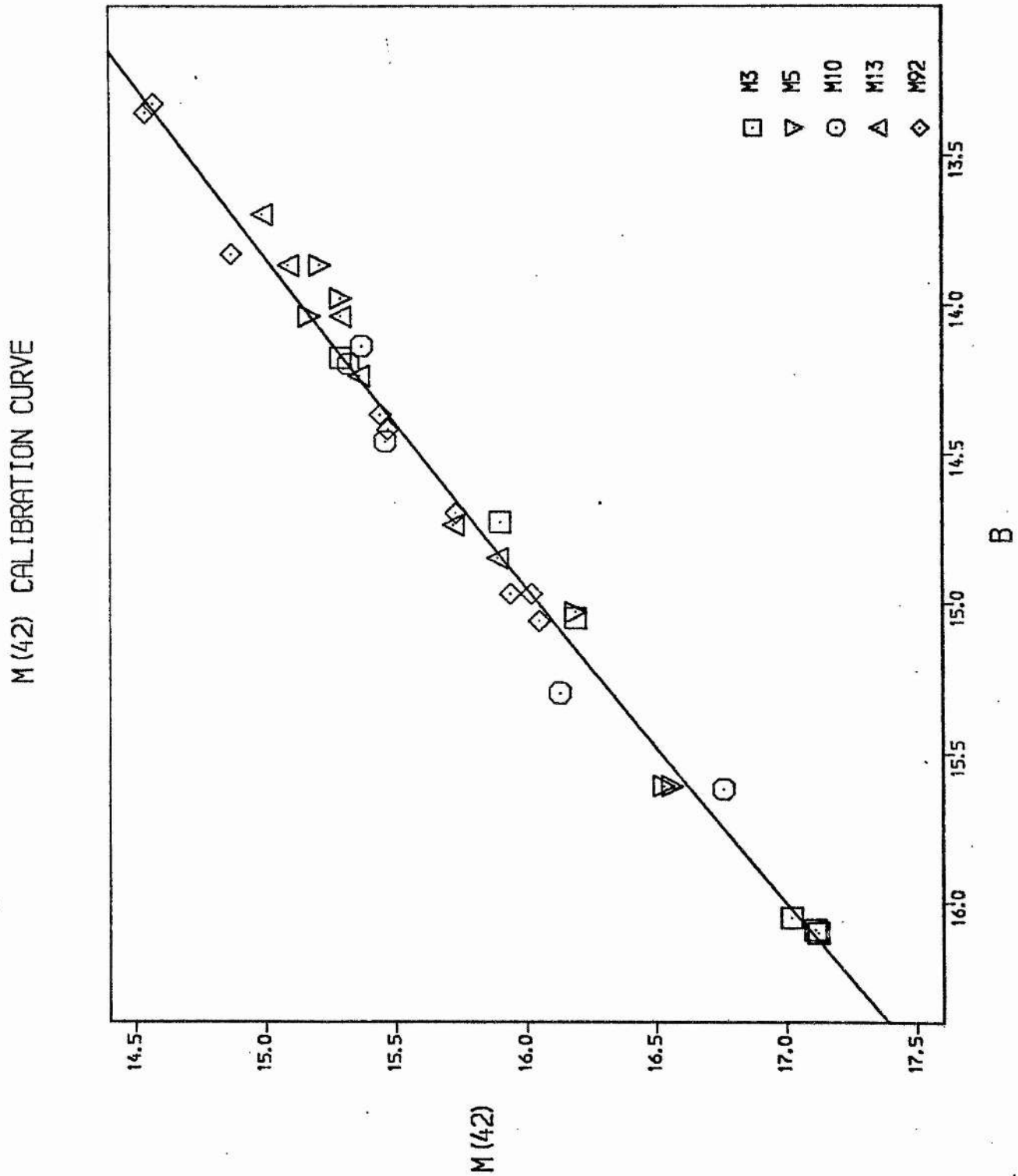

Figure 4

The calibration curve for m(42)

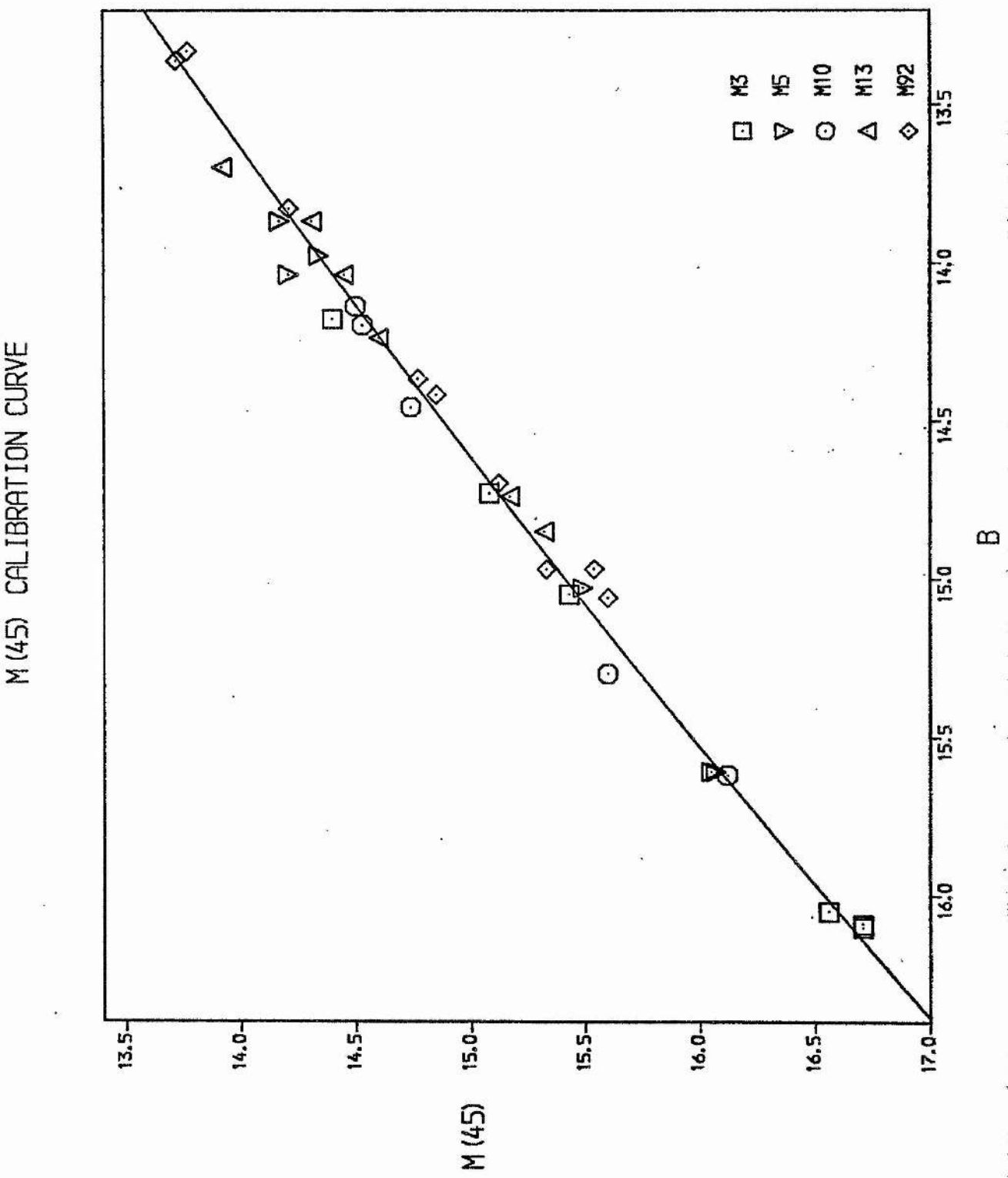

Figure 5

The calibration curve for m(45)

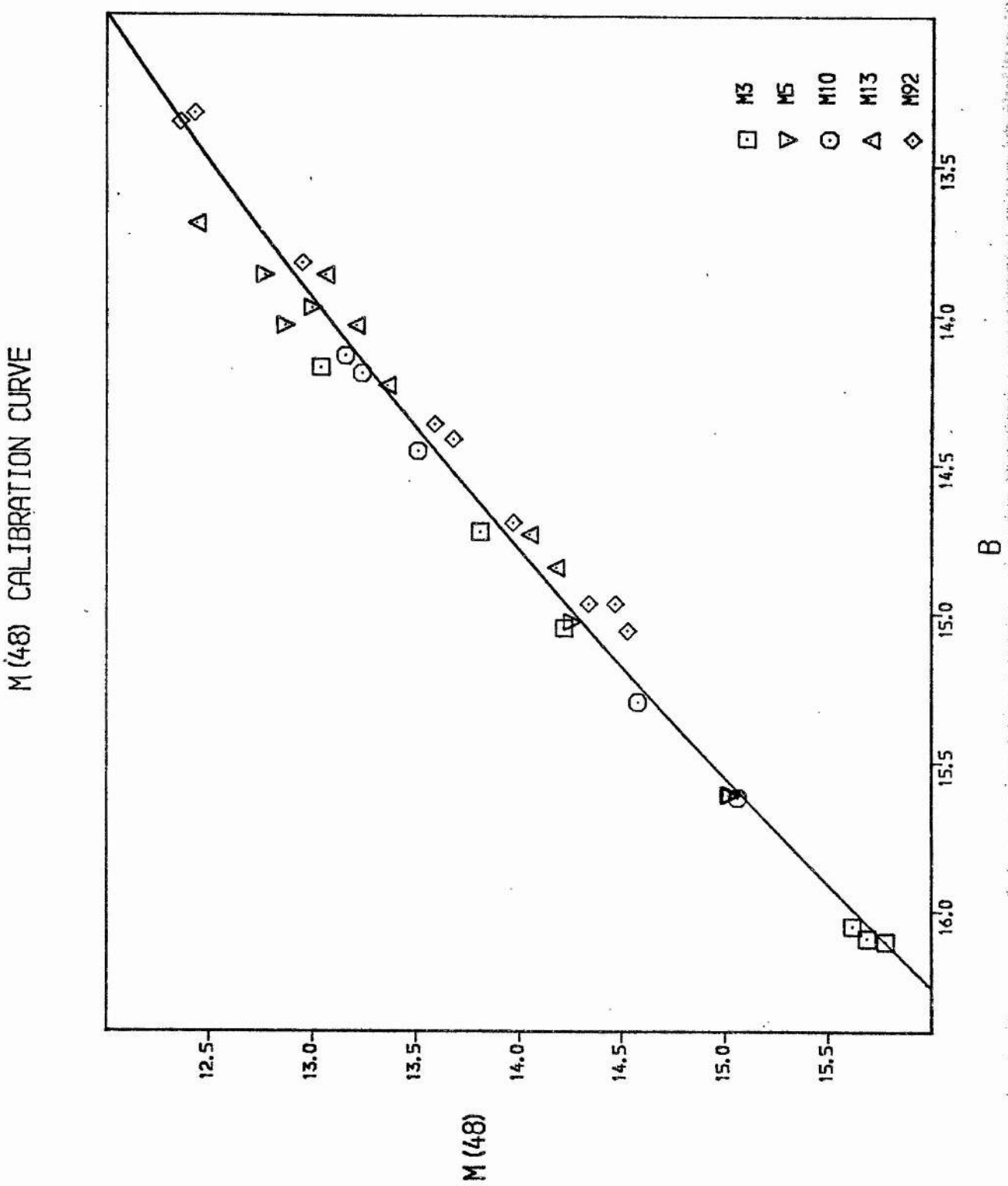

Figure 6

The calibration curve for m(48)

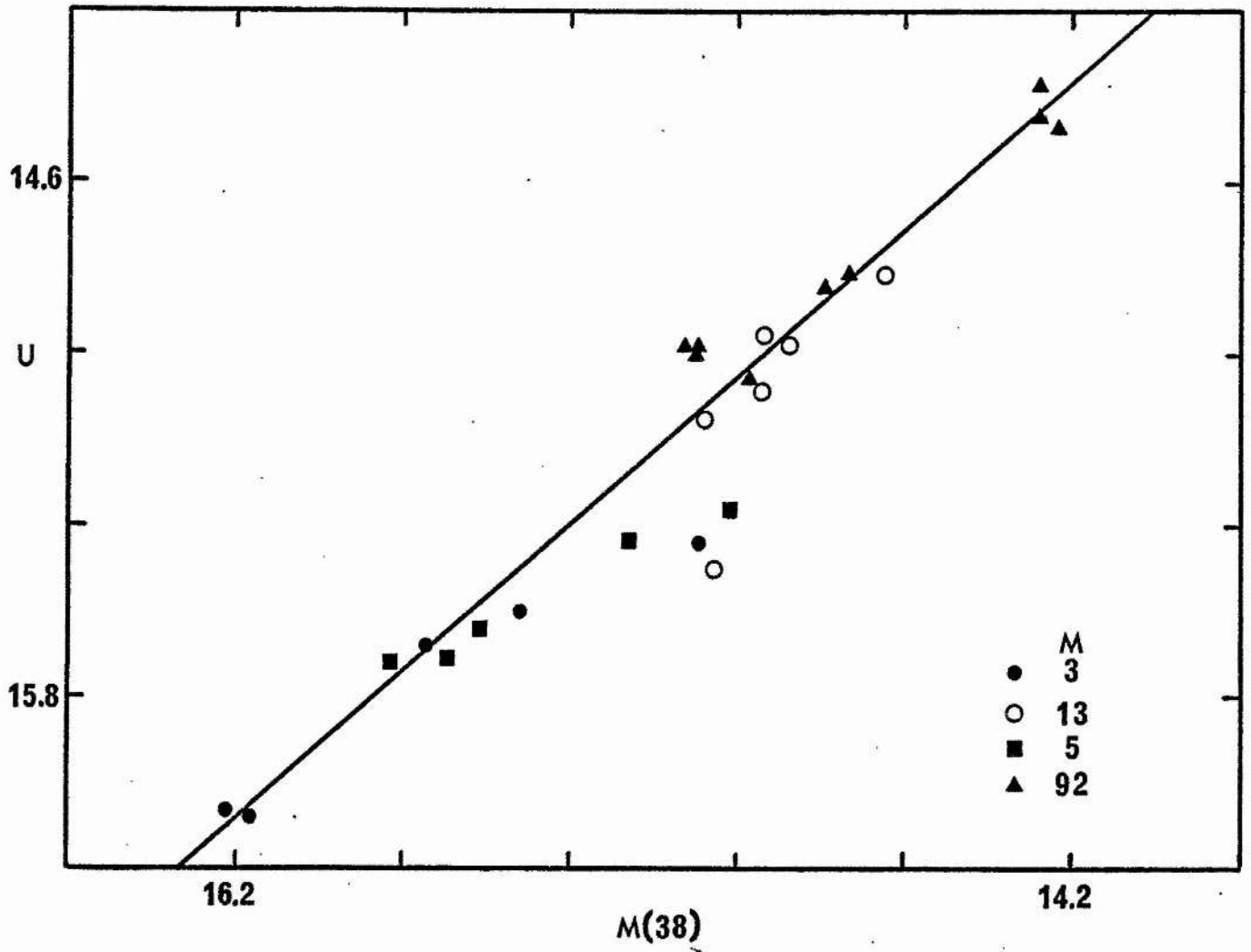

Figure 7

Calibration of the m(38) magnitude using the broad-band U magnitude

scheme is employed to obtain the final function. In Figures 3 - 6 the solid line is the function fitted by this program. For the uncertainties ascribed to each observation we have used Osborn's estimates for the DDO magnitudes and have estimated an error for the B values after considering the method of observation and the number of observations made. The absolute values of the errors may not be correct but it is expected that their relative values will be. All stars in Osborn's list were used in the calibrations except for stars 559 and 551 which were omitted in the m(41) plot since they are known to have strong CN absorption. The functions fitted to the data are given below.

$$m(41) = 9.352 + 0.011716\ B + 0.029274\ B^2$$

$$m(42) = 6.797 + 0.30280\ B + 0.020927\ B^2$$

$$m(45) = 8.089 - 0.11356\ B + 0.040117\ B^2$$

$$m(48) = 12.273 - 1.01961\ B + 0.076840\ B^2$$

Armed with these calibrations, we are in a position to calculate a predicted DDO magnitude for each star whose B magnitude is known. Clearly for individual stars this will not be very meaningful, but averaged over a few dozen stars we might expect the calculated magnitudes to enable us to derive a calibration curve for the photographic data, so that the final results will be very nearly linear.

The original photographic observations covered the clusters M 5, M 13, M 15 and M 92. For M 5 and M 13, these data have now been superceded by electronographic observations to be described later and consequently will not be considered further. Before we can utilise the calibrations of Figures 3 - 6, we require B magnitudes for the programme stars. For M 92 these were available from Sandage and Walker's (1966) photometry. For the majority of stars in M 15, only Arp's (1955) data were available. To obtain B magnitudes from these we have used the transformation (Arp, 1962)

$$B = m_{pg} - 0.16(CI) + 0.23$$

A subsequent comparison between these magnitudes and those given for some of the stars by Sandage (1970) showed that the transformed magnitudes were, on the whole, 0.12 magnitudes too bright and so they were corrected accordingly.

5.3 Observations

All of the photographic observations were obtained at the F/5.6 prime focus of the 36" Crossley reflector of Lick Observatory. The direct camera holds $3\frac{1}{4}$" x $4\frac{1}{4}$" plates and focussing is by means of a knife-edge inserted in place of the plate holder. The focus is usually determined with the filter in place, but in this case it was found that only with the very brightest stars was it possible to do the knife-edge focussing through the DDO filters. The method used was to determine offsets for each filter focus from the clear focus reading. This was done using αLeo (V = 1.3). The offsets determined are given in Table III. Since the values change very slowly with F ratio these values can be applied to other telescopes.

Table III

Filter	Offset (ins)	Thickness (mms)
41	0.184	13.6
42	0.181	13.6
45	0.180	13.6
48	0.187	14.2

When observing a cluster, the clear focus would be determined by observing a bright nearby star chosen from the ephemeris and the appropriate offset applied. The telescope was refocussed before observing a new cluster and every two hours or so if only one cluster was being

observed. Since the Crossley mirror was apt to show astigmatism at times, the focus was determined each time in the N-S and E-W directions and the mean value adopted. Two offset guide eyepieces were available, one on either side of the main beam, so with the main object centred, a systematic search for a guide star could be made. Most of the observations were taken during the bright of the moon, but, due to the narrow pass-band of the filters, the background density on the plates was still low. Indeed, the only disadvantage of the bright moon was that it made finding a guide star and guiding on the very comatic image somewhat more difficult. The photographic plates used were standard 103aD and 103aO. They were preflashed, developed in D19 for four minutes at 68° F with constant agitation, rinsed in dilute acetic acid, fixed for fifteen minutes and washed for at least forty-five minutes. A final rinse in photoflo ensured evenness in the drying.

5.4 Reduction for plates of M 15

A journal of the photographic plates obtained of the globular cluster M 15 is given in Table IV. These plates were measured at St. Andrews using the method of image scanning on the Joyce-Loebl, followed by profile fitting to the data. The resultant magnitudes were calibrated against the calculated magnitudes as described. Typical calibration curves derived by the program for a plate in each colour are illustrated in Figures 8 - 11. Figure 12 shows the intermediate step in the reduction of plate CD 1925 where the image-density magnitude is plotted against the dispersion of the profile. Since the images measured here only cover a range of about two magnitudes, this calibration is not as certain as the example illustrated earlier, though, in view of the earlier results, this step in the reduction procedure was retained. The magnitudes obtained with each of the four longer wavelength filters were then averaged and

TABLE IV

Observations of M 15

Plate No.	Filter	Emulsion	Start (UT 1974)		Exposure (mins)	Hour Angle End
CD 1923	41	103aO	1010	15 July	30	0-40 W
CD 1924	41	103aO	1049	15 July	30	1-20 W
CD 1925	41	103aO	1121	15 July	26	1-50 W
CD 1903	42	103aD	0926	10 July	27	0-25 E
CD 1907	42	103aD	0908	11 July	45	0-25 E
CD 1908	42	103aD	0957	11 July	45	0-24 W
CD 1922	42	103aO	0917	15 July	30	0-15 E
CD 1909	45	103aD	1103	11 July	15	0-56 W
CD 1920	45	103aO	0835	15 July	15	1-15 E
CD 1921	45	103aO	0855	15 July	15	0-55 E
CD 1917	48	103aD	0740	15 July	10	2-10 E
CD 1918	48	103aD	0805	15 July	10	1-45 E
CD 1919	48	103aD	0819	15 July	10	1-30 E

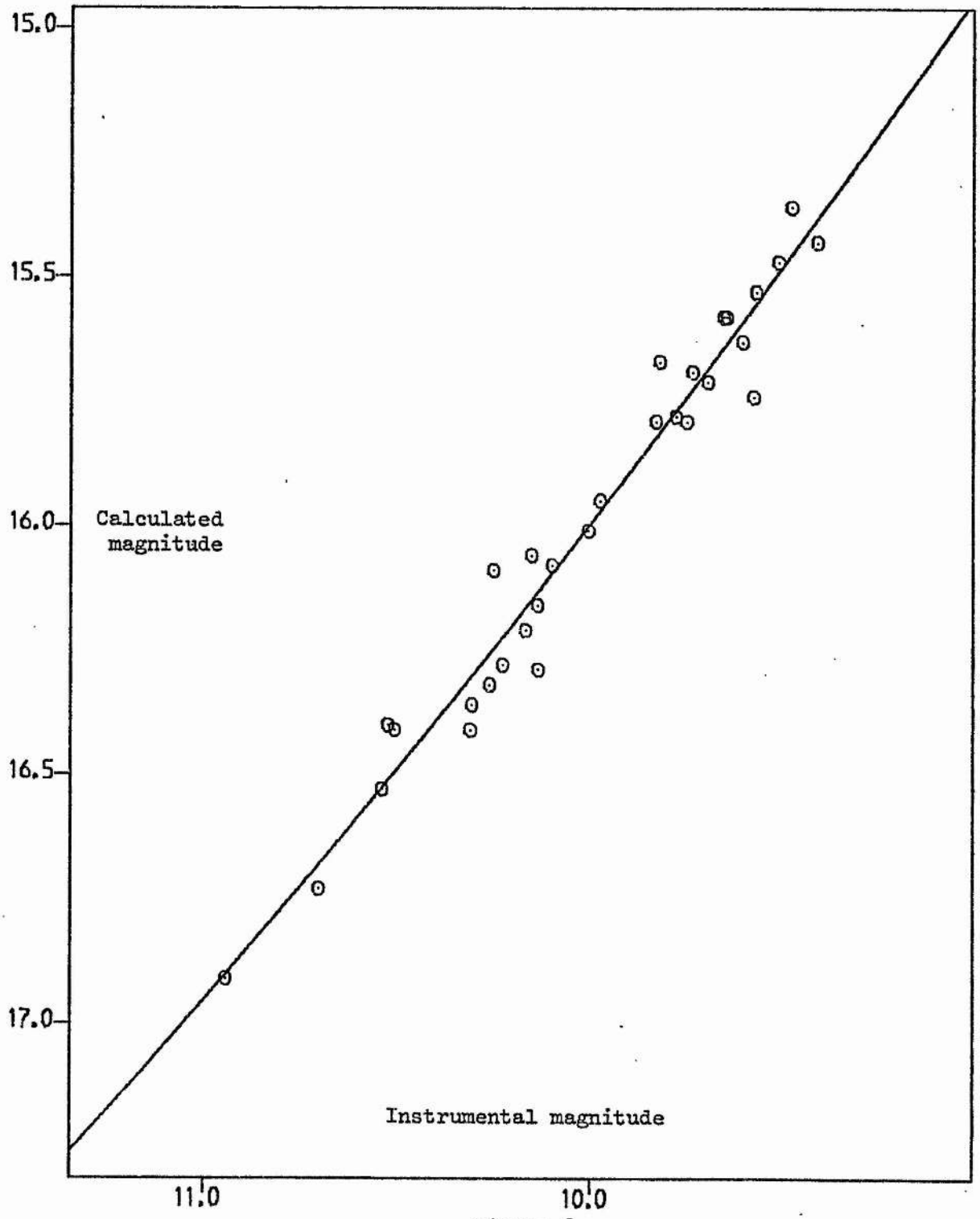

Figure 8
Calibration curve for m(41) from plate CD 1925 of M 15

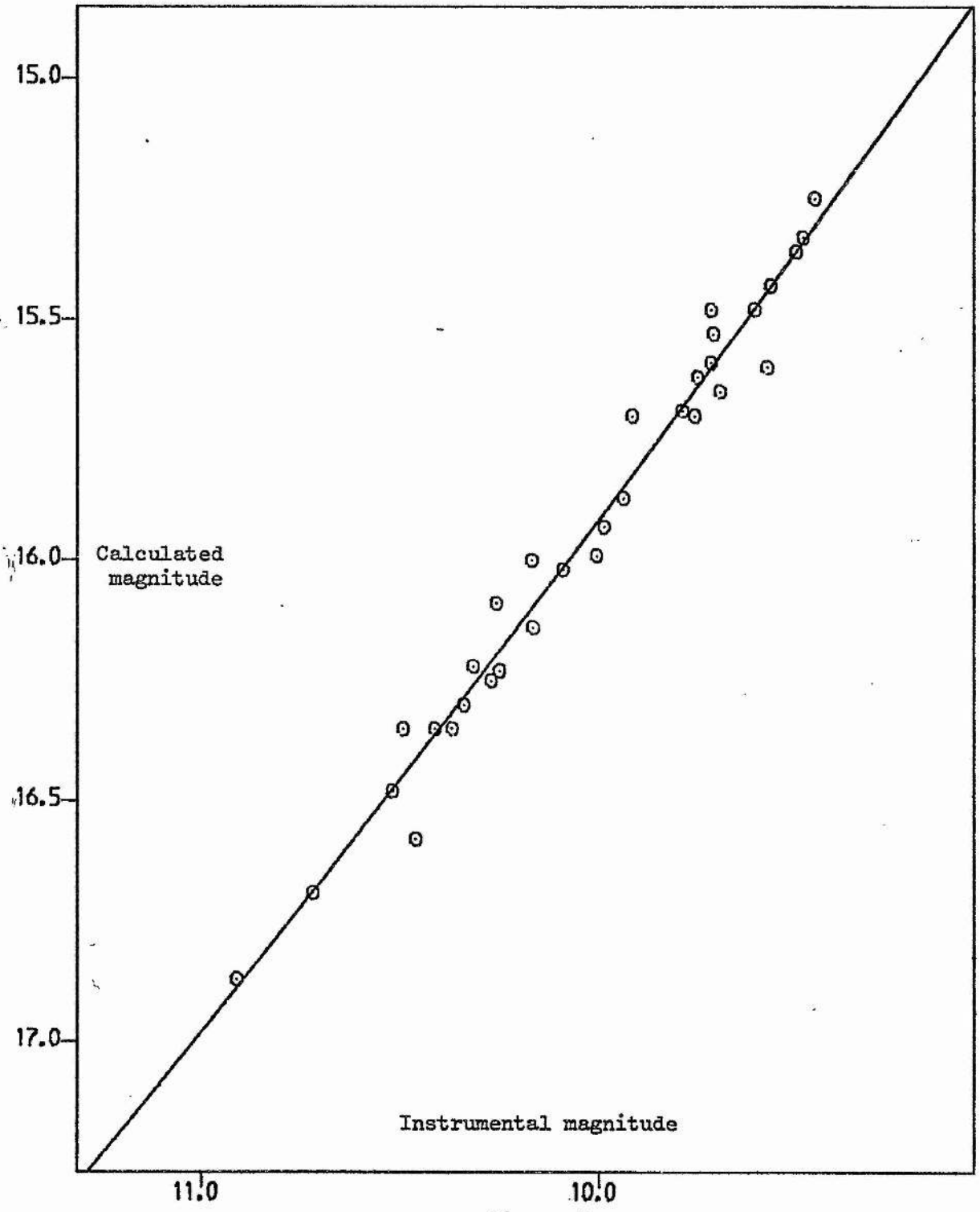

Figure 9

Calibration of m(42) from plate CD 1908 of M 15

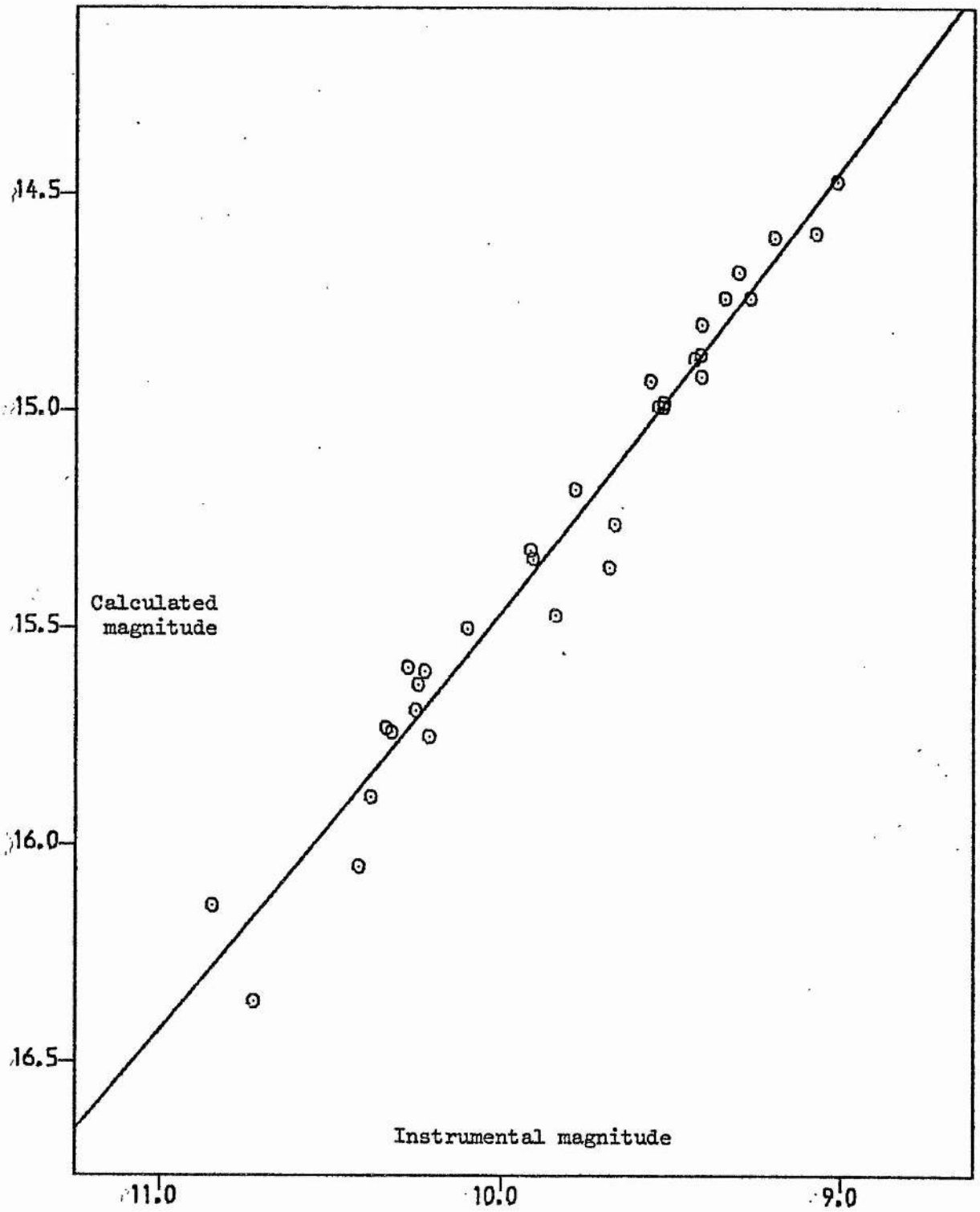

Figure 10

Calibration of m(45) from plate CD 1921 of M 15

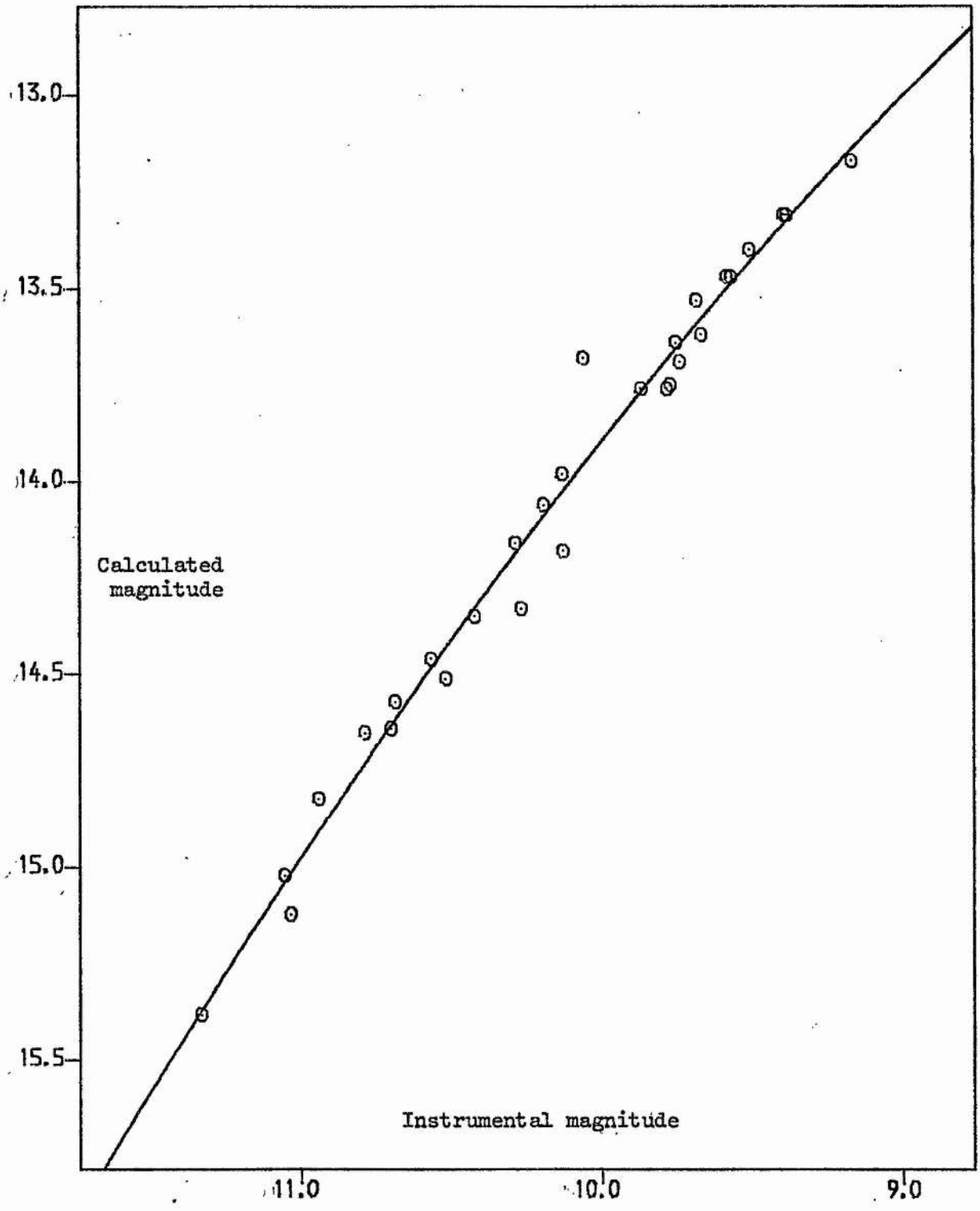

Figure 11

Calibration of m(48) from plate CD 1918 of M 15

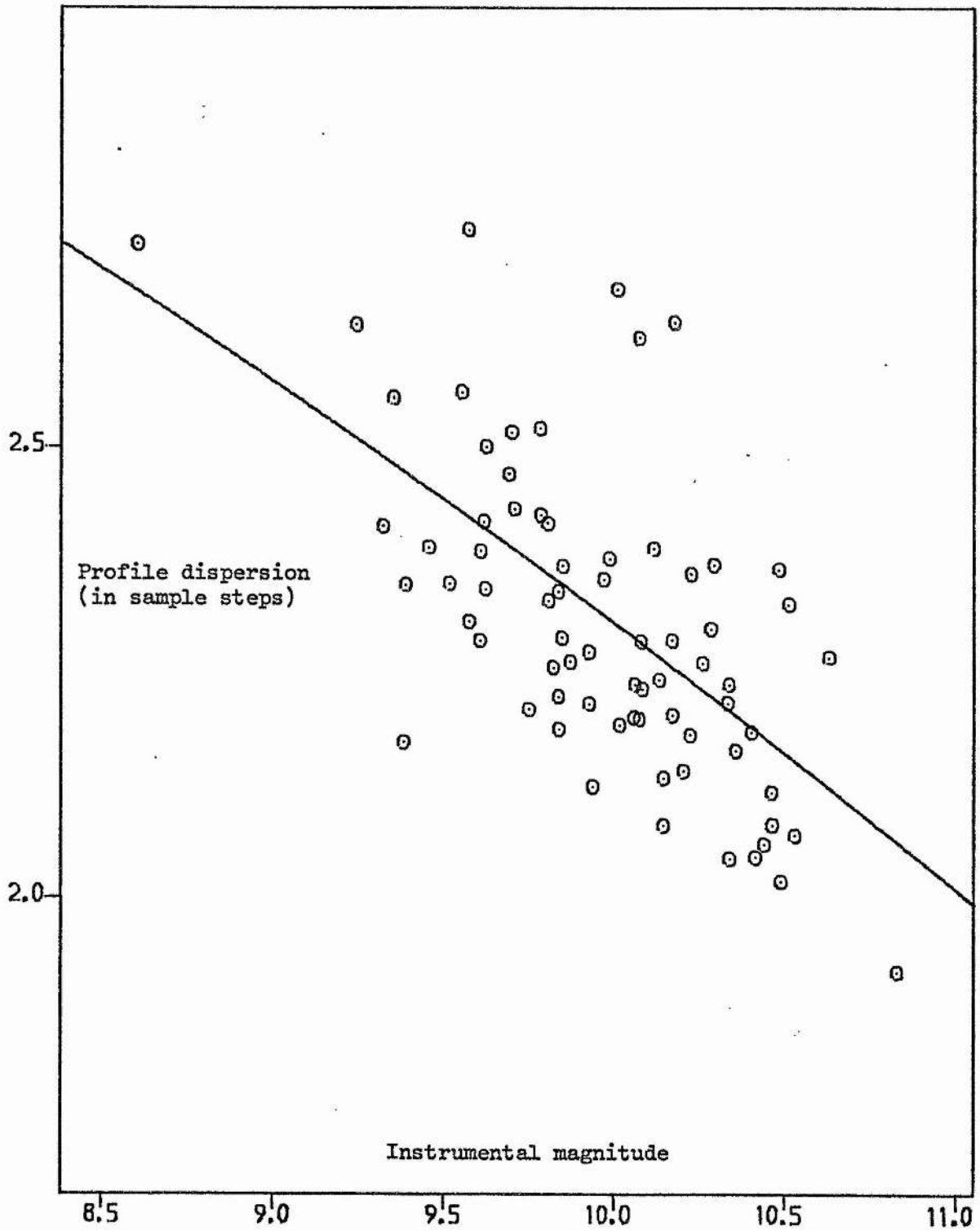

Figure 12

Calibration of the dispersion on plate CD 1925

the relevant colours formed. These are the CN band index C(4142), the temperature index C(4245) and C(4548), the gravity sensitive parameter. We are thus in a position to construct temperature-gravity (T-g) and CN band strength plots for the stars observed. The standard lines for luminosity classes Ib, III and V in the T-g plane have been given by Osborn (1971). Before a comparison between these lines and our data can be given, however, account has to be taken of the metal deficiency and reddening of the cluster. Osborn (1971) has derived blanketing coefficients for the relevant DDO colours. As these are luminosity class dependent, in order to be able to correct a given star's colours an initial approximation to its luminosity class must be known. To circumvent this difficulty, we have chosen instead to deblanket the standard lines, while at the same time applying the cluster reddening. For this we adopt a reddening of E(B-V) = 0.12 (Sandage, 1970) which implies reddening in C(4245) and C(4548) of 0.03 and 0.04 magnitudes respectively. Various estimates for the metal abundance of M 15 are available. All indicate an extreme metal deficiency of about $\left[\mathrm{Fe/H}\right] = -2.0$ and, as this agrees well with a recent determination by Butler (1974) using scanner observations of RR Lyrae stars, we have used this value to correct the colours of the standard luminosity class lines. If our deduced DDO colours are correct, then the data should coincide with the standard lines. When plotted, the agreement was surprisingly good with the expected trends in the data readily apparent.

The scatter of the points was, however, somewhat larger than had been hoped and this suggested that a remeasurement of the plates might be worthwhile. This was performed on the GALAXY machine in use at the RGO and a brief synopsis of the measurement procedure follows. The GALAXY machine can operate in either of two modes (Murray and Nicholson, 1975), search or measure. In the search mode, the plate is scanned within

specified limits and the positions of all images found above a given threshold limit are recorded. Later, using these positions, in measurement mode, the machine can return to the images and measure their position and density accurately enough for both astrometry and photometry. Since the programme stars here numbered only about one hundred, a complete search would have been wasteful and we therefore produced the rough positions of the relevant stars by measurement on the Zeiss two-coordinate measuring machine. These positions were then transferred to a disc file on the Nova minicomputer controlling the GALAXY, to be used later in the measurement mode. To obtain the transformation between the Zeiss and GALAXY coordinates, three bright stars on each plate were measured on the Zeiss and these were then found manually on the GALAXY prior to measurement. Several optics are available for the GALAXY, their use depending on the image scale of the plate. Some initial runs were made with the x75 optic, although the accuracy achieved with this turned out to be inadequate and subsequent measures employed the x240 lens. GALAXY performs photometry by obtaining a scan of the image and then matching the slope of the profile sides to that of a set of preloaded profiles. It outputs the parameter of the profile best matching that of the observed image. The plates were calibrated against the calculated DDO magnitudes using a least-squares routine and magnitudes and colours derived as previously.

Due to the novelty of the first reduction technique, it is perhaps instructive to compare the two sets of results. Comparisons of the C(4245) and C(4548) data are shown in Figures 13 and 14. The overall agreement is good. The standard deviation of the points from the 45° line in Figures 13 and 14 is 0.04 magnitudes. There are a number of points in Figure 14 which fall significantly below the line i.e. the Joyce-Loebl colour is larger than the GALAXY measure. In most cases, this is attributable to one magnitude being significantly different,

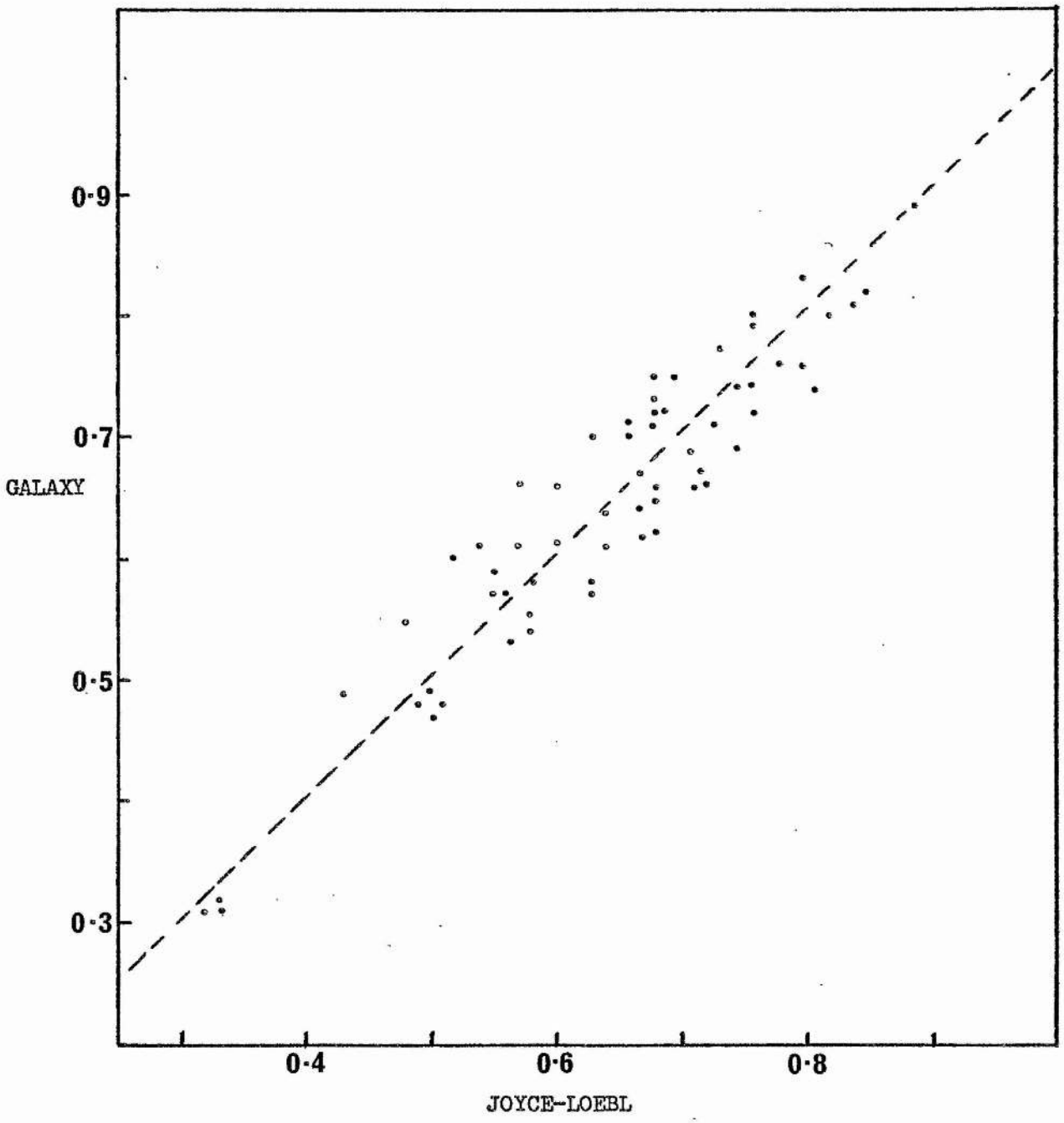

Figure 13

A comparison of C(4245) obtained by different reduction techniques

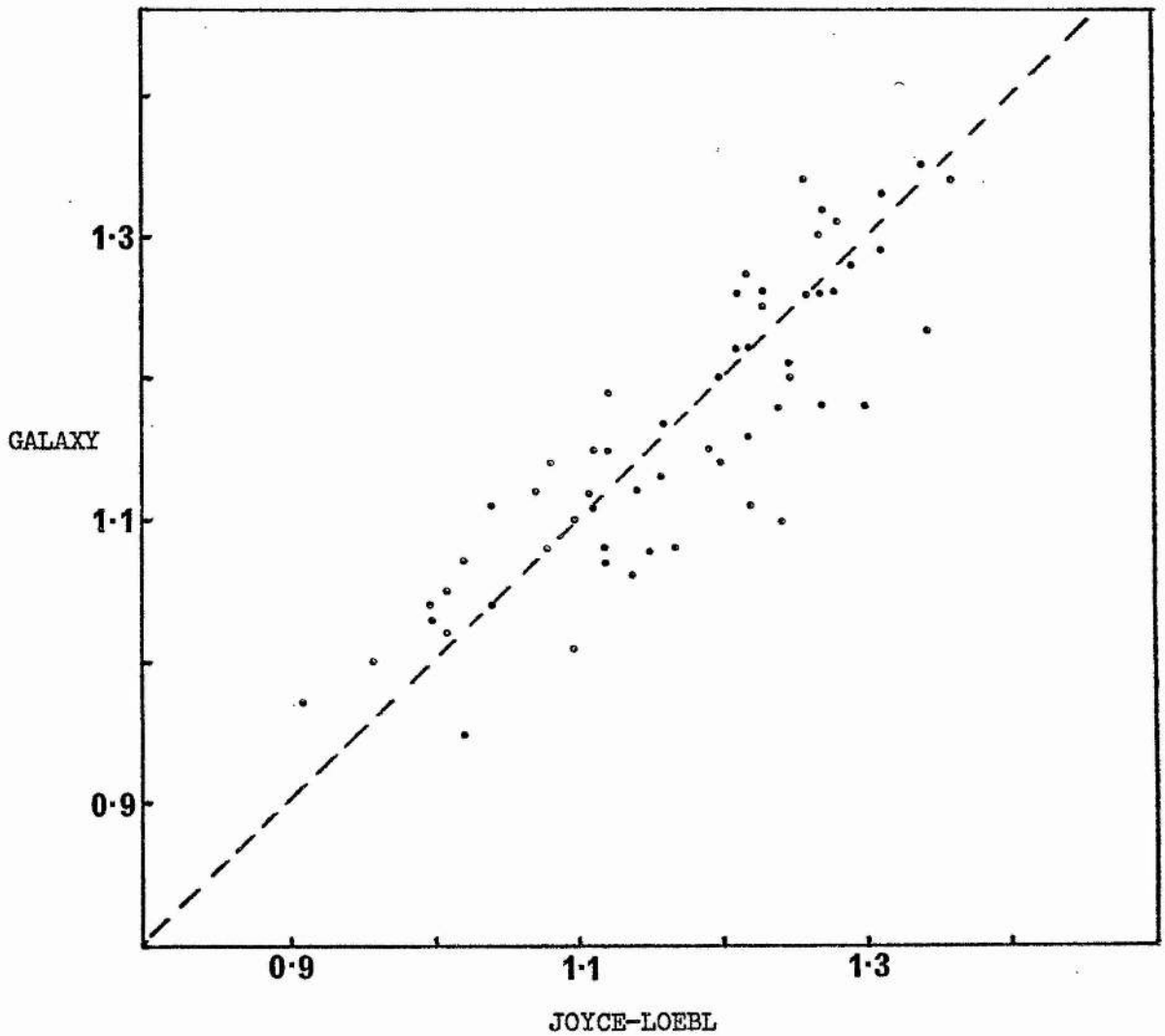

Figure 14

A comparison of C(4548) obtained by different reduction techniques

though the cause of this is uncertain as the individual plate measures are in accord. However, in view of the general agreement, we have averaged the colours obtained by the two methods to yield the final results. All of the brighter stars in the cluster which were within the photometric field and visible on both the '41' and '48' plates were measured. These are shown in Figure 15 which is a reproduction of plate CD 1925. The sequence of measurement by both methods is also indicated. Some of the stars were later identified from the photometry as being blue horizontal branch or variable stars and so the results for these and for the stars with discordant colour measures are omitted from Table V, which gives the final colours for the remaining programme stars. Where a former identification for the star is given by Arp (1955) or Sandage (1970), this is shown in column two.

5.5 Results

In Figure 16 we have plotted the T-g diagram from the data obtained on M 15. The data points agree surprisingly well with the calculated standard lines, considering the uncertainties inherent in the calibration procedure. At the lower temperatures, that is the upper end of the giant branch, a luminosity class of Ia-b is indicated, while this changes as expected to class II - III as we proceed down the giant branch. There appears to be a fairly well defined group of stars falling below the luminosity class III line. We have added to the diagram the unreddened standard line for luminosity class V stars of solar abundance. The agreement of this line with the aforementioned stars reinforces the suspicion that these are foreground field dwarfs. From a check on the individual magnitudes of the stars it does seem that the observed deviations from the cluster sequences are significant. The stars in this group are numbers 1, 3, 13, 14, 20, 21, 33 and 35 and clearly spectroscopic

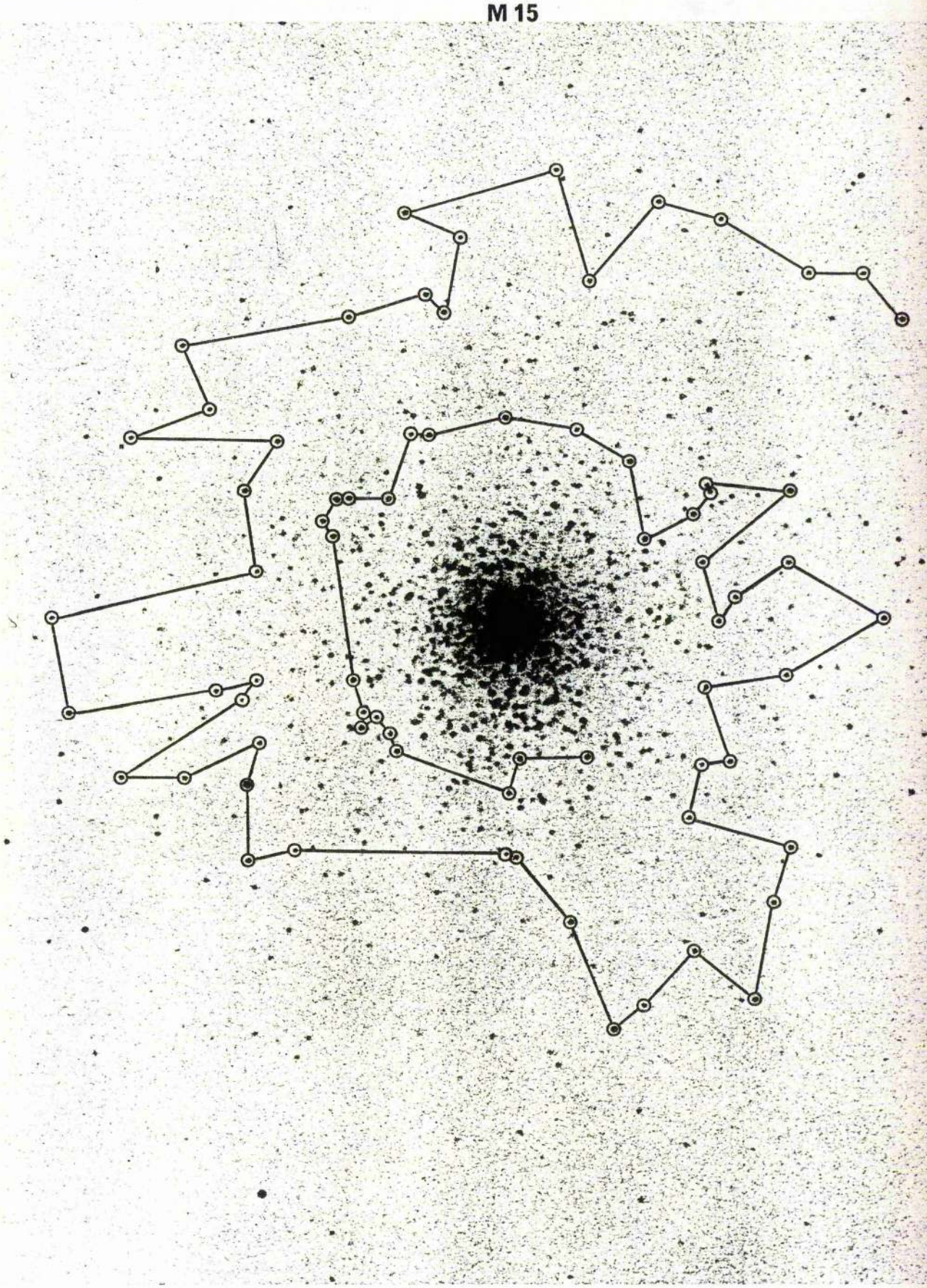

Figure 15

The stars observed in M 15

TABLE V

Colours of stars observed in M 15

	Star	C(4142)	C(4245)	C(4548)
1		-0.07	0.75	0.98
2		0.07	0.67	1.13
3		0.07	0.70	1.08
4		0.01	0.63	1.11
5		0.11	0.58	1.11
8		0.10	0.78	1.35
10	S1	0.03	0.81	1.29
11	S3	0.08	0.74	1.22
12		0.02	0.70	1.20
13		-0.07	0.65	0.98
14		0.09	0.66	1.03
15		0.08	0.54	1.10
16	II-64	0.08	0.78	1.23
17	II-75	0.17	0.74	1.30
20		0.00	0.65	1.04
21	III-8	-0.02	0.98	1.05
24		0.11	0.58	1.24
25		0.06	0.72	1.22
26		0.09	0.56	1.13
28	S7	0.05	0.67	1.28
29		0.05	0.56	1.07
32		0.03	0.70	1.14
33		-0.05	0.61	1.02
35	S23	0.00	0.89	1.10
36	S8	0.06	0.72	1.26
37		0.10	0.52	1.11
38		0.04	0.57	1.23
39	IV-48	0.06	0.57	1.09
40	IV-30	0.06	0.56	1.11
41	IV-29	0.15	0.59	1.20
42		0.04	0.73	1.16
43		0.06	0.70	1.24
44		0.08	0.78	1.26
45	I-74	0.07	0.67	1.17
46	I-41	0.08	0.65	1.16
47	I-38	0.00	0.60	1.21
48	I-43	0.08	0.68	1.17
50	I-56	0.20	0.56	1.12
51		0.09	0.65	1.11
52	I-50	0.06	0.71	1.19
53		0.08	0.72	1.30
54	I-12	0.15	0.77	1.35
55	I-63	0.09	0.68	1.04
57	II-42	0.12	0.67	1.30
58	II-40	0.08	0.48	1.17
59		0.06	0.82	1.22
60	II-31	0.07	0.83	1.24
61		0.12	0.77	1.30
62	II-30	0.16	0.67	1.22
63	II-29	0.15	0.69	1.32

TABLE V - continued

	Star	C(4142)	C(4245)	C(4548)
64	III-14	-0.01	0.49	1.10
65		0.10	0.54	1.14
66	III-27	0.07	0.69	1.25
67	III-26	0.00	0.50	1.10
69	III-48	0.03	0.75	1.27
70	III-83	0.08	0.62	1.17
71		0.13	0.69	1.23
72	IV-38	0.18	0.81	1.37

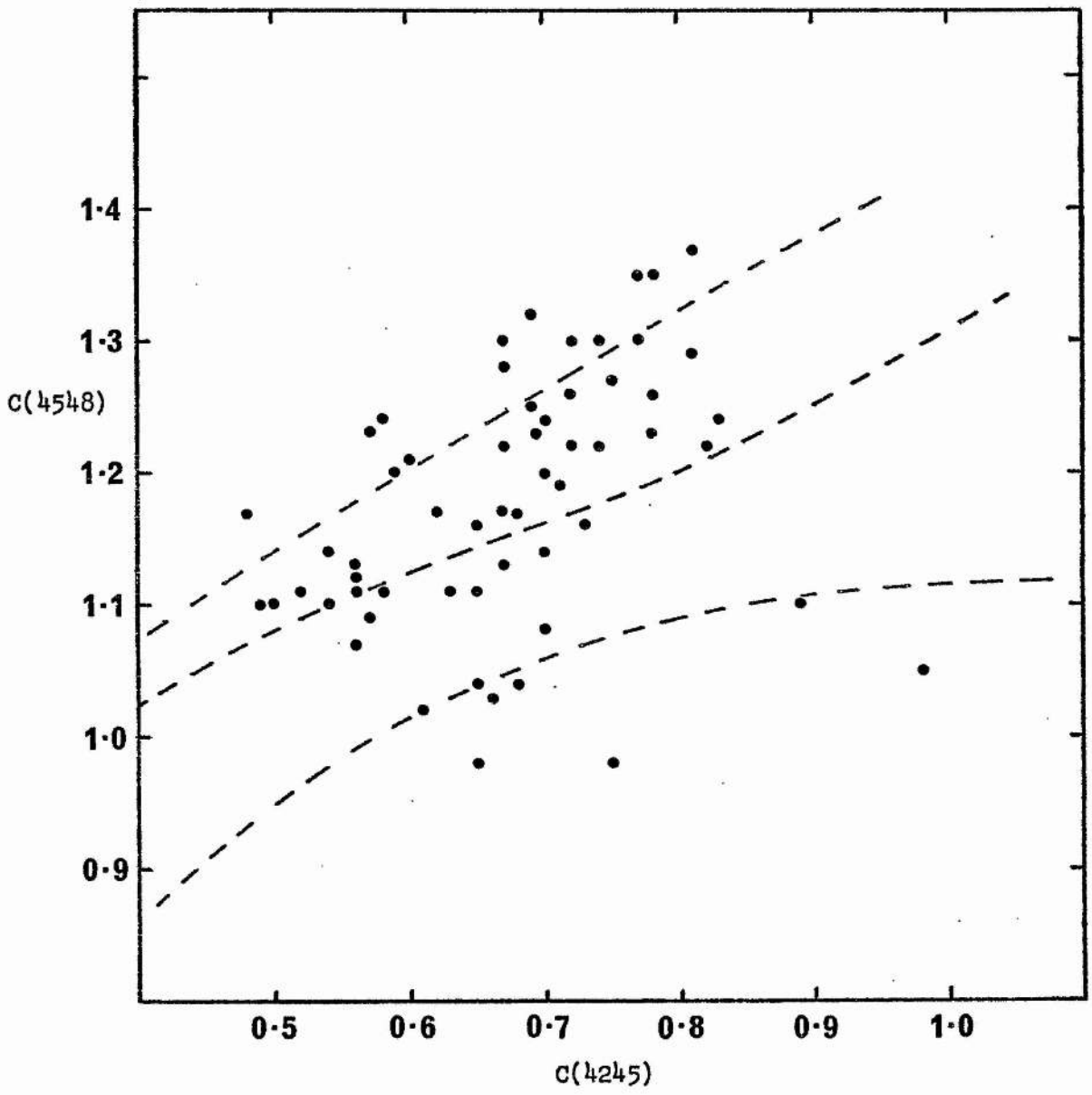

Figure 16

The temperature-gravity plot for M 15

observations would be desirable to investigate the accuracy of this classification.

Sandage (1970) lists several stars as being field stars, but it is clear from a colour-magnitude and two-colour diagram plotted with his data that his classification rests solely on the basis of their deviation from the cluster sequences. Since the discovery, for example, that many bright blue stars seen in the C-M diagram of globulars are indeed members (Strom et al, 1970; Zinn et al, 1972) these criteria should perhaps be viewed with suspicion. Equally, there are certain to be field stars whose broad-band colours place them fortuitously in coincidence with the cluster sequences. We suspect that such a star is number 35 (S23) which falls exactly on Sandage's (1970) fiducial giant branch. Osborn (1971) has demonstrated a tight correlation between (B-V) and C(4245) for the different luminosity classes and this provides a means of checking the observed C(4245) colours. To use the largest sample of stars we could employ Arp's (1955) colour index (CI) in place of (B-V), but such a plot shows a disappointingly large scatter. Recently Lloyd-Evans (1975) has demonstrated that early measurements of CI, when compared to modern (B-V) values are liable to show errors of typically 0.1 - 0.2 magnitudes. More precise values of (B-V) are available from the photometry of Sandage (1970), though only for a few stars. The plot of (B-V) against C(4245) is shown in Figure 17. The two reddest stars, numbers 17 and 54 (open circles), deviate from the sequence, possibly indicating an error in the C(4245) calibration for the very red stars, though their position in Figure 16 is not anomalous. Star number 35 is shown by a filled square and again, lying 0.2 magnitudes to the red of the cluster sequence, coincides with the luminosity class V position. We note, however, that an error in the '45' magnitude could be responsible for its position in both Figures 16 and 17.

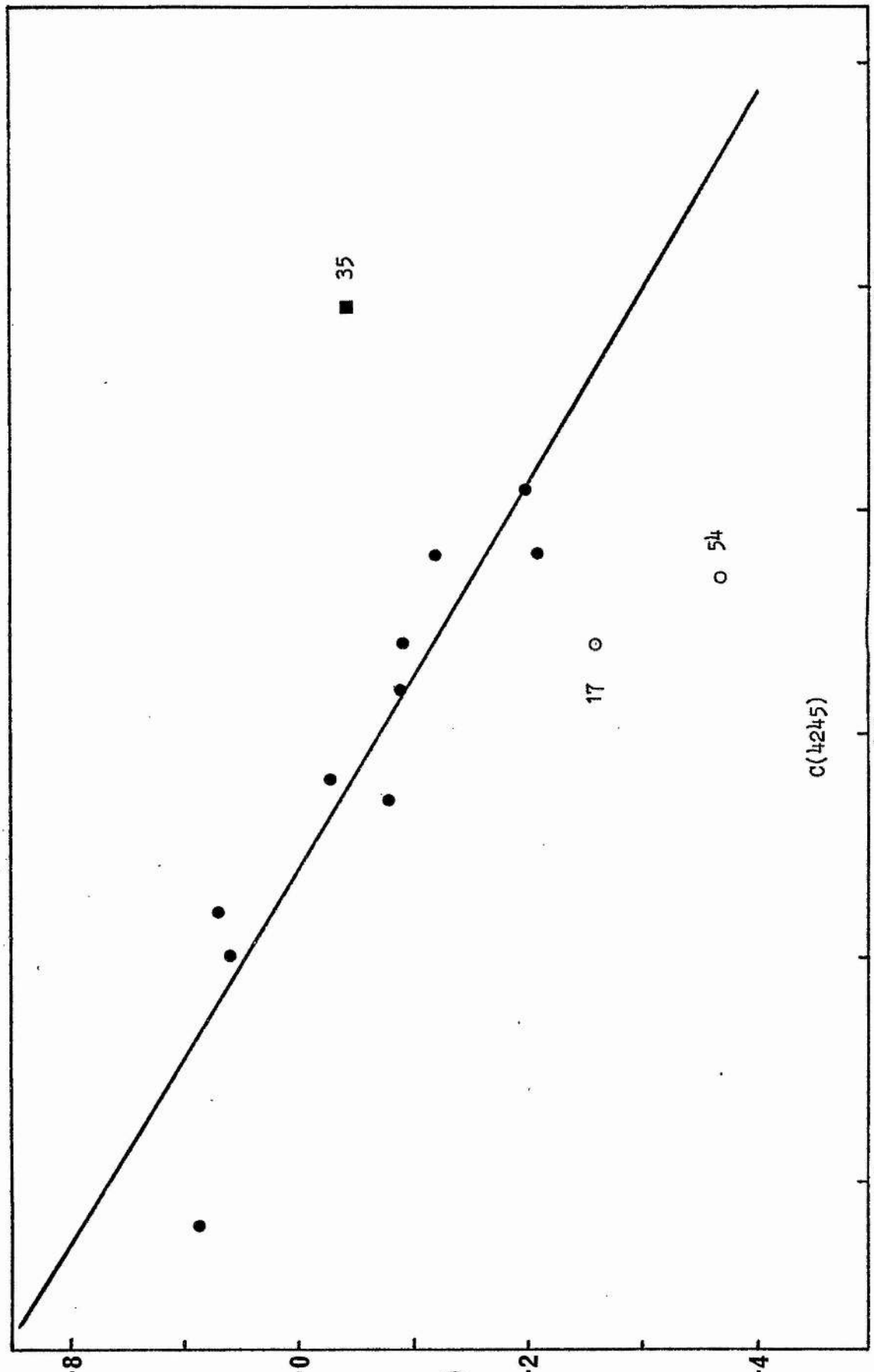

Figure 17. The relation between (B-V) and C(4245)

When these reductions had been completed, independent evidence for the identification of stars 35 and 21 as field stars became available. Cudworth (1976), in an astrometric study of the cluster, found that the proper motion gave an excellent membership criterion and concluded that stars 35 and 21 are indeed non-members. It is therefore clear that this kind of photographic survey using the DDO system is capable of a high success rate in distinguishing members. This is not altogether a trivial matter, since the number of stars observed on each sequence of the C-M diagram is related to the time scale of evolution at that stage and for the red giant and horizontal branches this has been related by stellar models to the helium content of the cluster (Iben et al, 1969; Demarque et al, 1972). These attempts so far have led to values for the helium content somewhat lower than other methods (variables, planetary nebula, etc.), but this at worst says something about the stellar models. The ability to correct the C-M diagram relatively easily for the presence of field stars is a necessary step in using this technique.

From the data in Table V we may also plot the C(4142) - C(4548) diagram. In Population II stars the 0-1 CN band at 4215A is normally too weak to measure, although the band strength does increase sharply with decreasing gravity (Schadee, 1968). The standard sequence line thus rises sharply at large values of C(4548). The diagram plotted from our data is shown in Figure 18. The C(4548) axis has been fitted as calculated, but a shift in the ordinate between the data and standard line (Osborn, 1971) was needed to bring the two into coincidence. Osborn's data indicate that there is an intrinsic scatter in the ordinate of this diagram of the order of 0.05 magnitudes and so the appearance of Figure 18 is considered satisfactory, especially since the increase of C(4142) with decreasing gravity is shown. Of particular interest is star number 50 (I-56) which is seen to stand above the expected sequence. Allowing

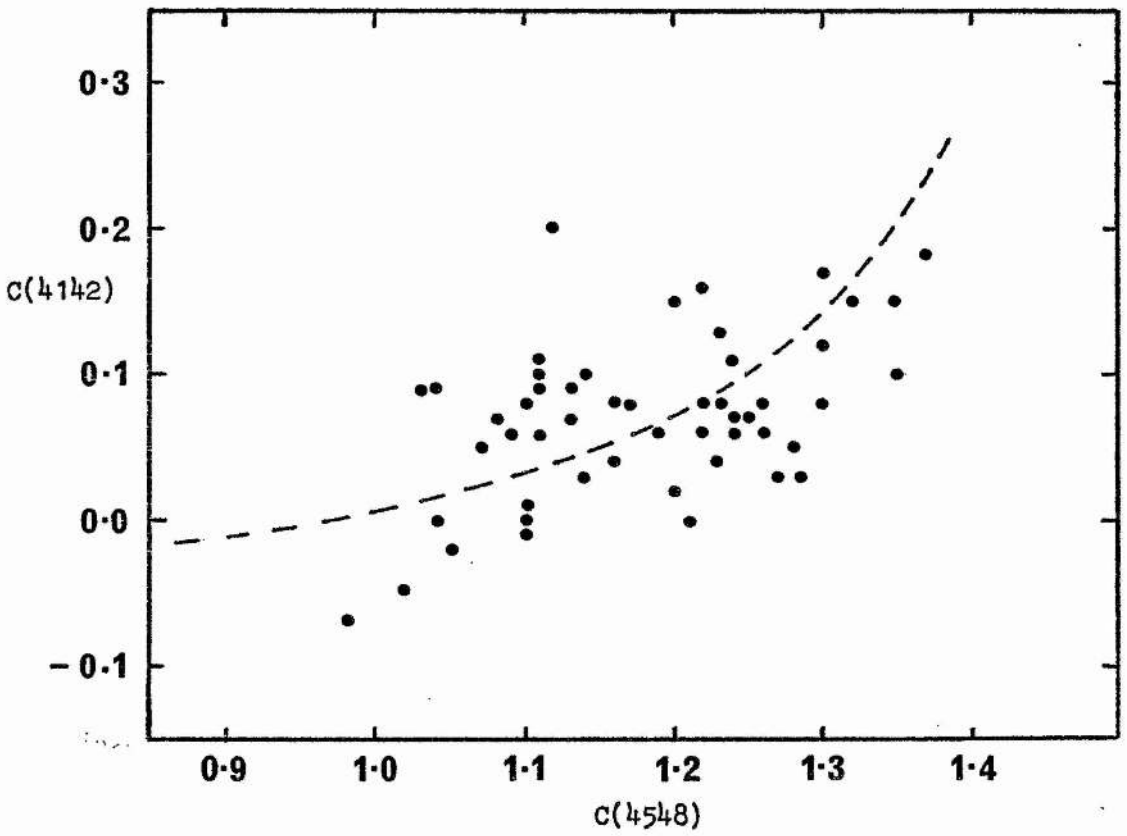

Figure 18

The CN-band strength plot for the red giants in M 15

for errors of ±.05 magnitudes in each colour, the deviation is still marginally significant. The deviation is in the correct sense for the star to have an anomalously strong CN band similar to those found by Osborn. From the star's position in the C-M diagram of M 15, its absolute magnitude is somewhat less than the other CN strong stars. Furthermore, from a sample of this number of stars, one might argue that statistically one star might be found this far from the general sequence. Clearly, a spectroscopic investigation would be worthwhile.

The photographic observations of stars in M 92 were obtained and reduced in exactly the same manner as described for M 15. The quality of the plates was somewhat lower however and the results less satisfactory in terms of the agreement between the two reduction methods and the scatter in the final diagrams. In general, the conclusion that this is an efficient means of determining cluster membership stands. In particular, star IX-81 (which is a known radial velocity non-member - Zinn, 1973) fell on the luminosity class V sequence, as did stars XI-50 and XI-14. The former of these was also categorised as a field star by Sandage and Walker (1966) from UBV photometry.

One observation for which a quick survey such as this will be useful is in the study of NGC 6273. This cluster has a highly elliptical form and Bessell and Norris (1976) have suggested that the associated angular momentum may well have affected the structure of individual stars to the extent where mixing may be important in the later stages of evolution. As this is one possible explanation for the anomalous abundances observed in the ωCen giants, which cause the cluster to have an intrinsically wide giant branch, Bessell and Norris have suggested that the C-M diagram of NGC 6273 may well exhibit the same feature. Harris et al (1976) have obtained the C-M diagram of this cluster, but the result is unsatisfactory due to the presence of many field stars.

We propose that observations along the lines described here will easily be able to separate the field dwarfs and that observations of the CN band strength and/or the UV excess will distinguish the giants of the nuclear bulge, allowing the true nature of the cluster's red giant branch to be observed.

References

Arp, H., 1955. A.J., 60, 317.

Barker, D. R. & Diana, L. M., 1974. Amer. J. Phys. 42, 224.

Bessell, M. & Norris, J., 1976. Preprint.

Butler, D., 1974. Thesis, University of California.

Clutton Brock, M., 1967. Technometrics, 9, 261.

Crawford, D. L., 1961. A.J., 66, 281.

Cudworth, K. M., 1976. A.J., 81, 519.

Demarque, P., Sweigart, D. & Gross, P. G., 1972. Nature Phy. Sci., 239, 85.

Harris, W. E., Racine, R. & de Roux, D., 1976. Ap. J. Suppl., 31.

Iben, I., Rood, R. T., Strom, S. E. & Strom, K. M., 1969. Nature, 224, 1006.

Johnson, H. L. & Morgan, W. W., 1953. Ap. J., 117. 313.

Lloyd Evans, T. L., 1975. Mon. Not. R. ast. Soc., 171, 647.

McClure, R. D., 1976. A.J., 81, 182.

McClure, R. D., & Bergh, S. van den, 1968. A.J., 73, 313.

Murray, C. A. & Nicholson, W., 1975. Image Processing Techniques in Astronomy. D. Reidel Pub. Co., Dordrecht. Pg 171.

Newell, E. B., Rodgers, A. W. & Searle, L., 1969. Ap. J., 156, 597.

Osborn, W. H., 1971. Thesis, Yale University.

Philip, A. G. D., 1972. Ap. J. (Letters), 171. L51.

Philip, A. G. D., 1973. Ap. J., 182, 517.

Sandage, A., 1970. Ap. J., 162, 841.

Sandage, A. & Walker, M. F., 1966. Ap. J., 143, 313.

Schadee, A., 1968. Ap. J., 151, 239.

Strom, S. E., Strom, K. M., Rood, R. T. & Iben, I., 1970. Astr. & Astroph., 8, 243.

York, D., 1966. Canadian J. Phys., 44, 1086.

Zinn, R. J., 1973. Astr. & Astroph., 25, 409.

Zinn, R. J., Newell, E. B., & Gibson, J. B., 1972. Astr. & Astroph., 18, 390.

CHAPTER 6

INTERMEDIATE BAND ELECTRONOGRAPHY OF M 5 AND M 13

6.1 Introduction

In the previous chapter, we described the results of a photographic survey of M 15 using the DDO photometric system which was obtained as a backup programme when electronographic observations at that time proved no longer feasible. Nevertheless, we still wished to obtain electronographic observations, both for the astronomical goals described previously and to investigate the feasibility of intermediate band electronography for such a programme.

In April and June 1976, time was allocated to obtain this data using the 4 cm McMullan camera at the South African Astronomical and Wise Observatories. The observing run at the former was a complete failure due to inclement weather and equipment problems. (We did however obtain one exposure of ωCen with the '48' filter, which was important at the time, since we believe it to be the first such observation!) The observing at the Wise Observatory was fortunately more successful and observations were obtained on six and a half out of seven nights allocated.

6.2 Observations

The McMullan camera, mounted at the F/7 Cassegrain focus of the Wise Observatory's 1-metre telescope has a usable field of approximately 20'. In this case, it was reduced somewhat since the interference filters had to be mounted at a distance of 10 cm from the focus, with the consequence that the outer three millimetres of the photocathode were vignetted. This still left sufficient usable field to contain the whole of the clusters under study. The necessity to mount the filters there was indeed not altogether undesirable, since one of the potential problems with using interference filters for two-dimensional stellar photometry is the possibility of the occurrence of variations in the filter characteristics across its area. Meaburn (1966) has investigated these effects, but

for much larger filters than those used here. He concludes that this is only likely to be a problem for filters with larger diameters than about 5 cm. The fact that the filters, when used for the electronographic exposures, were 10 cm from the focus implies that the stellar light was covering an annulus of diameter ~15 mm at the filter. This would considerably smooth out any small scale variations if they were present. A further indication that this is not a problem comes from inspection of the results taken when the positioning of the images was different for different exposures. There was no evidence that the internal scatter for the results from each position was less than that obtained when comparing the results from different positions.

The telescope was equipped with an offset guide eyepiece and, as there was no facility for viewing the main field directly, the use of the same guide star, with the guide eyepiece unmoved during the day, ensured the identical positioning of the field relative to the photocathode when this was required. Exposures were obtained primarily of two clusters, M 5 and M 13. A journal of these exposures is given in Table I. In order to calibrate the sensitivity of the cathode at the four wavelengths observed, exposures of the twilight sky were made. Details of these are given in Table II.

All of the films were developed according to the precepts given in Chapter 1. The only modification found necessary was that the developer had to be changed after processing of each batch of four films, because it clouded very rapidly after the development. The precise cause of this is not known, but it can probably be linked to the fact that the films are developed while still mounted on to plastic rings by a non-setting glue. Presumably, a reaction between the glue and developer is responsible.

Table I

Electronographic Exposures of M 5

Film No.	Filter (DDO)	Exposure (min)	Emulsion	UT Start (1976)		H.A. End
43	41	30	G5	June 17	19.14	0W29
44	41	30	G5	June 17	19.48	1W03
45	41	40	G5	June 17	20.22	1N48
46	41	40	G5	June 17	21.05	2W31
65	41	40	G5	June 18	19.29	0W58
66	41	40	G5	June 18	20.12	1W42
67	41	30	G5	June 18	21.09	2W28
27	42	20	G5	June 16	20.56	1W58
28	42	20	G5	June 16	21.20	2W22
29*	42	20	G5	June 16	21.44	2W46
40	42	20	G5	June 17	17.56	0E58
41	42	20	G5	June 17	18.20	0E35
42	42	20	G5	June 17	18.43	0E11
63	42	25	G5	June 18	18.32	0E14
64	42	25	G5	June 18	19.00	0W15
22	45	10	G5	June 16	19.34	0W25
23	45	10	G5	June 16	19.49	0W41
24	45	10	G5	June 16	20.05	0W57
25	45	10	G5	June 16	20.20	1W12
26	45	10	G5	June 16	20.39	1W31
61	45	10	G5	June 18	17.59	1E01
62	45	10	G5	June 18	18.14	0E47
1	48	10	L4	June 15	18.46	0E28
18	48	17	L4	June 16	18.07	0E54
19	48	15	L4	June 16	18.28	0E36
20	48	15	L4	June 16	18.47	0E16
21	48	15	L4	June 16	19.07	0W03
59	48	3	G5	June 18	17.48	1E20
60	48	3	G5	June 18	17.54	1E14

* Film badly scratched – exposure not reduced.

Table I (continued)

Electronographic Exposures of M 13

Film No.	Filter (DDO)	Exposure (min)	Emulsion	UT Start (1976)		H.A. End
97	41	40	G5	June 20	18.13	1E33
98	41	40	G5	June 20	18.56	0E50
99	41	40	G5	June 20	19.41	0E06
100	41	40	G5	June 20	20.25	0W39
101	41	40	G5	June 20	21.14	1W49
102	41	40	G5	June 20	22.18	2W32
87	42	25	G5	June 19	21.31	1W27
88	42	25	G5	June 19	21.59	1W55
89	42	25	G5	June 19	22.27	2W24
90	42	25	G5	June 19	22.56	2W53
91	42	25	G5	June 19	23.30	3W27
103	42	20	G5	June 20	23.01	2W55
81	45	10	G5	June 19	19.47	0E32
82	45	10	G5	June 19	20.00	0E20
83	45	10	G5	June 19	20.22	0W03
84	45	10	G5	June 19	20.40	0W21
85	45	10	G5	June 19	20.54	0W35
86	45	10	G5	June 19	21.07	0W49
92	45	15	G5	June 19	23.59	3W46
75	48	15	L4	June 19	17.50	2E24
76	48	15	L4	June 19	18.09	2E05
77	48	15	L4	June 19	18.27	1E47
78	48	15	L4	June 19	18.45	1E29
79	48	15	L4	June 19	19.09	1E05
80	48	15	L4	June 19	19.27	0E47

Table II

Twilight exposures reduced to obtain sensitivity corrections

Film No.	Filter	Emulsion	UT Start (1976)		Exposure (secs)
36	41	L4	June 17	17.05	15
55	41	L4	June 18	17.05	15
71	41	L4	June 19	17.05	15
37	42	L4	June 17	17.09	20
56	42	L4	June 18	17.09	25
72	42	L4	June 19	17.09	30
38	45	L4	June 17	17.12	20
57	45	L4	June 18	17.12	25
73	45	L4	June 19	17.12	25
39	48	L4	June 17	17.15	30
58	48	L4	June 18	17.15	30
74	48	L4	June 19	17.15	30

6.3 Reductions

The early electronographs obtained at Lick Observatory were always sealed between sheets of glass, using a cement of the kind used in bonding filters and lenses. Although inert in contact with glass, the cement was found to react with the developed grains of the electronographs, eventually rendering them unfit for measurement. The films obtained at the Wise Observatory were therefore left unmounted and, when measured, were held in place by a weighted piece of glass. This was somewhat unsatisfactory when large pieces of debris, embedded in the emulsion, held the glass sufficiently clear of the film for Newton's rings to form. This, though, was a relatively rare and localised effect which, when present, did not usually affect more than a single image. During measurement, sharp focussing of the whole 40 mm field was occasionally troublesome, but it was always found possible to focus the whole plate within the limits where the change in focus has a negligible effect upon the derived magnitudes.

From the number of exposures listed in Table I, it will be apparent that, as there were initially one hundred stars in M 5 and about one hundred and thirty in M 13 to be measured, it was necessary to employ an automatic reduction scheme of the kind described in Chapter 4. At the Royal Greenwich Observatory, a reduction process along these lines had been developed independently by A. J. Penny (1976) and, as it was geared to the use of existing hardware (a PDS microphotometer and PDP 11), we have employed this system to reduce our electronographs. The process is the same in concept as that described earlier, although the mechanics of measurement are different and will therefore be outlined briefly.

The reduction program runs on line and fits a two-dimensional Gaussian, with variable background level, to the array of data points obtained from each image. The dispersions of each exposure's image-

profile are found as before from full-fits to a sample of the brighter stars. Thereafter, fixed dispersion profiles are fitted to the programme stars. The volume of the least-squares fit profile is then taken as a measure of the stellar magnitude. The PDS is a single beam microphotometer which measures transmission and converts this to density via a logarithmic amplifier. The output is not linear with density, however, and must therefore be calibrated. The calibration is stored in a look-up table for use with analysis programs. One useful facility incorporated into the scheme is that a file of stellar positions can be created by manually driving the PDS from image to image and recording the positions. This can later be accessed from the measurement program. Thus, once any given exposure has been orientated to match the file positions, the program can move from star to star through the whole file, measuring and fitting the profile sequentially. Instrumental magnitudes, together with data on the scan and profile parameters are then output at the teletype. In its present form, the program can measure approximately ninety stars per hour. This rate could be enhanced quite easily as the time taken per star is shared almost equally between the scanning, the profile fitting and the output of data!

The profile fitting program in its present form is extremely sensitive to the effects of image crowding. This arises both from the fact that the background level is allowed to vary and also that deviant points cannot be rejected without disturbing the overall balance of the least-squares fit. To investigate the performance of the fitting program in the presence of other images, we carried out a number of numerical tests. Data were generated from a two-dimensional Franz profile with parameters approximating to those found for stellar images. Least-squares fits were then made of a Gaussian to these data in the manner of Figure 11 in Chapter 4. A 30 x 30 data array was used and various degrees of contami-

nation simulated by adding a constant factor to the 36 data points in one corner. The peak height of the data profile was taken as 100 units. The results can best be seen by reference to Table III, where the degree of contamination is given with the resulting magnitude.

TABLE III

Test of contamination on the derived magnitudes

Contamination	Derived Magnitude
0	10.304
1	10.304
5	10.314
10	10.325
15	10.346
20	10.357
35	10.388
100	10.419

Thus it is clear that virtually any contamination of the array is unacceptable and certainly any visible signs of nearby images preclude the measurement of that star. The programme stars were chosen from photographs of the clusters taken as described in the previous chapter. All stars which were visible on both the '41' and '48' exposures and which appeared sufficiently uncrowded on these prints were measured on the electronographs. As it happens, this was not a strict enough criterion and it was found necessary to inspect the electronographs themselves to judge whether a large enough area surrounding each image was uncrowded. The maximum step size used in reducing the electronographs was 12μ for the 30 x 30 array. We therefore require the image to be in an uncrowded area of 360μ square which, at the scale of approximately 30"/mm used here, corresponds to 11" square. We are thus approaching a selection criterion almost as stringent as that necessary for photo-

electric photometry and, indeed, more restrictive than normally needed for photographic photometry.

The PDS, in common with other microphotometers, has a serious tendency to drift, both optically and electronically, during the first few hours of operation. It is consequently necessary to monitor for this by measuring a star repeatedly throughout the measurement of the plate. In this case, the first star was remeasured every tenth image and the results checked for any systematic changes. During most runs (which typically lasted about one hour, since the maximum number of stellar positions allowed in the file was ninety-three) drifts were apparent. They were normally only one or two hundredths of a magnitude, unless caused by changes in the position of the measurement aperture, in which case magnitude changes of up to seven or eight hundredths were recorded. Any corrections found necessary in this way were applied prior to the final averaging procedure.

The instrumental magnitudes of the standard stars were calibrated (for the zero point) against Osborn's (1971) photoelectric standards (Table I; Chapter 5) and the results from all plates taken with the same filter averaged. In this process, the initial mean magnitude and standard deviation were calculated and any measure deviating by more than two standard deviations omitted. Thereafter, the standard deviation and standard error of the mean were recalculated. While delegating such procedures to a computer ensures complete objectivity, this is not always necessarily correct and can lead to anomalies. As a precaution, those cases in which more than one observation from the set was omitted, the results were checked by hand.

6.4 Sensitivity Corrections

Accurate correcting of the observed magnitudes and colours for

the varying response of the photocathode is a good deal more difficult in practice than one would suspect. In theory, all that is required is to measure the relative densities on an exposure taken with uniform illumination of the photocathode. The potentially most uncontrollable part of this procedure is the uniformity of the emulsion used for the exposures. In terms of calibrating the system, any such variations will mean that one is using a new instrument for each exposure. Estimates of these variations in sensitivity range from one to a few percent (Penny, 1976; Mackay, 1975; Wlerick et al, 1974). The quality of nuclear emulsion is visibly very variable and, indeed, if the film is inspected before use, patches where the emulsion is thinner can be seen. Since simple variation in emulsion thickness is almost certainly a major cause of its variable sensitivity, careful selection of the film used is liable to eliminate any gross effects. In further attempts to safeguard against these effects, we have taken the average result from three uniformity exposures at each wavelength. The resultant mapping of the sensitivity variations should then closely match the variations inherent to the photocathode, which are constant over the time scale considered here.

The photocathode of the image tube employed at the Wise Observatory was one of the earlier ones manufactured and, as such, has a myriad of pinholes. As we have seen in the case of profile fitting, their presence becomes more troublesome the more automatic the reduction procedure becomes. When digitizing a uniformity exposure, for example, these small defects could be eliminated satisfactorily if a sufficiently fine grid of data points were taken. The problem then becomes one of handling a vast amount of data. Here we have chosen an intermediate and interactive-type process where the data is restricted to a 425 x 425 point array. Some smoothing is done numerically and the rest by eye.

Using the indents set in the photocathode, the exposures can be

aligned on the PDS so that matching can be achieved easily to within $\pm 50\mu$. The uniformity exposures were scanned with a 55μ square aperture at 75μ steps - giving the size of array mentioned. Each line of data was then smoothed by taking the running mean of successive five-point groups and rejecting any point greater than 2σ from the mean. With the clear plate level subtracted, the differences from a mean density of the exposure were then converted to magnitude corrections. Since the scan was set up so as to measure areas of clear plate at the beginning and end of each scan, it was possible to again check for drift in the measurements. If this was detected, a slope for the clear plate perpendicular to the lines of the scan was written into the program and it was rerun. This happened only once, however, as these scans were not obtained unless the PDS had been running for several hours beforehand. The cathode positions of all the stars measured in the clusters were then calculated in terms of their coordinates in the scan array and the nine points surrounding each stellar position printed out. From visual inspection, it was then usually possible to see which, if any, of these points were affected by cathode defects. When these had been accounted for, the mean of the good points was taken as the correction for the star at the position.

The exposures of M 13 were taken with identical positioning on the photocathode, but for the observations of M 5, the positioning was changed for the three nights of observation. (The positioning on film number one was sufficiently close to the following night not to warrant a separate correction) For each star in M 5, therefore, there were three corrections. Overall, this gave approximately 430 points on the cathode at which the sensitivity was known. By plotting these out, the coverage of the area was comprehensive enough to allow a further check for anomalous points, on the expectation that the variation would be smooth with a scale length

of the order of millimetres. From these magnitude-correction maps, it was also possible to plot maps of the colour corrections. For M 13, these corrections could be applied directly to the observed colours, but for M 5 the magnitude corrections were applied before the averaging procedure. Using this technique, we estimate that the internal consistency of the corrections is ±0.005. We still have no way of accounting for variations if they occur in the emulsion used for the cluster exposures, but these differences will be recorded as part of the general error in the final mean magnitudes.

6.5 The Globular Cluster M 5

6.5.1 Introduction

Despite the fact that it is one of the brightest globular clusters, M 5 (NGC 5904) appears in recent years not to have received as much attention as its equally magnificent northern companions. The initial broad-band photometry was given by Arp (1955) and this was later transformed by him (Arp, 1962) to the UBV system and extended to reach some three magnitudes below the main sequence turn-off. This later work permitted estimates of the reddening of the cluster (essentially zero) and its metallicity ($\left[\mathrm{Fe/H}\right] = -1.2$, derived from the observed UV excess of the stars) to be made. Morphologically, M 5 is a prototype intermediate metallicity cluster. The horizontal branch is evenly populated and has a large number of variables (Sawyer Hogg, 1973), while the giant branch locus gives $\Delta V = 2.58$ (Sandage and Wallenstein, 1960).

The photometry of the bright stars in M 5 given by Arp (1962) was simply his earlier observations transformed to the BV system. Since these had only one measure in each colour, we suspect that the errors in the magnitudes are likely to be more than the 0.02 magnitudes quoted by

Arp (1955). A more recent study of the bright stars in M 5 has been given by Simoda and Tanikawa (1970). Through the use of more abundant plate material and careful selection and calibration procedures, they achieved a much improved accuracy which is borne out by the appearance of their C-M diagram. This indicates a very narrow giant branch, but somewhat puzzling though is the fact that the asymptotic giant branch (AGB) shows more scatter in this later work than did the original and, in fact, tends to clump into two regions with visual magnitudes of 13.5 and 14.2. This effect is considered real, however, due to the improved quality of the observations.

The reddening estimate for this cluster has also recently been revised. Johnson and McNamara (1969) deduced a value of $E(B-V) = 0.034$ from integrated ubvy photometry and the presently adopted value, $E(B-V) = 0.06$, is larger still and is derived from integrated photometry and spectroscopy (Burstein and McDonald, 1974; Harris and van den Bergh, 1974). Three recent estimates of the metal abundance are available (Osborn, 1971; Kjaergaard, 1969; Butler, 1974) and these give $\left[\text{Fe/H}\right] = -0.68$, -0.9 and -1.01 respectively. The first two investigations used photometry of individual giants, while Butler used image tube scanner observations of the RR Lyrae stars. We feel that the first of these determinations should be treated with reserve, both because of the large range exhibited by the individual stars (-0.17 to -1.01) but, more seriously, because the star measured as having $\left[\text{Fe/H}\right] = -1.01$ was the same star in which a strong 0-1 CN band at 4215A was detected. Now, the CN band at 3800A is intrinsically much stronger and should therefore have affected the flux in the metallicity filter of the DDO system, leading to an abnormally high value for the deduced metallicity (see for instance the correlations between the CN band strength and derived metallicity found by McClure and Norris, 1974 and Bessell and Norris, 1976).

Furthermore, Osborn (1976) found certain discrepancies when attempting to determine the helium content of M 5 from his observations, which, he notes, could be resolved if the cluster were considered slightly more metal poor - i.e. more in line with Butler's (1974) value.

6.5.2 Results

As described earlier, the magnitudes derived from each plate were calibrated for the zero point only, by a least-squares fit of a unit slope line to the comparison between the electronographic and photoelectric magnitudes. When the sensitivity corrections had been applied, and all the plates averaged, the calibrations showed obvious magnitude or colour equations. At this juncture, it was also apparent that the measures of star IV-19 were anomalous, in the sense that the measured C(4548) colour alone was grossly different from the photoelectric value. The cause was clear from the calibration plots. The measured '41', '42' and '45' magnitudes each indicated the star to be a tenth of a magnitude fainter than the photoelectric value, while the '48' magnitude was in good agreement. A number of explanations for this are possible, none of which however is very satisfactory. It seems unlikely that observational errors would produce the same deviations in the unrelated '41', '42' and '45' magnitudes (especially since the difference is greater than three standard errors of the mean) and so these measures would suggest that the star is variable. This is not a totally unlikely situation in view of the star's position near the top of the red giant branch, especially since one of the DDO standards in M 13 was suspected of variability from BV photographic photometry (Pike and Meston, 1977). This possibility still leaves the problem of the 'correctness' of the '48' magnitude since, if the star is variable, we can think of no reason why this should not have been registered in this pass-band as well. Although there is no a priori

reason either (e.g. cathode defects or companions) why the observations should be unreliable, we have been unable to resolve the anomaly and have therefore omitted this star from the magnitude calibrations. Least-squares fits to the slope and zero point then gave the following corrections:

$$m(41) = 1.155\ m^*(41) - 2.428$$

$$m(42) = 1.127\ m^*(42) - 1.948$$

$$m(45) = 1.126\ m^*(45) - 1.832$$

$$m(48) = 1.116\ m^*(48) - 1.590$$

where m*(DDO) represents the observed magnitude. The magnitudes and colours for the standard stars obtained after application of these equations are given in Table IVa.

Table IVa

Colours for the DDO Standards in M 5

	Electronographic (Photoelectric)		
Star	C(4142)	C(4245)	C(4548)
III-3	0.188 (0.179)	1.047 (1.044)	1.414 (1.401)
IV-19	0.156 (0.164)	0.958 (0.960)	1.445 (1.337)
IV-59	0.220 (0.226)	0.954 (0.954)	1.302 (1.335)
II-51	0.183 (0.192)	0.681 (0.700)	1.248 (1.228)
IV-86	0.094 (0.074)	0.525 (0.515)	1.023 (1.031)

The residuals are plotted as a function of C(4245) in Figure 1.

Although stars reaching nearly to the horizontal branch were just visible on the electronographs, it was clear from the residuals that the photometric accuracy achievable from these images (particularly on the G5 emulsion) would be insufficient to give meaningful colours. In order

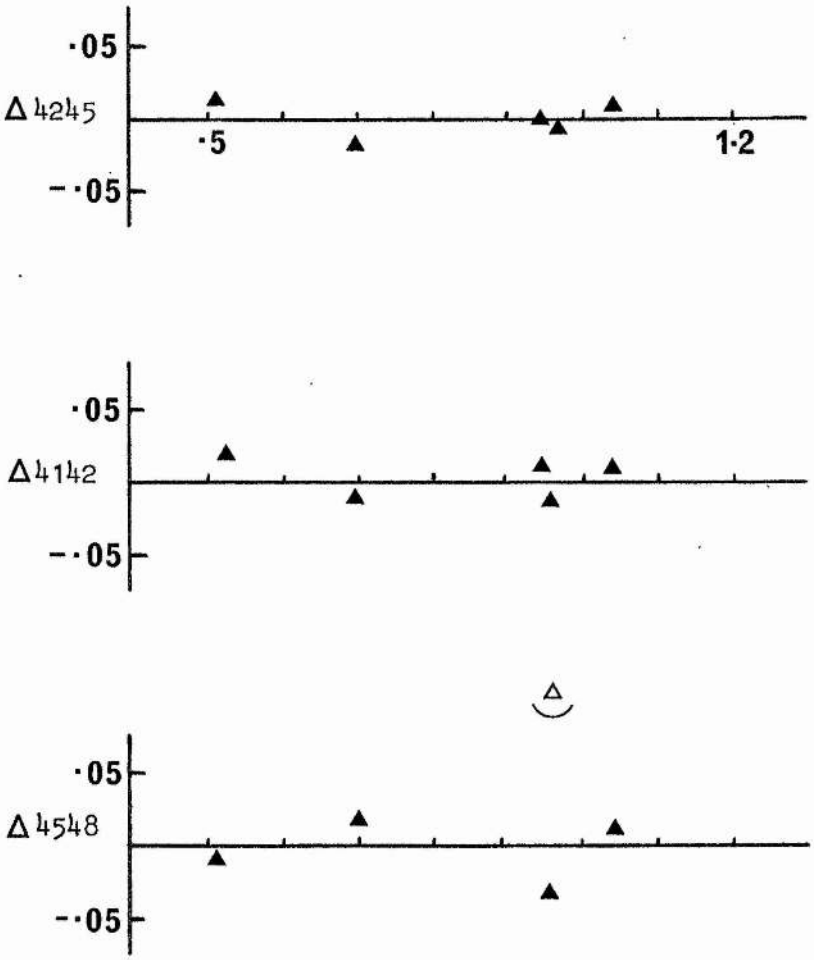

Figure 1

The residuals for the standard stars plotted in the sense (electronographic-photoelectric)

therefore to try and preserve the reliability of the results, we have limited the survey to those stars having $V \leq 14.0$. This corresponds in the majority of cases to those stars whose images were strong enough to give errors in the mean magnitudes of ≤ 0.02 magnitudes. For the stars brighter than $V = 13.5$, the sample was initially complete for all but two of the stars observed by Arp (1955) and included six stars not observed by him. A number have since been omitted though due to unacceptably large residuals or crowding problems. In the range $13.5 \leq V \leq 14.0$, the final sample was approximately 60% complete once the various selection criteria had taken their toll.

Before it is possible to use the calibration of the system to derive physical parameters for the stars, the observed colours must first be corrected for the effects of reddening and line blanketing - or lack of it - to bring them into line with solar abundance colours. Osborn (1971) gives blanketing coefficients as they apply to different luminosity classes. The values however are rather uncertain and, coupled with the accuracy of the present observations, do not justify individual corrections for the stars. We have therefore taken the blanketing coefficients appropriate to luminosity class II stars and applied the corrections these give. In view of our remarks earlier, we have adopted $\left[\text{Fe/H}\right] = -1.0$ for the cluster's metal abundance. This in turn implies blanketing corrections of

+0.065 in C(4548) and +0.170 in C(4245)

The adopted reddening of $E(B-V) = 0.06$ gives reddening corrections of

-0.02 in C(4548) and -0.015 in C(4245)

No blanketing or reddening corrections have been applied to C(4142) since they are minimal.

Table IV gives the observed magnitude and corrected colours for each star in the final list, together with the broad-band observations of Simoda and Tanikawa (1970).

TABLE IV

Magnitudes and colours for the stars in M 5

Star	Arp (1955)	m(48)	C(4142)	C(4245)	C(4548)	V	B-V
1	IV-30	13.672	0.089	0.828	1.308	13.52	0.93
6:	IV-26	13.708	0.046	0.828	1.251	13.62	0.88
7:	IV-34	13.291	0.160	1.046	1.362	13.06	1.20
8:	IV-36	14.176	0.168	0.883	1.276	13.99	1.04
10	IV-12	13.771	0.274	0.931	1.283	14.46	0.90
13	IV-82	13.488	0.075	1.037	1.302	13.27	1.15
14	IV-81	12.578	0.289	1.286	1.502	12.17	1.63
16:	IV-78	13.648	-0.006	0.733	1.084		
17	IV-73	14.116	0.153	0.767	1.175	13.93	0.83
18	IV-72	13.184	0.089	1.094	1.332	12.83	1.31
19	IV-74	13.775	0.181	0.927	1.280	13.51	1.11
21	IV-47	12.852	0.227	1.202	1.418	12.38	1.50
23	IV-65	14.010	-0.050	0.753	1.056	14.02	0.48
25	IV-59	13.018	0.220	1.108	1.347	12.63	1.34
28	I-25	14.015	0.102	0.926	1.266	13.62	1.09
30	I-35	14.370	0.080	0.950	1.209	14.12	0.99
31	I-39	13.357	0.211	1.099	1.318	13.08	1.28
35:	I-21	14.260	0.162	0.939	1.267	13.93	1.03
36	I-81	14.180	0.154	0.893	1.298	13.83	1.02
37	I-20	12.861	0.197	1.199	1.409	12.50	1.44
38	I-14	13.324	0.054	1.107	1.334	13.02	1.27
39	I-71	13.345	0.137	1.026	1.324	13.10	1.20
40	I-68	12.851	0.158	1.254	1.404	12.42	1.55
41	I-67	14.180	0.011	0.744	1.158	14.02	0.80
42	I-61	13.620	0.015	1.023	1.324	13.36	1.17
43	I-58	13.556		0.978	1.280	13.29	1.15
46:	I- 4	13.670	0.041	0.972	1.291	13.40	1.13
47	I-55	13.873	0.040	0.788	1.205	13.68	0.91
48	II-86	13.640	0.047	0.829	1.275	13.49	0.99
49	II-85	12.742	0.225	1.263	1.518	12.29	1.59
50	II-74	14.010	0.134	0.940	1.297	13.80	1.05
52	II-61	13.685	0.156	0.859	1.290	13.53	0.97
61	II-51	14.203	0.183	0.835	1.293	14.05	0.99
62	II-50	14.093	0.102	0.902	1.280	13.89	1.02
67	III- 3	12.784	0.188	1.201	1.459	12.37	1.50
70	III-19	14.384	0.148	0.876	1.236	14.14	0.93
71:	III-18	13.503	0.079	0.856	1.296	13.30	1.00
72	III-36	13.143	0.280	1.077	1.321	12.76	1.33
77		12.654	0.307	1.262	1.466		
79		13.263	0.232	0.993	1.301		
83:	III-56	13.575		0.932	1.240	13.36	0.94
88:	III-66	14.405	0.081	0.879	1.209	14.12	0.95
91		13.400	0.236	1.049	1.359		
92:	IV- 4	14.374	0.070	0.943	1.177	14.10	0.93
95		12.663	0.197	1.175	1.411		
97		13.173	0.165	0.954	1.320		
98		13.682	0.139	1.015	1.268		

6.5.3 Discussion

From the data in Table IV, we may plot the two standard DDO diagrams. They are the C(4245) - C(4548) (temperature-gravity) plot and the C(4142) - C(4548) (CN band strength) diagram. The former of these is shown in Figure 2, where we have drawn in the standard luminosity class Ib and III lines. From the average errors in the electronographic magnitudes, we expect errors in each colour of 0.02 - 0.03 magnitudes. The stars for which the measures would admit of an error greater than 0.03 magnitudes in either colour are plotted as open circles and marked with a colon in Table IV. For comparison, we show in Figure 3 the composite T-g plot taken from all the photoelectric data on red giants given by Osborn (1971) after suitable reddening and blanketing corrections have been applied. The comparison between Figures 2 and 3 would indicate that our error estimates are realistic.

The most interesting feature of Figure 2 is the clump of stars that lies above the Ib sequence at about (0.8, 1.27) in the C(4245) - C(4548) plane. These points are immediately reminiscent of the star found by Osborn in this position. (Our measurements of this star appear to confirm the previous photometry) Of the six stars that most clearly define this clump, one (No. 71) has a probable error of 0.036 magnitudes in C(4245). In an attempt to assess further the significance of this grouping, we have an independent check on the observed colours in the form of a comparison between (B-V) and C(4245). Using the broad-band colours given by Simoda and Tanikawa, this plot is shown in Figure 4. Apart from stars 83 and 92 (which have uncertain DDO photometry anyway) the scatter in this intrinsically tight relationship is well within the quoted errors. Although we are prepared to concede that our photometry could be at fault with stars 83 and 92, it is perhaps worth noting that for these stars, the (B-V) colours given by Simoda and Tanikawa (1970) and Arp (1962) differ

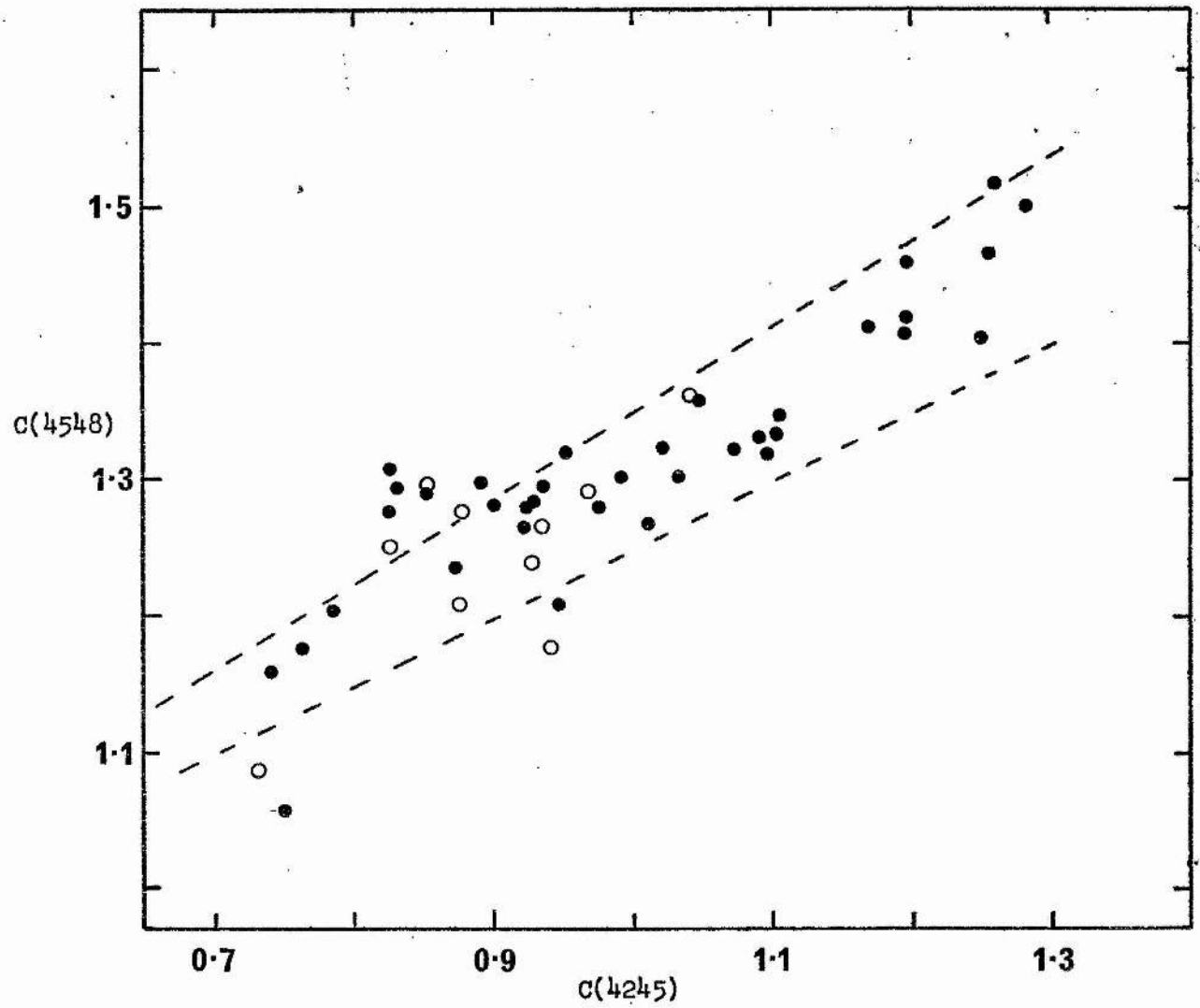

Figure 2

The T-g plot for the stars observed in M 5

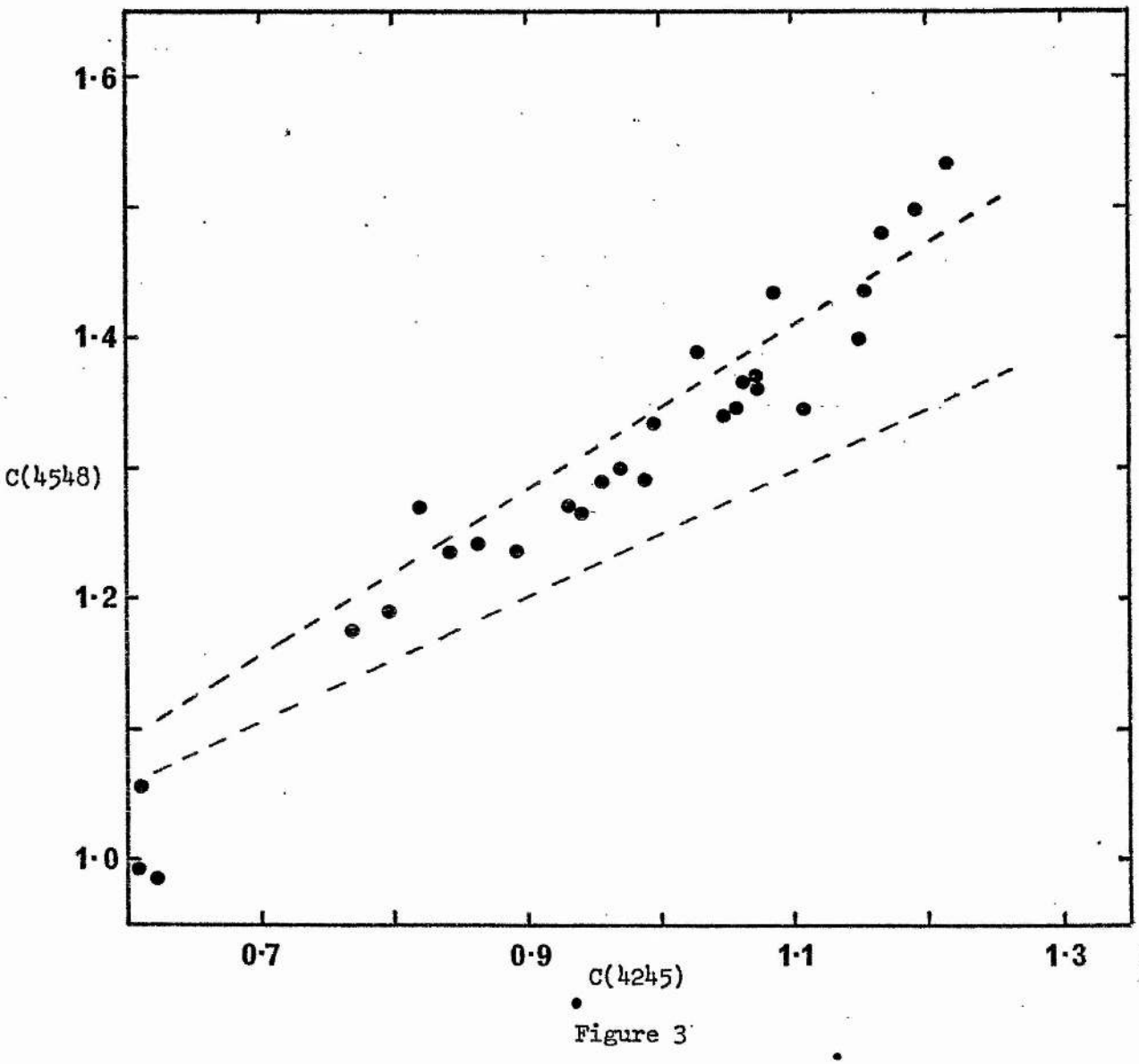

Figure 3

The T-g plot for Osborn's (1971) photoelectric observations of several clusters

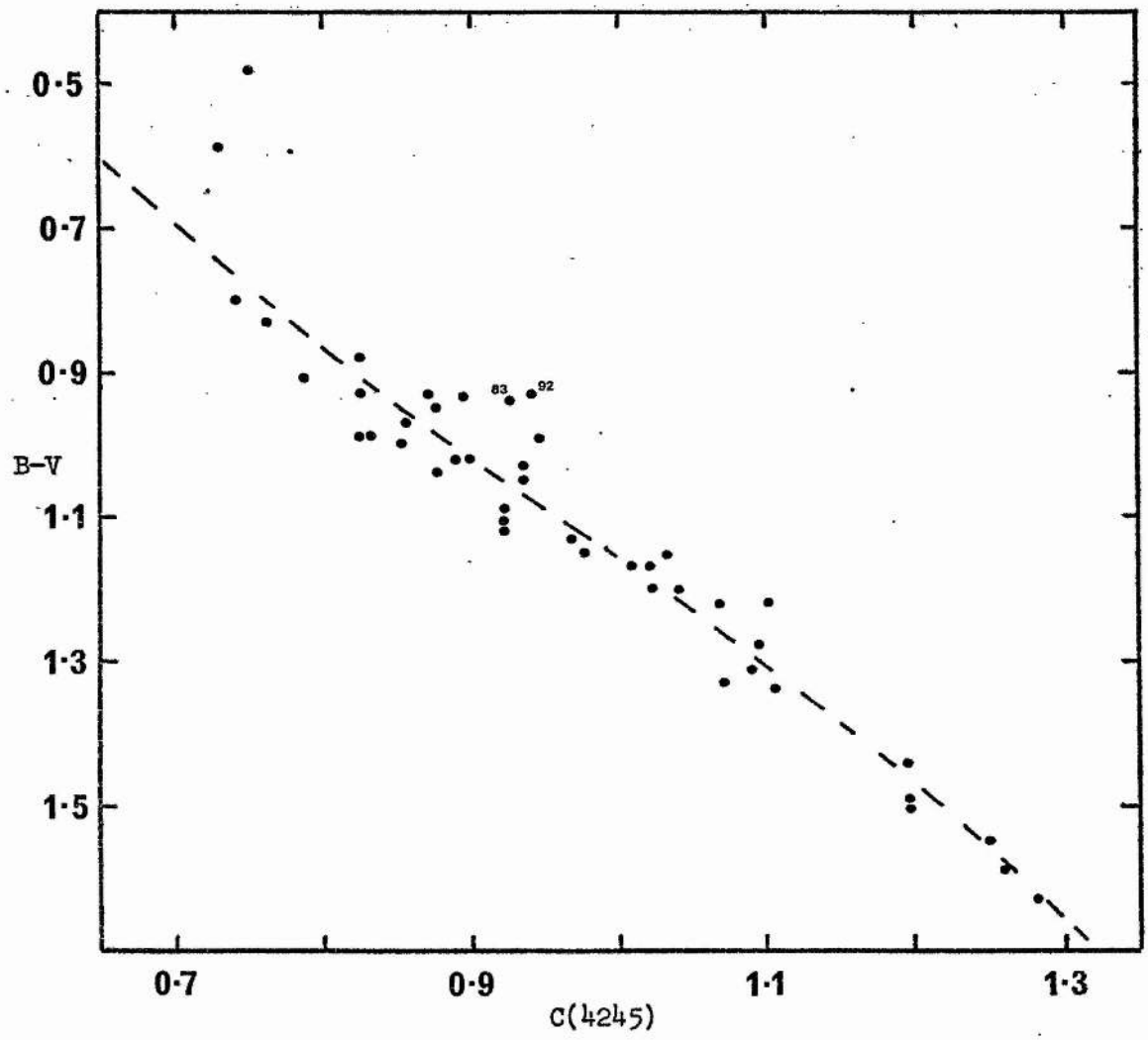

Figure 4

Comparison of (B-V) and C(4245) for the M 5 stars

by more than 0.1 magnitudes and, were we to arbitrarily use Arp's values in Figure 4, the points would return to the mean line!

Perhaps the most significant observation concerning the clump of stars, however, comes from Figure 5, where we have plotted the C-M diagram of M 5. Stars 1, 48, 52 and 71 are clearly on the upper AGB. Indeed, the photometry is not inconsistent with all the stars in the upper AGB belonging to this region of the T-g plane. Stars 36 and 61 are the two most obvious exceptions to this.

It is not impossible that an undetected colour equation could be responsible for the anomaly, as the standards available all fell on a virtually linear relationship in the C-M diagram. In a photometric system as filter-defined as the DDO one however, any colour equations are likely to be small. We note further that the stars 41 and 17 do not show the effect as markedly, nor indeed do stars 16 and 23, even though they occur at the same magnitude level but to the blue of the AGB group.

If we assume for the moment that the colours do indicate a low gravity, then this will lead to an estimate of a low mass for these stars. Thus, when the observations given in Table IV are run through the DDO calibration procedure, we may derive masses for the stars from the equation

$$\log(M/M_o) = \log g - 4\log T_e - 0.4M_{Bol} + 12.49$$

which is deduced using the standard solar values of $\log g = 4.45$ $T_e = 5{,}785^{\circ}K$ and $M_{oBol} = +4.72$. The results of the calibration are given in Table V. The bolometric corrections are taken from Schlesinger (1969) and the distance modulus for M 5, $(m-M)_v = 14.51$, from Harris (1974). The mean $\log (M/M_o)$ for the six AGB stars is -0.76 ± 0.52, while the other giants yield 0.10 ± 0.36. This difference clearly no more than reflects the positioning of the stars in the T-g plane.

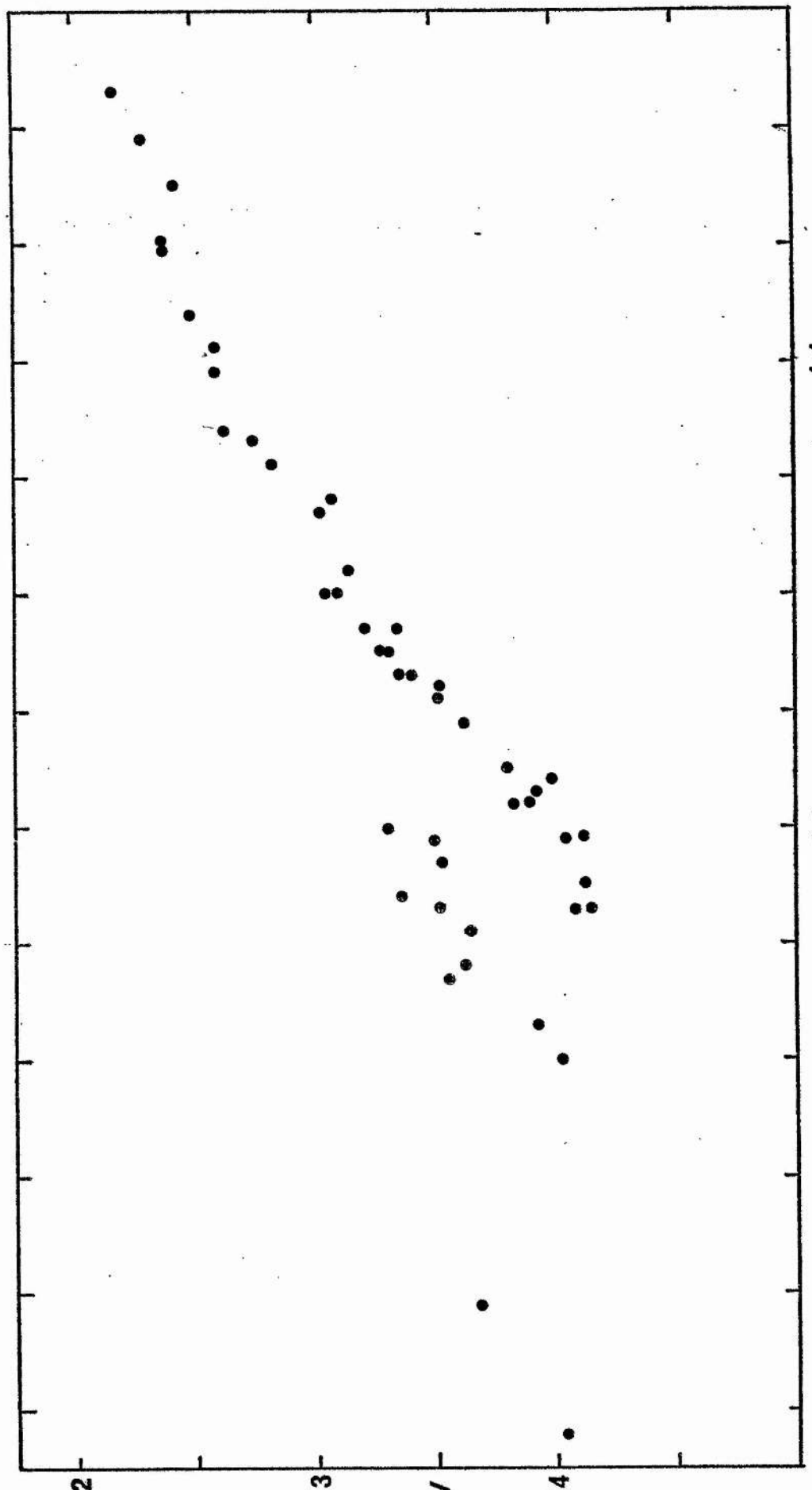

Figure 5. The C-M diagram for the stars observed in M 5

TABLE V

Physical Properties of the Stars in M 5

Star	MK class	B.C.	M_{Bol}	log g	log T.	log M/M$_\odot$
1	G3 Ia	-0.30	-1.29	0.4	3.732	-1.522
10	K0 Ib	-0.67	-0.72	1.4	3.681	-0.546
13	K2 II	-0.66	-1.90	1.6	3.638	0.298
14	K5 Ib	-1.27	-3.61	0.6	3.597	0.146
17	G4 II	-0.28	-0.86	1.8	3.716	-0.230
18	K3 II-III	-0.76	-2.44	1.5	3.623	0.474
19	G9 Ib-II	-0.50	-1.50	1.4	3.681	-0.234
21	K3-4 II	-0.88	-3.01	1.1	3.602	0.386
23	G8 V	-0.17	-0.66	4.6	3.732	
25	G3 II	-0.25	-2.13	1.4	3.623	0.250
28	K0 II	-0.53	-1.42	1.5	3.677	-0.150
30	K1 III	-0.47	-0.86	2.4	3.655	0.614
31	K3 III	-0.74	-2.17	1.6	3.618	0.486
36	G6 Ib	-0.40	-1.08	1.0	3.703	-0.890
37	K3-4 II	-0.88	-2.89	1.2	3.602	0.438
38	K3 III	-0.74	-2.23	1.5	3.618	0.410
39	K1 II	-0.59	-2.00	1.4	3.648	0.098
40	K4 II	-0.95	-3.04	1.3	3.591	0.642
41	G3 II	-0.25	-0.74	1.8	3.720	-0.294
42	K1 II	-0.59	-1.74	1.4	3.648	-0.006
43	K1 II	-0.59	-1.81	1.6	3.658	0.182
47	G4 Ib	-0.34	-1.17	1.5	3.716	-0.406
48	G4 Ib	-0.34	-1.36	0.8	3.724	-1.062
49	K5 Ib	-1.27	-3.49	0.5	3.607	-0.042
50	G9 Ib	-0.58	-1.29	1.3	3.681	-0.418
52	G4 Iab	-0.37	-1.35	0.8	3.716	-1.034
61	G4 Iab	-0.37	-0.83	0.6	3.724	-1.474
62	G7 Ib	-0.45	-1.07	1.3	3.690	-0.542
67	K3 Ib	-0.86	-3.00	0.8	3.613	0.038
70	G8 II	-0.38	-0.75	1.6	3.690	-0.370
72	K2 II	-0.66	-2.41	1.6	3.628	0.542
77	K4 Ib	-0.95		0.8	3.597	
79	K1 II	-0.59		1.5	3.658	
91	K1 Ib	-0.71		1.2	3.648	
95	K3 II	-0.80		1.1	3.613	
97	G8 Ib	-0.48		1.2	3.681	
98	K1 II-III	-0.50		1.8	3.658	

One problem which it was hoped this investigation would shed light upon was that of the systematic difference in mass between the asymptotic and red giant branch stars. It is well known for instance (Iben, 1971) that the observed widths of globular cluster horizontal branches can only be reproduced by model stars if a mass spread is allowed. This implies that some variable mass loss must occur prior to the horizontal branch stage of evolution. Numerous studies , both observational and theoretical (Newell et al, 1969; Iben and Rood, 1970), indicate that the horizontal branch is best modelled with stars of about 0.6 M_o, which is approximately 0.2 M_o less than the predicted main sequence turn-off mass. Thus the differences found here, although in the correct sense, are far too large to be realistic and an additional cause for the observed colours should be sought. This can only be in the form of spectral features (or lack of them) being inherent to the AGB stars and not to the normal giants. The obvious comparison - and possible explanation - is with the weak-G-band effect discovered by Zinn (1973) and studied by Norris and Zinn (1977). They found that stars predominantly on the AGB have systematically weaker G-bands (due to the CH molecule at about 4300A) than the other giants. The other salient points of their investigation were that a few stars on the normal lower giant branch exhibit the same weak-G-band effect, but that no stars above the confluence of the asymptotic and red giant branches in their sample had the same features. They suggest an explanation in which mixing both on the lower giant branch, but more particularly at the helium flash, causes a deficiency of carbon in the atmosphere. However, to explain the effect on the AGB would then require the horizontal branch stars to show a deficiency of carbon and present observations (Greenstein and Sargent, 1974), though not conclusive, do not support this.

The deviant stars found here in the T-g plane are thus analogous in three ways to the weak-G-band stars. They are mainly, but not

completely (Nos. 61 and 36), confined to the known AGB in the C-M diagram and the distinction is not apparent on the upper giant branch.

There has been some suggestion (Butler, 1976) that the '42' filter is sufficiently contaminated by the G-band that variations in the band's strength will significantly change the flux in this filter. It does seem unlikely that such an effect could be responsible for the difference in colour observed here - although it is certainly in the correct sense - as the corresponding shift in the C(4142) colour is not apparent. An alternative explanation is that there is some extra absorption in the pass-band of the '45' filter which accompanies the effect of the G-band variations.

Star no. 61 is still an interesting case. As well as its anomalous position in the T-g plot, Osborn found it to have strong CN absorption. By interpreting the photometry as indicative of very low gravity, he suggested that this was the cause of the strong CN. There is very little evidence though (Janes, 1975; Sneden, 1973) that the 4215A CN band is detectable, even at low gravities, for metallicities less than about $\left[\text{Fe/H}\right] = -0.7$. As we believe M 5 to be probably more metal poor than this, this star should probably be viewed as a true CN star.

Two other stars of note in Figure 2 are nos. 16 and 23. These are two of the UV-bright stars found by Zinn et al (1973) and seen in Arp's (1962) C-M diagram. Although many stars found in this region of the C-M diagram are now known to be bona fide cluster members (Strom et al, 1970), the photometry obtained here is consistent with both of them, in this instance being field stars.

Part of the reason for choosing M 5 for this study was the fact that abundance anomalies had already been noted and so this cluster provided a good opportunity to test the photometry by seeing whether we could reproduce these results and, at the same time, gave a high

chance of discovering new stars with similar properties.

The C(4142) - C(4548) plot for the stars observed is shown in Figure 6. The two high CN-index stars found by Osborn are indicated by crosses. Clearly due to the scatter in our observations, these stars would not have been selected as peculiar on the basis of Figure 6. Their positions, however, are not inconsistent with previous photometry. More interesting are stars 10, 72 and 79, which show even larger deviations from the main trend and for which the photometry appears reliable. Obviously, spectroscopic observations will be needed to investigate the correctness of the classification of these stars as CN stars.

Pending such observations, if we assume this classification, then it appears that M 5 contains at least five CN stars on the upper giant branch. Demarque and Zinn (1975) have suggested that the mixing necessary to produce CN and CH stars is more likely to occur at the helium core flash than during the helium shell flashes. The latter, they argue, could not produce mixed stars fainter than about $M = -1.3$. Of the M 5 CN stars, only star 61 is decidedly fainter than this and hence our observations are unable to provide a preference for the site of mixing.

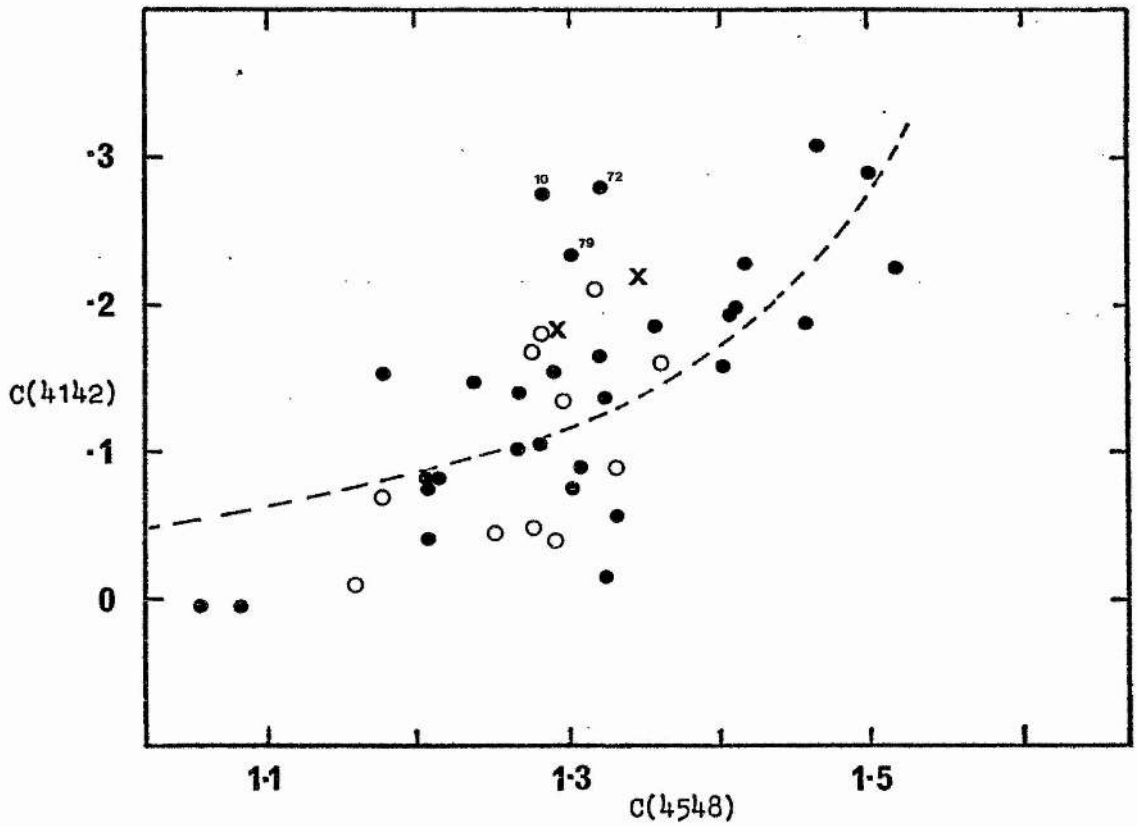

Figure 6

The CN band index plot for M 5

6.6 The Globular Cluster M 13

6.6.1 Introduction

The bright northern globular cluster M 13 (NGC 6205) is a fascinating object in many respects. As it has been the subject of many observational programmes, its general features and characteristics are well known, although it might be argued that more questions have been raised by the results of these investigations than have been answered by them. Broad-band photometric studies of the brighter stars abound (Sandage, 1970 and references cited therein) and the main sequence, identified as early as 1954 by Baum, has been observed and the photometry revised by Baum et al (1959) and Sandage (1970).

The derivation of the metal abundance of M 13 appears problematical. The traditional metallicity parameters (Deutsch, 1955; Morgan, 1959; Sandage and Wallerstein, 1960) indicated an intermediate metal abundance slightly greater than that of $\left[\text{Fe/H}\right] = -1.4$ derived by Helfer et al (1959) from spectroscopic studies. The contradiction of this with the extremely blue population of the horizontal branch was soon recognised as an important anomaly - indeed the 'M 13 anomaly' - the counterpart of which was not found until the observations of NGC 362 and NGC 7006 were made. More recent abundance determinations cannot be said to have clarified the situation any. Osborn (1971) derived a mean metal content of $\left[\text{Fe/H}\right] = -1.6$ but with a spread in the individual determinations of from -1.2 to -2.0. Butler (1974) was able to observe only one of the RR Lyraes which yielded $\left[\text{Fe/H}\right] = -1.04$. More recent DDO observations by Norris and Zinn (1977) give a mean cluster abundance of $\left[\text{Fe/H}\right] = -1.1$ although the scatter was even larger, ranging from -0.5 to -1.59. It seems apparent that high dispersion spectroscopic studies are needed both to resolve the problem of the correct abundance (if indeed there

is such a thing for the cluster as a whole) and perhaps to indicate why the present determinations appear, at least superficially, to disagree.

The reddening of the cluster is small. We have here assumed a value of E(B-V) = 0.02 (McClure and Racine, 1969; Burstein and McDonald, 1974).

A further characteristic of M 13 which was becoming established, was that concerning the interpretation of its variable star content. The paucity of the variables is one problem, their nature was another. Sandage (1970) considered the RR Lyraes to be unique and suggested an association with the asymptotic rather than horizontal branch. Bohm-Vitense et al (1969) encountered further difficulty when they attempted to compare theoretical and observational data for the Cepheids in M 13. They concluded that two of the Cepheids had either a very high helium content or very low masses. It would seem though that M 13 can be spared these embarrassments, as improved photometry of the variables (Pike and Meston, 1977) has shown that these stars are in reality quite normal Population II variables, whose former interpretation was distorted by inaccurate photometry.

6.6.2 Results

The reduction of the electronographs of M 13, listed in Table I, proceeded exactly along the lines described for those of M 5. The individual calibration plots, however, showed that on some plates the measurements of the standards were badly in error. It was possible to ascribe this to the fact that parts of some of the films were out of focus, not optically, but in the sense that the film had not made sufficiently intimate contact with the mica window. This is one of the potential hazards with the Spectracon line of image tubes, since if the contact between emulsion and mica is not perfect, scattering and absorp-

tion of the electrons in the intervening region normally renders the image unfit for measurement.

The exact manner in which to achieve this contact in the McMullan cameras took a while to develop. Electrostatic forces were employed, but found unsuitable due to their effect upon the electron imaging. The scheme employed at present simply introduces a small pressure behind the film which pushes the film into final contact. This can only be effective, naturally, over very small distances and what we suggest happened here is that either the piston on which the film-carrying ring is loaded, stopped fractionally short of the correct position, or that the film ring itself was seated not quite squarely upon the piston when it approached the mica window. Due to the automation of the film advancing mechanism in the McMullan camera, this procedure is beyond the control of the operator. However, provision has been made in the new generation of cameras now being constructed for the mechanism to give an extra final impulse to the piston, so that the likelihood of this failure occurring in the future should be small.

From the size of the effect which this failure had upon the measurement of the standard stars, it was clear that the final averaging routines would reject these measures anyway and so we persevered with the analysis as previously. The initial plot of the data in the C(4245) - C(4548) diagram showed an unacceptably large scatter which would most easily be explained by errors in the '45' magnitudes. Confirmation of this came from the observation that there was a strong systematic trend relating the stars' positions both in the C(4245) - C(4548) plot and in the comparison of C(4245) with the broad-band colours, with the position of the image on the film. The inference from this was that the effects of the loading error were variable across the plate and in the cases where the departure had been insufficient for the measures to be rejected, it

had caused a systematic trend in the final magnitudes.

The method adopted to deal with the situation was to inspect the films and reject any showing obvious signs of the defocussing effect. As a result, three exposures with the '45' and two with the '48' filter were discarded, after which the averaging procedures were repeated. There was no guarantee that the visual inspection would be a definitive indication of the quality of the exposure and, indeed, when the revised data were replotted, a smaller systematic trend still remained. From the fact that the '45' exposures appeared the most likely to be in error, a systematic correction to each star's m(45) was applied in regard to its position on the film. The standard stars were treated in exactly the same manner as the rest and the resulting colours are given in Table VI. We consider the good agreement with the photoelectric values to be both fortuitous and misleading since, due to the statistical nature of the corrections that were applied and to the decreased number of observations used, errors of the order of 0.04 - 0.05 magnitudes in the colours would have been expected.

TABLE VI

Colours of DDO standards in M 13

	Electronographic (Photoelectric)		
Star	C(4142)	C(4245)	C(4548)
9	0.30 (0.28)	1.06 (1.07)	1.46 (1.49)
35	0.10 (0.13)	0.75 (0.75)	1.26 (1.24)
47	0.10 (0.09)	0.77 (0.80)	1.25 (1.25)
59	0.11 (0.09)	0.83 (0.84)	1.25 (1.25)
81	0.07 (0.07)	0.59 (0.55)	1.11 (1.12)

In order to correct the colours to the solar abundance, we have retained Osborn's (1971) value for the metal abundance of $\left[Fe/H\right] = -1.6$. The colours and magnitudes of the programme stars, corrected for blanketing and reddening, are given in Table VII. The T-g diagram plotted from these data is shown in Figure 7. Also given in Table VII are the colours and magnitudes observed by Arp (1955) or Savedoff (1956), from which we have plotted the C-M diagram (Figure 8) for the stars studied here. From the uncorrected T-g plot, stars 5, 43 and 60 were shown to be field stars and consequently their colours have not been corrected. Due to the problems encountered in the photometry of this cluster, we consider that it would be premature to apply the calibration procedure to these data.

As far as we can tell, the '41' and '42' filter exposures were not subject to the same problems encountered with the others. It is therefore still possible to use these data to search the cluster for stars having anomalously strong CN bands. From our discussion earlier, we concluded that the CN band at 4215A is not detectable under normal conditions in these stars. C(4142) will thus in general only measure the equivalent of a continuum gradient and so will increase with the stars' decreasing temperature. In order that the errors likely to be present in the C(4548) colours should not mask any effect in the survey, we have chosen to plot instead the C(4142) colour against the broad-band colour index (CI). Most of the stars measured by Arp (1955) had four measures in each colour and they can be expected to be more accurate than those of M 5. The normal C(4142) - C(4548) diagram was also plotted as a check for the few cases where no CI was available. The C(4142) - CI plot is shown in Figure 9. There is no evidence that any of the stars observed have detectable CN bands.

Table VII

Magnitudes and colours for the stars in M 13

	Star	m(48)	C(4142)	C(4245)	C(4548)	m_{ps}	CI
1	II-33	13.04	0.080	1.15	1.48	12.54	1.25
3	II-34	12.76	0.126	1.21	1.50	12.20	1.39
4	II-28	13.91	0.037	0.95	1.26	13.56	0.82
5	II-30	14.21	0.038	0.74	1.05	13.85	0.86
8	II-23	14.12	0.047	0.93	1.28	13.93	0.81
9	II-67	12.53	0.300	1.32	1.56	12.06	1.54
12	II-63	14.53	0.066	0.86	1.28	14.50	0.72
14	B361	13.84	0.062	0.93	1.28	13.72	0.81
17	II-72	14.15	0.029	0.77	1.16	14.08	0.56
20	III- 7	13.50	0.122	0.98	1.32	13.31	1.01
22	III-18	12.90	0.241	1.02	1.39	12.70	1.17
23	III-73	12.65	0.250	1.15	1.42	12.25	1.31
24	B286	13.66	0.123	0.96	1.27	13.51	0.89
25	B273	13.75	0.066	0.90	1.30	13.56	0.87
26	A171	12.10		1.27	1.51	11.96	0.99
27	B252	14.47	0.005	0.87	1.27		
30	III-64	14.12	0.047	0.77	1.21	14.12	0.58
32	III-63	12.45	0.210	1.18	1.45	12.14	1.34
35	B651	13.31	0.099	1.03	1.36	13.12	0.93
36	IV-15	13.06	0.041	0.98	1.37	12.88	0.98
37	IV-16	14.13	0.044	0.93	1.31	14.09	0.80
38	IV-17	14.13	0.053	0.92	1.27	13.99	0.86
39	IV-18	13.78	0.060	0.94	1.32	13.69	0.88
40	IV-19	13.68	0.044	0.99	1.37	13.58	0.89
43	IV-24	14.04	0.037	0.74	1.04	14.04	0.68
44	IV-22	13.94	0.089	0.97	1.31	13.79	0.90
47	B171	13.01	0.097	1.03	1.35	12.78	0.95
50	IV-80	14.26	0.060	0.91	1.26	14.23	0.78
58	I-76	13.86	0.128	0.91	1.28	13.74	0.84
59	A371	13.18	0.083	1.09	1.35	12.93	1.03
60	A367	13.86	0.130	0.65	1.01	13.92	0.52
61	I-72	14.46	-0.037	0.98	1.34	14.49	0.75
62	I-71	14.35	0.028	0.60	1.05	14.66	0.06
66	I-65	14.10	0.081	0.92	1.28	13.99	0.83
68	I-62	14.58	0.021	0.95	1.24	14.67	0.67
69	I-67	14.32	0.061	0.90	1.29	14.36	0.73
70	B 67	14.41	0.086	0.88	1.28	14.34	0.76
74	I- 2	14.40	0.037	0.94	1.26	14.21	0.78
77	II-10	14.42	0.016	0.94	1.30	14.26	0.82
79	II- 9	14.23	-0.005	1.04	1.33	14.03	0.84
80	II- 7	14.38	-0.030	1.04	1.39	14.27	0.75
81	II-14	14.10	0.070	0.85	1.21	13.93	0.64
82	II-40	13.05	0.038	1.08	1.35	12.70	1.08
83	II-41	14.13	0.018	1.02	1.36	13.80	0.89
88	II-94	13.80	0.141	0.94	1.29	13.53	0.92
89	II-95	14.13	-0.025	1.03	1.35	13.74	0.88
90	II-90	12.45	0.238	1.23	1.53	12.01	1.50
91	II-87	13.52	0.133	0.97	1.32	13.19	0.99
93		13.08	0.145	1.06	1.36		
94	III-12	13.74	0.016	0.98	1.28	13.49	0.88

Table VII (continued)

	Star	m(48)	C(4142)	C(4245)	C(4548)	m_{pg}	CI
95	III-25	14.17	0.085	0.79	1.20	14.16	0.62
96	III-30	13.28	0.109	0.99	1.34	13.06	1.06
98	III-36	14.05	-0.005	0.93	1.29	13.86	0.87
99	III-37	12.95	0.174	1.07	1.35	12.67	1.17
101	III-41	13.34	0.144	0.90	1.26	13.23	0.88
104	III-50	13.57	0.034	1.01	1.35	13.43	0.95
105	III-51	13.40		1.15	1.40	13.20	1.02
106	III-52	12.81	0.137	1.12	1.40	12.53	1.21
107	III-59	12.75	0.200	1.08	1.44	12.46	1.24
108	III-56	12.45	0.279	1.20	1.55	11.97	1.51
111	IV- 6	14.51	0.034	0.95	1.28	14.35	0.83
113	IV-34	13.32	0.158	0.95	1.33	13.04	1.03
115	IV-28	13.20	0.123	1.00	1.37	12.88	1.11
116	IV-25	12.39	0.313	1.21	1.51	12.01	1.52
117	IV-35	13.28	0.107	0.95	1.31	13.03	0.96
118	IV-36	13.80	0.016	0.93	1.25	13.63	0.77
119	IV-37	13.54	0.148	0.98	1.33	13.25	0.99
120		14.43	0.150	0.80	1.24		
121	IV-38	13.92	0.056	0.79	1.21	14.18	0.58
122	IV-48	12.56	0.298	1.17	1.51	irr. var.	
124		14.04	0.057	0.90	1.27		
128		12.50	0.312	1.21	1.50		
130	I-86	13.30	0.207	1.00	1.33	13.01	1.05
131	I-49	14.09	0.013	0.97	1.30	13.89	0.85
132	I-48	12.39	0.285	1.29	1.58	11.91	1.60
133	I-54	13.81	0.016	0.89	1.24	13.67	0.74
136	I-24	13.08	0.079	1.08	1.39	12.77	1.11
137	I-23	13.30	0.087	0.99	1.28	13.07	0.95
138	I-18	14.00	0.002	0.97	1.28	13.84	0.86
139	I-19	13.94	0.092	0.96	1.28	13.77	0.92
140	I-13	12.83	0.082	1.14	1.47	12.42	1.29
141	I-12	13.63	0.071	1.01	1.36	13.47	0.94
142		13.78	0.048	1.01	1.37		
153	IV- 4	13.90	0.044	0.96	1.28	13.57	0.90

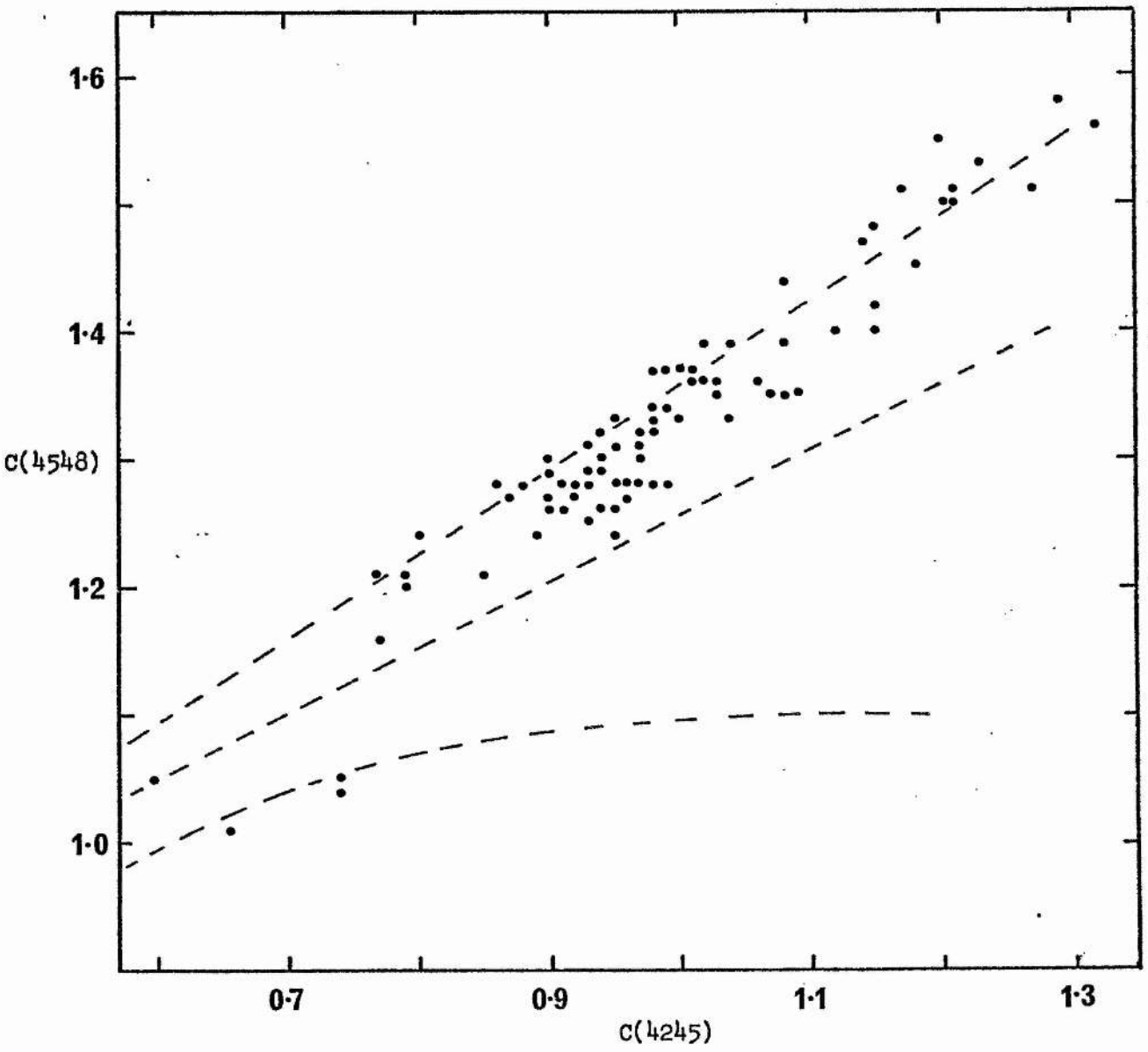

Figure 7

The T-g plot for the stars observed in M 13

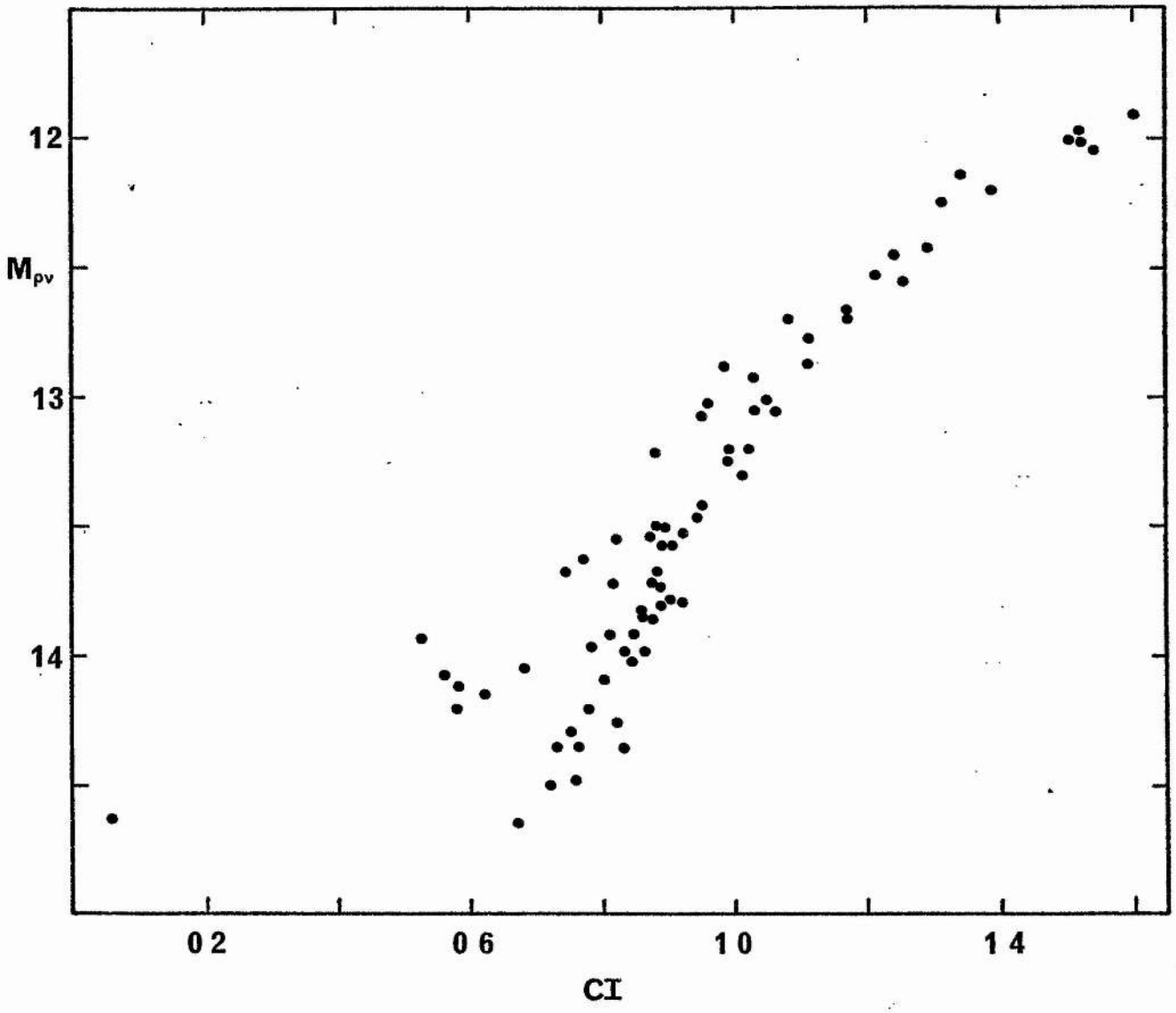

Figure 8

The C-M diagram for the stars observed in M 13

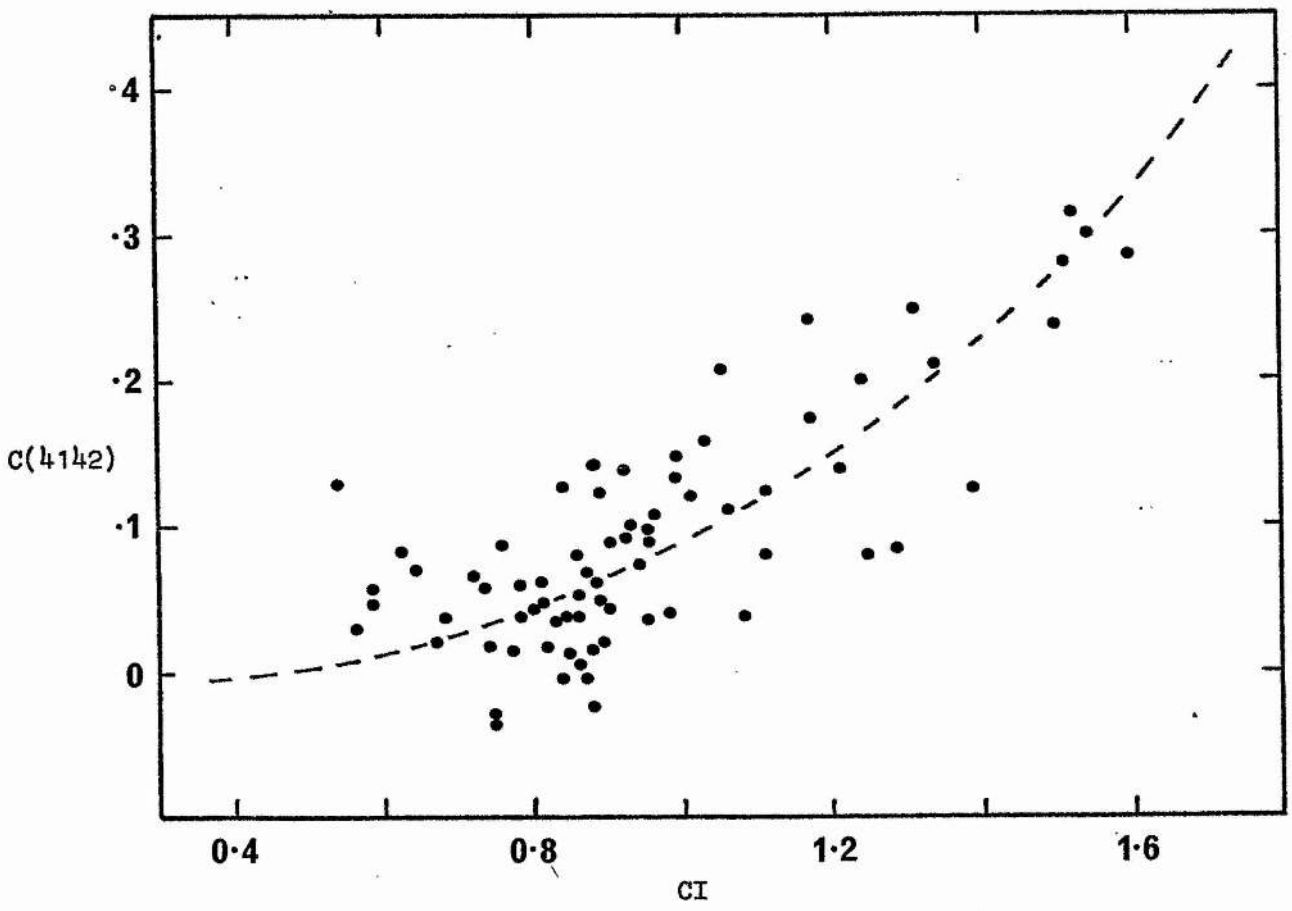

Figure 9

C(4142) versus CI for the stars in M 13

6.7 Summary

We believe that, notwithstanding the technical problems encountered, we have in this chapter demonstrated the feasibility of using intermediate-band electronography for this kind of study. From the photometry of M 5 we have been able to derive temperatures and gravities for many of the giants in the cluster. By comparing our results for the stars also observed by Osborn (1971) - i.e. the standard stars - the temperatures and gravities given in Table V are seen to be accurate to ±150°K and ±0.3 dex. A further independent check of the derived temperatures can be made by a comparison with the infra-red photometry of Eggen (1972). After conversion of his colours to the Johnson system (Eggen, 1971) and application of the appropriate reddening corrections, we may employ the temperature calibrations given by Johnson (1966). For the stars indicated as luminosity class II in Table V, we have taken the mean of Johnson's class I and III calibrations. The comparison for the four stars in common with Eggen (1972) is shown in Table VIII and is a further indication that the error estimates are correct.

TABLE VIII

Comparison of DDO and infra-red temperatures

Star	$(R-I)_{J,o}$	Temperature °K (R-I)	DDO
21	0.75	4000	4000
40	0.76	4000	3900
42	0.66	4250	4450
67	0.77	4000	4100

All clusters so far studied exhibit the weak-G-band effect (Norris and Zinn, 1977) and, in terms of the current interpretation, this implies that mixing must occur to some extent in all globular clusters. Subject to limitations on the accuracy and completeness of the sample, Figures 6

and 9 support the hypothesis that mixing, sufficient to produce CN stars, occurs extensively in the giants of M 5 but not in those of M 13. While the detection of but one CN star is sufficient to indicate the presence of the effect (e.g. M 10; Osborn, 1971), it is clear that only with systematic searches of the kind presented here can any particular cluster be said to be free of the phenomenon. Therefore, unless some theoretical cause for this kind of mixing is forthcoming, observations of many more clusters will be needed to piece together an overall picture in an attempt to isolate observationally the necessary or sufficient conditions for its occurrence. In the meantime, we are limited to speculation.

The presence of an excess of angular momentum has been postulated as a cause of the effect in ωCen (Bessell and Norris, 1976) but ωCen is unique in that it contains CH as well as CN stars and probably represents an extreme case. For the less drastic instances found in other clusters, there is, as yet, no obvious indication from the clusters' integrated properties to distinguish the haves from the have-nots. Should subsequent observations confirm that the stars in M 13, and possibly other clusters, are free of the phenomenon, then this would support the case for the cause being associated with some common property of the cluster stars. In the event that isolated cases are eventually found in all clusters, then these stars must represent a possible phase of Population II stellar evolution, whose existence is determined by the physical conditions pertaining to each individual star.

References

Arp, H. C., 1955. A.J., 60, 317.

Arp, H. C., 1962. Ap. J., 135, 311.

Baum, W. A., 1954. A.J., 59, 422.

Baum, W. A., Hiltner, W. A., Johnson, H. L. & Sandage, A. R., 1959. Ap. J., 130, 749.

Bessell, M. & Norris, J., 1976. Preprint.

Bohm-Vitense, E., Szkody, P., Wallerstein, G. & Iben, I., 1974. Ap. J., 194, 125.

Burstein, D. &McDonald, L. H., 1974. A.J., 80, 17.

Butler, D., 1974. Thesis, University of California.

Demarque, P. & Zinn, R., 1975. Preprint.

Deutsch, A., 1955. In: Principes Fondementeaux de Classification Stellaire (C.N.R.S., Paris), p 25.

Eggen, O. J., 1971. Ap. J. Suppl., 22, 389.

Eggen, O. J., 1971. Ap. J., 172, 639.

Greenstein, J. L. & Sargent, A. I., 1974. Ap. J. Suppl., 28, 157.

Harris, W. E., 1974. Thesis, University of Toronto.

Harris, W. E. & Bergh, S. van den, 1974. A.J., 79, 31.

Helfer, H. L., Wallerstein, G. & Greenstein, J. L., 1959. Ap. J., 129, 700.

Iben, I., 1971. P.A.S.P., 83, 697.

Iben, I. & Rood, R. T., 1970. Ap. J., 161, 587.

Janes, K. A., 1975. Ap. J. Suppl., 29, 161.

Johnson, H. L., 1966. Ann. Rev. of Ast. & Astroph., 4, 193.

Johnson, S. L. & McNamara, D. H., 1969. P.A.S.P., 81, 415.

Kjaergaard, P., 1969. Thesis, University of Copenhagen.

Mackay, C. D., 1976. Adv. in E. & E.P., 40B, 847.

McClure, R. D. & Norris, J., 1974. Ap. J., 193, 139.

McClure, R. D. & Racine, R., 1969. A.J., 74, 1000.

Meaburn, J., 1966. App. Optics, 5, 1757.

Morgan, W. W., 1959. A.J., 64, 432.

Newell, E. B., Rodgers, A. W. & Searle, L., 1969. Ap. J., 156, 597.

Norris, J. & Zinn, R., 1976. Preprint.

Osborn, W. H., 1971. Thesis, Yale University.

Osborn, W. H., 1976. Mon. Not. R. astr. Soc., 176, 1.

Penny, A. J., 1976. Thesis, University of Sussex.

Pike, C. D. & Meston, C. J., 1977. Mon. Not. R. astr. Soc., in press.

Sandage, A., 1970. Ap. J., 162, 841.

Sandage, A. & Wallerstein, G., 1960. Ap. J., 131, 598.

Savedoff, M., 1956. A.J., 61, 254.

Sawyer Hogg, H. B., 1973. Publ. D. D. Obs., 3, No. 6.

Schlesinger, B. M., 1969. Ap. J., 157, 533.

Simoda, M. & Tanikawa, K., 1970. Publ. Astr. Soc. Japan, 22, 143.

Sneden, C., 1973. Ap. J., 184, 839.

Strom, S. E., Strom, K. M., Rood, R. T. & Iben, I., 1970. Astr. & Astroph., 8, 243.

Wlerick, G., Michet, D. & Labeyne, C., 1974. Electronography and its astronomical applications, p 177.

Zinn, R. J., 1973. Ap. J., 182, 183.

Zinn, R. J., Newell, E. B. & Gibson, J. B., 1973. Astr. & Astroph., 18, 390.

CHAPTER 7

CONCLUSIONS

We conclude by reviewing the results of the previous chapters and giving some thoughts and suggestions for the future of electronography.

The studies of NGC 5053 and NGC 6366 provide a good example of programmes in which electronography can be used to advantage. The ability to extrapolate photoelectric sequences clearly does save much large-telescope time. For studies such as these, the utmost accuracy is not essential provided sufficient numbers of stars are observed. As long as there are no systematic effects in the photometry, then the important features of the C-M diagrams will be apparent and from these a number of interesting properties of the clusters can be deduced, as has been the case for NGC 5053 and NGC 6366. The fact that electronography did not provide all the photometric data used on the two clusters was due to technical problems with the image tubes, rather than to any inherent shortcoming in the technique. It is pertinent to note here perhaps that, although because of linearity, results can still be obtained from cathodes as bad as that used in Chapters 2 and 3, this should not be regarded (as sometimes happens) as an advantage of electronography, since the quality of the detectors is a feature of the technique itself.

The developments in data handling described in Chapter 4 are clearly only a first, but very necessary, step in achieving the efficient retrieval of substantial amounts of information from electronographs. We believe that Chapter 6 records the first substantial use of this kind of reduction scheme. While it has enabled the reductions to be completed in a reasonable time, the restrictions already noted show that the system is still inadequate in many ways and efforts should be increased to develop the alternative approach, also given in Chapter 4, of using a more realistic profile (in this case the two-dimensional Franz profile). The application to multiple image groupings is particularly important as it employs the advantages of electronography to the full and makes available data totally

lost by the more traditional methods of photometry. Testing the results from multi-image analysis presents a slight problem in that, by the very nature of the stars observed, there will be nothing with which to compare the resultant electronographic magnitudes. One way around this will be to obtain special electronographs in which a group of stars is simulated by a number of exposures of one star, with the telescope moved slightly between exposures. Accurate timing of the exposures will then give the expected relative magnitudes of the images in the group.

In Chapter 6 we employed electronography on a potentially very rewarding astronomical programme and one which would seem ideal for an accurate two-dimensional detector. In theory, the results should have enabled a complete survey of the cluster to be made with (if the current literature is to be believed) an accuracy normally associated with photoelectric photometry. Ignoring the instrumental difficulties, the results indicate that only a partially complete survey was possible. This was due primarily to:

1) Image crowding problems which precluded the measurement of a number of stars. That a two-dimensional linear detector should be restricted in this way is clearly unacceptable.
2) Defects on the cathode which occasionally coincided with the positions of images. Even when this was not directly visible, its effects probably explain the cause of some measures having large residuals.
3) The fact that on G5 film the results indicate that an image must be approximately one magnitude above the plate limit before a measuring accuracy of 0.05 magnitudes is achieved. This set the limit of the photometry somewhat brighter than we had anticipated.

The results from the use of fine grain L4 emulsion were always noticeably better than those on G5 and, if at all practicable, L4 should

be used for this kind of work. However, as it takes approximately five times the exposure to achieve the same visibility on L4 (we do not subscribe to the 'the-information-is-there-but-you-just-cannot-see-it' philosophy) this would have required exposures of about three hours for the M 5 observations. Obtaining many of these is not very practicable. Nonetheless, the results of Chapter 6 show that this kind of photometry can yield useful information on the temperatures and gravities of globular cluster giants.

Stellar photometry is, of course, not the only field in which electronography is being used. Numerous studies of two-dimensional objects (galaxies, nebulae, etc.) are in progress, but here again it remains to be seen whether the full potential of the technique can be realised. In this regard, it seems at present to be Mackay (1976) versus the rest. Whether the interpretation of this should be that Mackay is the only one prepared to be truly objective about the situation must await further work. We are in fact beginning an investigation to compare the capabilities of electronography with other techniques in the field of galaxy surface photometry. Surface photometry of galactic halos to less than 1% of the sky brightness is now commonplace using modern photographic emulsions. The question is whether the known complications of electronography i.e. cathode sensitivity variations and emulsion problems, can be compensated for accurately enough to allow photometry to this level. In collaboration with J. J. Lorre of the Jet Propulsion Laboratory we hope to apply their image processing techniques to some electronographs in the expectation that, at least in this case, the reduction procedures will not be found wanting.

As regards improvements in the accuracy of stellar photometry, we can but list some of the basic requirements that have become apparent from our experiences:

a) The quality of the basic materials, i.e. photocathode and emulsion, must be improved. An immediate improvement is no doubt technically possible, if those responsible are given sufficient encouragement and incentive by the users.

b) Conditions prevailing in most darkrooms are not adequate for processing electronographs. The conditions required are closer to the 'clean room' situation common in many scientific fields, than to the average observatory darkroom. At the very least, automatic temperature control of the chemicals, filtered washing water and, most important, a dust-free drying area should be available.

c) An effort equivalent to that expended in the development and manufacture of the electronographic cameras must be put into devising further improved reduction schemes. While speed and simplicity are excellent ideals, in the end they are no substitute for accuracy.

In conclusion, we would suggest that the results of the thesis as a whole indicate that the use of electronography is advantageous for certain projects, but that with present equipment and reduction techniques we are still a good way from the realisation of electronography as two-dimensional photoelectric photometry.

Reference

Mackay, C. D., 1976. Adv. in E. & E.P., 40B, 847.